SIGNAL DESIGN STUDY FOR SHUTTLE/TDRSS KU-BAND UPLINK

FINAL REPORT

AUGUST 1976

Prepared for
NATIONAL AERONAUTICS and SPACE ADMINISTRATION
JOHNSON SPACE CENTER
HOUSTON, TEXAS

Under Contract No. NAS 9-14842
CDRL No. 2
TRW No. 29210

TRW
DEFENSE AND SPACE SYSTEMS GROUP

ONE SPACE PARK • REDONDO BEACH, CALIFORNIA 90278

TRW

CONTENTS

TRW

CONTENTS (Continued)

TRW

ILLUSTRATIONS

TRW

ILLUSTRATIONS (Continued)

1. INTRODUCTION

This final report is submitted in compliance with CDRL No. 2 of contract NAS9-14842 and summarizes the results of the Signal Design Study for Shuttle/TDRSS Ku-Band Uplink. This study was conducted by the TRW Defense and Space Systems Group for the Johnson Space Center of the National Aeronautics and Space Administration. The duration of the uplink study was 9 months beginning 1 December 1975 and ending 1 September 197

The remainder of this introduction to the final report serves to identify the uplink study tasks, the methodology employed in the accomplishment of these tasks, and the organization of this final report document.

1.1 OBJECTIVES OF STUDY

The objectives of the uplink signal study were directed by the following task statements taken from the amended Statement of Work for the Signal Design Study for Shuttle/TDRSS Uplink.

Task 1: Assessment of Baseline Signal Design for TDRSS/Orbiter Uplink. Evaluation and assessment of the adequacy of the signal design approach chosen for the TDRSS/Orbiter Uplink. Critical functions and/or components associated with the baseline design shall be identified, and design alternatives shall be developed for those areas considered high risk.

Task 2: Development of Performance Specifications for TDRSS/Orbiter Ku-Band Uplink. Development of a detailed set of RF and signal processing performance specifications for the Orbiter hardware associated with the TDRSS/Orbiter Ku-band Uplink. Any changes to existing TDRSS performance specifications, as supplied by NASA, which appear reasonable and desirable shall be identified and definitized.

Task 3: Detailed Design and Parameter Optimization. Performance of a detailed design of the PN despreader, the PSK carrier synchronization loop, and the symbol synchronizer. Critical parameters shall be identified and optimized.

Task 4: Performance Evaluation of the Downlink Signal. *Performance evaluation of the downlink signal (Modes 1 and 2) by means of computer simulation to obtain a realistic determination of BER degradations.*

Task 5: Analytical Performance Evaluation of the Three-Channel PM Downlink Signal Structure (3-Channel Interplex). *Evaluation of the three-channel PM downlink signal by means of analysis and computer simulation.*

1.2 METHODOLOGY

To the extent possible this final report investigates various alternative approaches to the K-band Orbiter Receiver Design. In many cases a particular implementation is recommended for its commonality with the S-band approach. This is for obvious reasons of low risk and associated cost. This is particularly true in the detailed design of Task 3 and is reflected also in the parameters of the Orbiter Receiver Specification (Task 2). Apart from this consideration every effort was made during the study to maintain an "open mind" to the advantages of other techniques and to consider as far as possible the ramifications of these techniques.

1.3 ORGANIZATION OF FINAL REPORT

The introduction of the final report is followed by a summary of results and recommendations contained in Section 2 which is a concise overview of the basic conclusions achieved during the study. Section 2 concludes with a list of summary recommendations and rationale.

Sections 3 through 5 treat in order: the assessment of uplink signal design (Task 1), the development of performance specifications (Task 2), the detailed receiver design and parameter optimization (Task 3). Performance evaluation of the downlink signal (Task 4), and the analytical simulation of the three-channel downlink "interplex" signal (Task 5) is covered in Section 6.

This final report contains two appendices which complement the analytical aspects of Sections 5 and 6. Appendix A discusses the noncoherent AGC performance of the Ku-band Orbiter receiver. Appendix B treats intermodulation distortion in the Ku-band Shuttle mode 2 return link.

2. SUMMARY

2. SUMMARY

A summary of results and recommendations yields a concise overview of the basic conclusions achieved during the TDRSS/Orbiter Uplink Signal Design Study. Wherever possible, figures and tables illustrate the major points of this summary section.

An analytical tool finding continual use during the uplink study was the LINK computer simulation program. Use of the program allowed a realistic determination of bit error rate (BER) degradations for the forward link (Task 1) and the various downlink modes (Tasks 4 and 5). All of the resulting Ku-band communication link power budgets are summarized in Figure 2-1. Sources for the various items in each budget refer to the Rockwell RFP and the TRW proposal, references [28] and [3], respectively.

The uplink signal design assessment incorporates the best estimates presently available for the calculation of the Shuttle/TDRSS Ku-band uplink power budget, Orbiter G/T, system noise temperature, and link margin for the revised uplink signal (216 kbps PSK). These calculations indicate that the overall uplink circuit margin is approximately equal to the value of G/T. Ultimate results are given parametrically for different values of RF line loss and for two values of preamp gain and noise figure typical of those with and without a paramp. The basic conclusion of these calculations indicate that the paramp is not required to obtain high values of G/T. Error correction coding, similarly, is not required.

The forward link margin based on BER degradations from the referenced sources is 8.5 dB. Using the 2.4 dB BER degradation obtained by simulation of the LINK computer program, the forward link margin increases from 8.5 to 10.3 dB. Note that these comfortable margins are obtained without use of a paramp preamplifier.

Return link Mode 1 margins are 19.2, 15.0, and 7.0 dB for Channels 1, 2, and 3 respectively. For all the variable bit rate channels the highest bit rate and lowest bit error probability specified were used to determine worst-case margins. The margin on Channel 3 is sufficiently high (7.0 dB) so that the data rate could be increased from 50 Mbps to 60 or 70 Mbps with

A MARGIN SUMMARY

LINK	RFP REQUIRED MARGIN	MARGIN PROVIDED
FORWARD LINK	3 dB	8.5 dB (10.3 dB USING EXPECTED RATHER THAN SPECIFIED DEGRADATIONS)
RETURN LINK		
MODE 1		
CHANNEL 1	3 dB (GOAL)	19.2 dB
CHANNEL 2	3 dB (GOAL)	15.0 dB
CHANNEL 3	3 dB (GOAL)	7.0 dB
MODE 2		
3 CHANNEL CONFIGURATION		
CHANNEL 1	-	13.6 dB
CHANNEL 2	-	10.3 dB
CHANNEL 3		
ANALOG	-	8.9 dB
DIGITAL	-	13.6 dB
2 CHANNEL CONFIGURATION		
PM CHANNEL	-	13.6 dB
WIDEBAND CHANNEL		
ANALOG	-	8.9 dB
DIGITAL	-	13.6 dB

B FORWARD LINK

ITEM	VALUE	SOURCE
TDPS EIRP	48.0 dBw	PS 70.2.2.2.1F [12]
SPACE LOSS	-207.7 dB	PS 70.2.2.2.2A [12]
ANTENNA POLARIZATION LOSS	-0.1 dB	[3]
ANTENNA POINTING LOSS	-0.1 dB	[3]
RECEIVED SIGNAL POWER	-159.9 dBw	CALCULATION
RECEIVE ANTENNA GAIN	39.7 dBi	[3]
RECEIVER RF LINE LOSS (INCLUDED IN T_S)	-1.3 dB	[3]
SYSTEM NOISE TEMPERATURE, T_s	31.9 dB-K	[3]
ORBITER G/T	7.8 dB/K	[3]
BOLTZMANN'S CONSTANT	-228.6 dBw/Hz-K	-
P_{REC}/N_o	76.5 dB-Hz	CALCULATION
INFORMATION BIT RATE	53.3 dB-Hz	216 KBPS
E_b/N_o	23.2 dB	CALCULATION
RECEIVER DEGRADATION	[2.4 dB]	STUDY
BIT SYNC	-1.5 dB	PS 70.2.2.2.3C [28]
SPREAD SPECTRUM	-1.5 dB	PS 70.2.2.2.3G [28]
DEMODULATION LOSS	-0.7 dB	[3]
FILTERING LOSS	-0.5 dB	[3]
REQUIRED E_b/N_o	10.5 dB	PS 3.2.1.2.2.1.2.1J [28]
MARGIN	8.5 dB	CALCULATION
	[10.3 dB]	STUDY

C RETURN LINK - MODE 1

ITEM	VALUE	SOURCE
ORBITER TRANSMIT POWER	19.5 dBw	[3]
TRANSMIT CIRCUIT LOSS	-1.6 dB	[3]
TRANSMIT ANTENNA GAIN	40.3 dBi	[3]
ORBITER EIRP	58.2 dBw	[3]
ANTENNA POINTING LOSS	-0.1 dB	[3]
ANTENNA POLARIZATION LOSS	-0.1 dB	[3]
SPACE LOSS	-208.5 dB	PS 70.2.3.2A [28]
TDRS RECEIVER G/T	24.1 dB/K	PS 70.2.3.1A [28]
BOLTZMANN'S CONSTANT	-228.6 dBw/Hz-K	-
P_{REC}/N_o	102.2 dB-Hz	CALCULATION
TDRS TRANSPONDER LOSS	-2.0 dB	PS 70.2.3.1B [28]
TDRS AUTOTRACK LOSS	-1.0 dB	PS 70.2.3.1C [28]
DEMODULATION LOSS	-1.0 dB	PS 70.2.3.1D [28]
EFFECTIVE P_{REC}/N_o	98.2 dB-Hz	CALCULATION

ITEM	CHANNEL 1	CHANNEL 2	CHANNEL 3			SOURCE
MODULATION LOSS	-14 dB	-8 dB	-1 dB	-1 dB	-1 dB	RFP AMENDMENT 1 [28]
DATA RATE (MBPS)	0.192	2.0	50.0	30.0	10.0	-
DATA RATE (dB-Hz)	52.8	63.0	77.0	74.8	70.0	-
E_b/N_o (dB)	31.4	27.2	20.2	22.4	27.2	CALCULATION
BAND LIMITING EFFECT (dB)	0.0	0.0	-0.7	-0.3	0.0	PS TABLE XXVIII [28]
BIT SYNC DEGRADATION (dB)	-2.0	-2.0	-3.5	-3.0	-2.5	PS TABLE XXVIII [28]
OTHER LOSSES (dB)	-1.8	-1.8	-2.5	-2.1	-1.9	STUDY
BEP	10^{-4}	10^{-4}	10^{-6}	10^{-6}	10^{-6}	-
CODING GAIN (dB)	N/A	N/A	4.0	4.0	4.0	PS TABLE XXVIII [28]
REQUIRED E_b/N_o (dB)	8.4	8.4	10.5	10.5	10.5	-
CIRCUIT MARGIN (dB)	19.2	15.0	7.0	10.5	16.3	CALCULATION

D RETURN L

ITEM
FM IMPROVEMENT
FM DISCRIMINATO DEGRADATION (dB
MODULATION LO:
QPSK DEMODULAT LOSS (dB)
POST DETECTION
SNR OF INPUT DAT
SIGNAL TO IM RAT
COMBINED SNR (d
BANDPASS FILTERIN LOSS (dB)
TV INTERFERENCE
SUBCARRIER INTERF
BIT SYNC DEGRADATION (d
SNR (dB)
BEP
REQUIRED SNR (dB)
DATA MARGIN (dB)
CIRCUIT MARGIN

D RETURN LINK - MODE 2

ITEM	VALUE	SOURCE
ORBITER TRANSMIT POWER	19.5 dBw	[3]
TRANSMIT CIRCUIT LOSS	-1.6 dB	[3]
TRANSMIT ANTENNA GAIN	40.3 dBi	[3]
ORBITER EIRP	58.2 dBw	[3]
ANTENNA POINTING LOSS	-0.1 dB	[3]
ANTENNA POLARIZATION LOSS	-0.1 dB	[3]
SPACE LOSS	-208.5 dB	PS 70.2.3.2A [28]
TDRS RECEIVE G/T	24.1 dB/K	PS 70.2.3.1A [28]
BOLTZMANN'S CONSTANT	-228.6 dBw/Hz-K	-
TDRS P_{REC}/N_o	102.2 dB-Hz	CALCULATION
TDRS TRANSPONDER LOSS	-2.0 dB	PS 70.2.3.1B [28]
TDRS AUTOTRACK LOSS	-1.0 dB	PS 70.2.3.1C [28]
EFFECTIVE P_{REC}/N_o	99.2 dB-Hz	CALCULATION
PREDETECTION BW	75.6 dB-Hz	PS 70.2.3.3.3.3A[28]
SNR AT DISCRIMINATOR INPUT	23.6 dB	CALCULATION
FM THRESHOLD	10 dB	PS 70.2.3.3.3.3B [28]
FM THRESHOLD MARGIN	13.6 dB	CALCULATION

ITEM	CHANNEL 1 (192 KBPS)	CHANNEL 2 (≤ 2 MBPS)	CHANNEL 3 ANALOG OR DIGITAL		SOURCE
FM IMPROVEMENT (dB)	16.7	6.5	23.8	23.8	CALCULATION PS 70.2.3.3.3.1.2C [28]
FM DISCRIMINATOR DEGRADATION (dB)	-1.0	-1.0	-1.0	-1.0	PS 70.2.3.3.3.1.1C [28]
MODULATION LOSS (dB)	-7.0	-1.0	N/A	N/A	PS 70.2.3.3.3.1.1B [28]
QPSK DEMODULATION LOSS (dB)	-1.0	-1.0	N/A	N/A	PS 70.2.3.3.3.1.1A [28]
POST DETECTION SNR (dB)	31.3	27.1	46.4 $(\frac{rms}{rms})$	46.4	CALCULATION
SNR OF INPUT DATA (dB)	35.0	35.0	45.0 $(\frac{P-P}{rms})$	35.0	PS 3.2.1.2.3.3.1 [28]
SIGNAL TO IM RATIO (dB)	41.0	31.1	>60.0 $(\frac{P-P}{rms})$	41.1	STUDY
COMBINED SNR (dB)	29.4	25.2	44.5 $(\frac{P-P}{rms})$	33.8	CALCULATION
BANDPASS FILTERING LOSS (dB)	-0.4	-0.4	-0.1	-0.6	STUDY [28]
TV INTERFERENCE (dB)	-2.0	-2.0	N/A	N/A	PS 70.2.3.3.3.1.1D [28]
SUBCARRIER INTERFERENCE	N/A	N/A	-0.5	-0.5	STUDY
BIT SYNC DEGRADATION (dB)	-1.5	-2.0	N/A	-2.0	PS 70.2.3.3.3.1.1.E [28]
SNR (dB)	25.5	20.8	43.9	30.7	CALCULATION
BEP	10^{-6}	10^{-6}	N/A	10^{-6}	-
REQUIRED SNR (dB)	10.5	10.5	35.0 $(\frac{P-P}{rms})$	10.5	-
DATA MARGIN (dB)	15.0	18.3	8.9	20.2	CALCULATION
CIRCUIT MARGIN (dB)	13.6*	10.3	8.9	13.6*	CALCULATION

ITEM	8.5 MHz SCO CHANNEL	WIDEBAND CHANNEL ANALOG OR DIGITAL		SOURCE
POST DETECTION SUB-CARRIER/N_o (dB)	93.2	N/A	N/A	CALCULATION
FM IMPROVEMENT (dB)	N/A	23.8	23.8	CALCULATION PS70.2.3.3.31.2C**
FM DISCRIMINATOR DEGRADATION (dB)	-1.0	-1.0	-1.0	PS 70.2.3.3.3.1.2C**
DATA RATE (dB)	42.0	N/A	N/A	PS 70.2.3.3.3.1.1C**
POST DETECTION SNR (dB)	50.2	46.4 $(\frac{rms}{rms})$	46.4	CALCULATION
SNR OF INPUT DATA (dB)	35.0	45.0 $(\frac{P-P}{rms})$	35.0	PS 3.2.1.2.3.3.1 [28]
SIGNAL TO IM RATIO (dB)	48.0	60.0 $(\frac{P-P}{rms})$	41.1	STUDY
COMBINED SNR (dB)	34.7	44.5 $(\frac{P-P}{rms})$	33.8	CALCULATION
MODULATION LOSS (dB)	3.3	N/A	N/A	CALCULATION
PM DEMODULATION DEGRADATION (dB)	-1.0	N/A	N/A	PS 70.2.3.3 3.2 1d[28]
BANDPASS FILTERING LOSS (dB)	-0.2	-0.1	-0.6	STUDY
TV INTERFERENCE (dB)	-2.0	N/A	N/A	PS 70.2.3 3 3.1.1d[28]
SUBCARRIER INTERFERENCE	N/A	-0.5	-0.5	STUDY
BIT SYNC DEGRADATION (dB)	-1.5	N/A	-2.0	PS 70.2.3 3.3 1.1e[28]
SNR (dB)	26.7	43.9	30.7	CALCULATION
BEP	10^{-6}	N/A	10^{-6}	-
REQUIRED SNR (dB)	10.5	35.0 $(\frac{P-P}{rms})$	10.5	-
DATA MARGIN (dB)	16.2	8.9	20.2	CALCULATION
CIRCUIT MARGIN (dB)	13.6*	8.9	13.6*	CALCULATION

*CIRCUIT MARGIN IS CONSTRAINED BY FM THRESHOLD MARGIN **[28]

Figure 2-1. Link Power Budget Summaries

A SPREAD SPECTRUM PROCESSOR REQUIREMENTS vs CAPABILITIES

PS PARA.NO.	REQUIREMENT		CAPABILITY
3.2.1.2.2.2.2	PN CODE RATE	11.232 MEGACHIPS/SEC	11.232 MEGACHIPS/SEC
3.2.1.2.2.2.2	PN CODE LENGTH	2047	2047
70.2.2.1.1	PN CODE MODULATION	NRZ-L PSK	NRZ-L PSK
3.2.1.2.2.2.1.1	DATA RATE	216 KBPS	216 KBPS
3.2.1.2.2.2.1.1	DATA MODULATION	MANCHESTER II, BIPHASE L	MANCHESTER II, BIPHASE L
3.2.1.2.2.1.2.1	PN CODE ACQUISITION TIME	≤10 SEC	1.6 SEC
3.2.1.2.2.1.2.1	SPECIFIED SIGNAL LEVEL	-102 dBm*	3.8 dB MARGIN (FIG.C)
20.3.2.1.2.2.1.6.3**	DETECTION PROBABILITY	0.99	> 0.99
20.3.2.1.2.2.1.6.3**	FALSE ALARM PROBABILITY	10^{-6}	$< 10^{-6}$
3.2.1.2.1.2.2.C	CODE DOPPLER	± 400 Hz	± 400 Hz
3.2.1.2.1.2.2.A, B	IF FREQUENCY UNCERTAINTY	±1.0 MHz + RCVR LO VAR	± 1.1 MHz (0.1MHz FOR RCVR LO)
70.2.2.2.3	BER DEGRADATION	≤1.5 dB	0.4 dB AT 10^{-6} BER

*REFERED TO 34.6 dBi RECEIVE ANTENNA
**RFP AMENDMENT NO 1, CHANGE 5

B TWO BANDPASS FILTERS USED TO ACCOMMODATE TOTAL 2.2 MHz FREQUENCY UNCERTAINTY

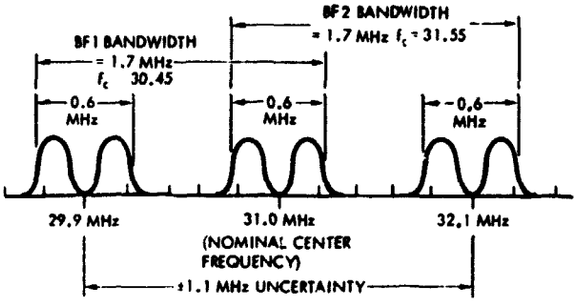

C 3 dB MINIMUM MARGIN AT DESIGN-POINT CARRIER-TO-NOISE DENSITIES

MINIMUM SIGNAL LEVEL FOR 10 SEC ACQUISITION (PS 3.2.1.2.2.1.2.1)	MINIMUM TDRS EIRP FOR ACQUISITION (RFP AMENDMENT NO. 1, CHANGES)
-102.0 dBm AT OUTPUT OF 34.6 dBi ANTENNA	36.6 dBw TDRS EIRP
+ 5.1 dB ΔGAIN OF 39.7 dBi ANTENNA	-207.7 dB SPACE LOSS
31.9 dB-°K SYSTEM NOISE TEMPERATURE (1549°K)	7.8 dB/°K G/T
-166.7 dBm/Hz N_o	-0.2 dB POLARIZATION AND TRACKING LOSS
69.8 dB-Hz C/N_o	65.1 dB-Hz C/N_o
66.0 dB-Hz DESIGN POINT	62.1 dB-Hz DESIGN POINT
3.8 dB MARGIN	3.0 dB MARGIN

D DWELL TIME vs P_{FA}

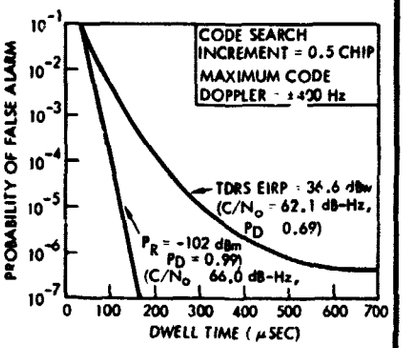

E MEASURED BER DEGRADATION

BER	MEASURED DEGRADATION (dB)
10^{-2}	0.6
10^{-3}	0.5
10^{-4}	0.4
10^{-5}	0.4

F SUMMARY OF KEY SSP DESIGN PARAMETERS

PARAMETER	RECEIVED SIGNAL -102 dBm	TDRS EIRP = 36.6 dBw	NOTES
CODE ACQUISITION TIME	1.6 SEC	7.2 SEC	>3 dB MARGIN
CODE PHASE ACQUISITION DWELL TIME	154.5 μSEC	154.5 μSEC	P_D 0.99 P_{FA} .999999 .0
CODE PHASE TRACKING DWELL TIME	309 μSEC	309 μSEC	
ACQUISITION PREDETECTION BANDWIDTH	1.7 MHz	1.7 MHz	DOPPLER FREQUENCY SEARCH
TRACKING PREDETECTION BANDWIDTH	4.6 MHz	4.6 MHz	
PROBABILITY OF LOSS OF LOCK	<0.0001	<0.01	DURING 100 MIN. TRANSMISSION
TRACKING LOOP BANDWIDTH (ACQUISITION)	400 Hz	400 Hz	
TRACKING LOOP BANDWIDTH (TRACKING)	6 Hz	7 Hz	
PULL-IN TIME	17 MSEC	20 MSEC	4 LOOP TIME CONSTANTS
DAMPING RATIO	0.707	0.77	
TRACKING LOOP LAG (WORST CASE)	0.007 CHIP	0.008 CHIP	
RMS TRACKING ERROR	0.04 CHIP	0.05 CHIP	
BEP DEGRADATION	<0.7 dB	<0.7 dB	WITH MAXIMUM DOPPLER

ure 2-2. Spread Spectrum Processor Design and Performance Summary

adequate margin. Alternatively, a 3.0 dB margin would be available without the 4 dB coding gain resulting from convolutional coding.

Return link Mode 2 margins vary from 8.9 to 13.6 dB. The margin for some channels is determined by the FM threshold margin of 13.6 dB rather than data margins. The typical signal (16 kbps PSK modulated on a 1.025 MHz sinusoidal signal) described in [28] Volume II, Paragraph 70.2.3.3.3.2.1, was used in determining circuit margin for the 8.5 MHz SCO channel of the two channel configuration.

As expected, the revised signal allows a great degree of commonality with the S-band receiver. Results (see Section 5.3) indicate that the same carrier recovery/demodulator approach (Costas loop) yields good performance, having a relatively fast acquisition time and low tracking errors.

A primary advantage of the revised uplink signal (216 kbps PSK) is that it allows the use of the SCTE NSP bit synchronizer without modification for the Ku-band Orbiter receiver bit synchronizer. The times required for bit synchronization for the higher SNR values in the Ku-band application are well within one second (see Section 5.4).

Greatly improved performance of the PN despreader, treated in detail in Section 5.2, was obtained for the revised uplink signal structure. Specifically, the improvements are in the areas of a faster code acquisition, allowed by the lower dwell times, and better threshold identification between signal plus noise and noise only. Brief summaries of design and performance for the despreader, carrier recovery loop, and bit synchronizer are presented below.

The requirements and capabilities of the Ku-band Orbiter receiver spread spectrum processor (SSP) are listed in Figure 2-2a.

The parameters having the most significant design impact on the despreader are required acquisition time, IF frequency uncertainty, code doppler, and the received signal power. The optimum acquisition bandwidth (with no frequency uncertainties) is approximately 70 percent of the null-to-null bandwidth or 0.6 MHz. Because of the large frequency uncertainties (1.1 MHz total), the required bandwidth for a conventional despreader would be 2.8 MHz resulting in a much lower SNR than the 0.6 MHz bandwidth.

Significant improvements in both margin and acquisition time result if the total bandwidth is divided in half with each filter (1.7 MHz bandwidth) covering one half the frequency uncertainty (see Figure 2-2b). The acquisition then consists of a check of all code positions with one filter and then with the other filter. The filters are switched after each complete search of all code positions, in addition to filter bandwidth changes. The code phase dwell times are reduced by a factor of 4 from SCTE; otherwise the KRCE spread spectrum processor (SSP) is identical to the SCTE SSP.

Acquisition time is largely determined by the code phase dwell time consistent with the P_D (0.99), and P_{FA} and the C/N_0 available for acquisition. The P_{FA} for -102 dBm is 10^{-6}. At the lower level for 36.6 dBW TDRS acquisition the false alarm rate will be somewhat higher than 10^{-6}. The only penalty resulting from this higher false alarm rate is the slight added time required for the despreader to reject erroneous code locks. For the false alarm rate provided, this time is negligible as discussed in Section 5.2. Design point carrier-to-noise densities are derived in Figure 2-2c showing at least a 3 dB margin. A plot of allowable dwell time versus P_{FA} for design values of C/N_0 and detection probability is shown in Figure 2-2d. All significant losses and degradations are included. A dwell time of 155 μsec has been chosen. For a P_D = 0.99 one complete search is required at 66.0 dB-Hz and four complete searches at C/N_0 = 62.1 dB-Hz.

Code acquisition time is computed for an overall 99 percent probability, with sufficient time allocated for the active code search plus time penalties caused by false alarms. Acquisition times for the design point carrier-to-noise densities of Figure 2-2c are 1.6 and 7.2 seconds at 66.0 and 62.1 dB-Hz, respectively.

After indication of code acquisition, the despreader switches to the track mode. During tracking the threshold is lowered to increase P_D to 0.999999999 so that the probability of loss of lock during a 100 minute transmission is $\leq$0.01. This approach at the 62.1 dB-Hz level (which corresponds to minimum acquisition TDRS EIRP of 36.6 dBW) yields a P_D = 0.999999999 and a $P_{FA} = 10^{-10}$ for each threshold check.

The SSP has capability to obtain code sync at significantly lower received signal levels than the abcve design points. Its measured bit error rate degradation is shown in Figure 2-2e. Allocation of key design parameters for the KRCE despreader are given in Figure 2-2f.

The carrier recovery loop parameters are indicated in Figure 2-3a and the tradeoff between loop bandwidth and acquisition time is shown in Figure 2-3b. This data shows that a loop bandwidth of at least 1 kHz is required if carrier acquisition is to occur within a time that is short relative to the one minute specification for total acquisition.

To reduce the carrier acquisition time, a 5 kHz loop bandwidth was selected. The $\pm$1.4 MHz sweep range was sized to accommodate the following factors: 500 kHz doppler, 500 kHz offset, 110 kHz receiver local oscillator offset, and 200 kHz allowance for variation in sweep circuitry.

The degradation due to phase noise for the 5 kHz loop bandwidth is shown in Figure 2-3c. The phase jitter estimates reflect both the front end thermal noise, that due to the VCXO, and the contribution of the VCO in the indirect X15 multiplier. In addition to the 0.1 dB degradation to bit error rate at nominal TDRS EIRP due to phase jitter, an additional 0.6 dB degradation is contributed by a static phase error of 17 degrees (current worst case SCTE estimate). This is due to phase shift differences in the signal paths to the Costas loop and the wideband data demodulator.

The KRCE bit synchronizer, identical to the SCTE unit, has demonstrated the capability of efficient operation at low signal-to-noise ratios, performing within 0.5 dB of theoretical at the forward link data rate of 216 kbps (Figure 2-4a). A summary of requirements and capabilities is shown in Figure 2-4b.

The key requirements for the bit synchronizer are a BER degradation of less than 1.0 dB and a capability of acquiring and tracking down to 0 dB signal-to-noise ratio. These requirements are met by an all-digital implementation to obtain accurate and stable matched filter detection and by employing a data transition tracking loop (DTTL) to allow the bit sync to operate at low values of signal-to-noise ratio.

A summary of the design values is given in Figure 2-4c for both acquisition and tracking. Mean acquisition times are plotted in Figure 2-4d for various values of SNR parametrically with transition density.

At the specified minimum of 0 dB SNR, the bit sync mean acquisition time is less than 0.7 seconds. For SNRs 5 dB below specification, acquisition time is only a few seconds and is relatively insensitive to transition density variations over a large range.

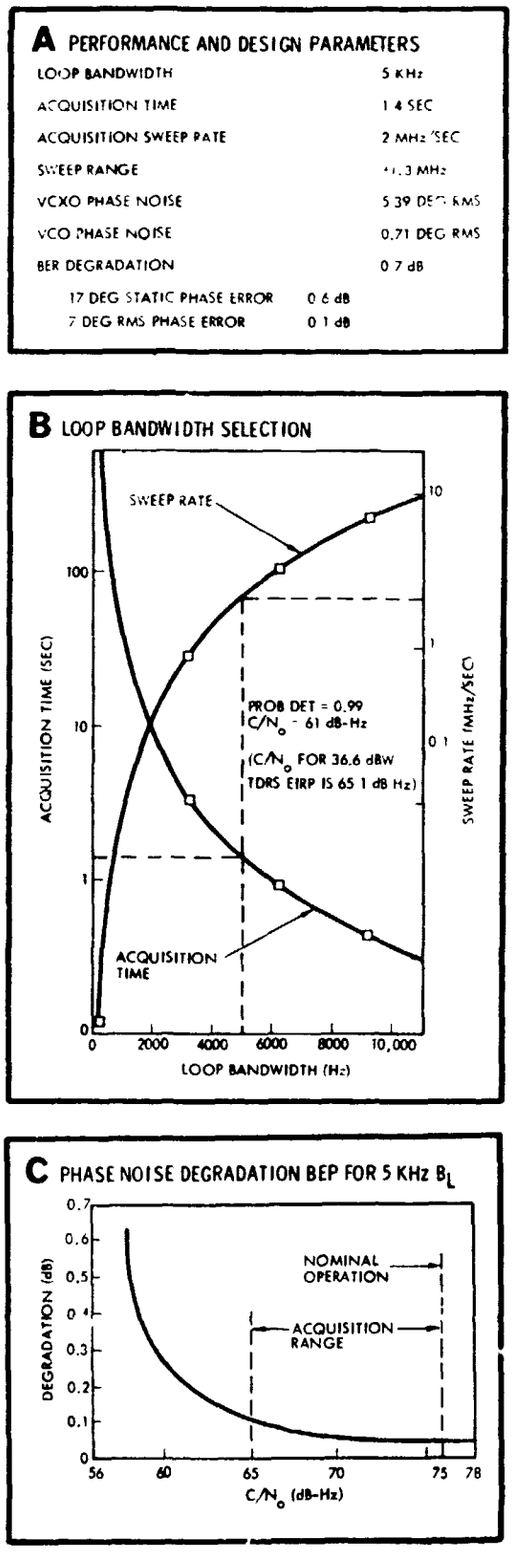

Figure 2-3. Carrier Recovery Loop Design and Performance Summary

A BIT SYNC BIT ERROR RATE IS WITHIN 0.5 dB OF THEORETICAL

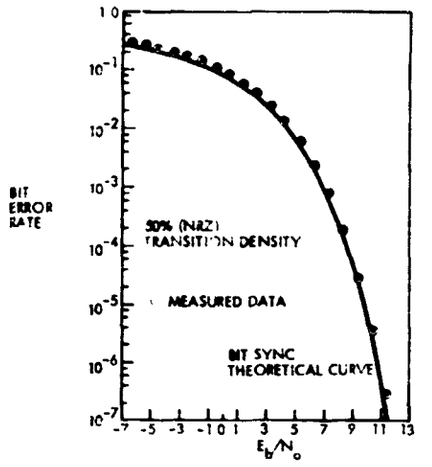

B SHUTTLE BIT SYNCHRONIZER REQUIREMENTS VERSUS CAPABILITIES

PARAGRAPH NO. (PS)	REQUIREMENT		CAPABILITY
7[illegible]2.1.1	INPUT CODE	MANCHESTER II, BIPHASE L	MANCHESTER II, BIPHASE L
10.3.2.1.2.1.2	BIT RATE	216 KBPS	216 KBPS
10.3.2.1.2.1.2	THRESHOLD SNR (E_b/N_o)	0 dB	< -5 dB
10.3.2.1.2.1.2	BER DEGRADATION	< 1 dB	0.5 dB
10.3.2.1.2.1.2.b	OUTPUT CODE	NRZ-L	NRZ-L
10.3.2.1.2.1.3	AMBIGUITY RESOLUTION	-	PROVIDED
NOT SPECIFIED	MEAN ACQUISITION TIME	-	< 0.7 SEC
10.3.2.1.2.1.3.a	LOCK INDICATION		PROVIDED

C DESIGN AND PERFORMANCE VALUES

$\frac{E_b}{N_o}$ (dB)	TRANSITION DENSITY (%)	LOOP BANDWIDTH B_L (Hz)	LOOP SNR (dB)	SYNC JITTER (%)	ACQ TIME (SEC)
0	50	80	36	<1.0	0.5
7	50	122	43	0.2	0.5

D MEAN ACQUISITION TIME AS A FUNCTION OF E_b/N_0

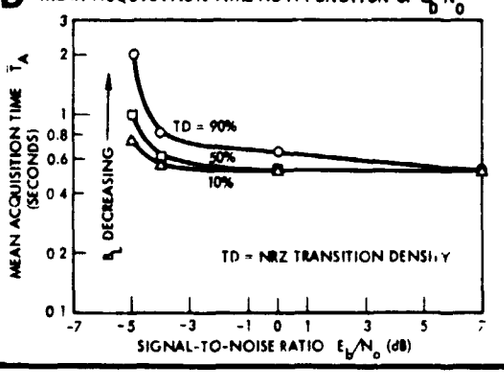

Figure 2-4. Bit and Frame Synchronizer Design and Performance Summary

The frame sync decoder acquires frame synchronization in an average of 9 milliseconds (four and one half frame periods). Thus, it is clear that the total time for bit and frame sync acquisition will be a few seconds, much less than the specified 10 second maximum. The frame sync decoder senses data polarity and inverts the data if required.

A complete Ku-Band Shuttle Orbiter Receiver Specification, developed during the Uplink Signal Design Study, comprises the bulk of Section 4. A brief list of TDRSS/Orbiter specification recommendations together with their rationale conclude Section 4. Specific recommendations concern ambiguities in the choice of return link center frequency and definition of the Mode 2 downlink signal.

3. ASSESSMENT OF UPLINK SIGNAL DESIGN (TASK 1)

Task 1 of the Signal Design Study for Shuttle/TDRSS Ku-Band Uplink is the assessment of the baseline design for the TDRSS/Orbiter uplink. Specifically Task 1 calls for the evaluation and assessment of the adequacy of the signal design approach chosen for the TDRSS/Orbiter uplink. Critical functions and/or components associated with the baseline design are to be identified, and design alternatives developed for those areas considered high risk. This section documents the work performed during the Ku-Band Uplink Signal Study in response to the above task definition.

3.1 UPLINK SIGNAL DESCRIPTION

The unbalanced QPSK modulation signal originally baselined for the Ku-band uplink specified a maximum channel rate of 3 Msps (coded) for the in-phase channel, operating with 80 percent of the available power, and 72 kbps in the quadrature channel with 20 percent of the total power. A requisite receiver must demodulate and detect this incoming quadriphase data. Code and carrier synchronization must first be provided to demodulate the two orthogonal biphase data streams which make up the quadriphase signal. Following demodulation, the baseband outputs must be filtered and sampled, and decisions must be made on the individual bits. Quadriphase demodulation requires the presence of a coherent carrier phase reference. Providing such a reference is difficult since there is no carrier component available to be tracked. A number of methods for performing the carrier recovery function were investigated early in this study and in related work at TRW. A satisfactory design solution was scoped as a relatively large-scale effort - particularly to obtain truly optimum performance for the variable high rate data channel.

The 72 kbps baseband data is forwarded directly from the QPSK demodulator to the S-band network signal processor. Bit synchronization of the 1 Mbps channel, however, must be performed in the Ku-band equipment. This is a non-trivival function for two reasons. First, a very low signal-to-noise ratio per channel symbol is implied due to the restricted TDRS EIRP and the rate 1/3 convolutional encoding.

Second, the 3 Msps symbol rate is relatively high making more optimum performance difficult to achieve in hardware sized within Orbiter constraints. Thus, symbol synchronizer design and performance analysis would have been a major task of this study.

Finally there would have remained the problem of high rate symbol stream. This is difficult only because the Orbiter constrains power and weight in the hardware. Total BER degradation of the decoder would take into account a number of small but significant effects arising from AGC action, carrier instability, and bit sync impact jitter.

Very early in the Ku-Band Uplink Signal Study a reevaluation by NASA of the variable, high-rate data channel led to the revision of the TDRSS/ Orbiter Ku-band uplink signal structure. The variable (1 Mbps) data channel was reduced to a fixed 144 kbps and time-division-multiple-accessed with the 72 kbps channel. Coding of the resultant 216 kbps PSK waveform was, for the purposes of this study, left as an open issue. In addition, the PN code rate of the spread spectrum uplink was reduced from 14.5 Megachips/sec to 11.234 Megachips/sec - the same as that used for the SCTE. A comparison of the original and revised versions of the Ku-band uplink signal is given in Table 3-1.

The attendant advantages allowed by the uplink signal revision in the Orbiter receiver design is discussed briefly in Section 3.5. The detailed design and parameter optimization of the PN despreader, PSK carrier synchronization loop, and bit synchronizer is contained in Section 5.

Table 3-1. Comparison of Original and Revised Ku-Band Uplink Signal Structure

Parameter	Original	Revised
Number of Data Channels	2	2
High Rate Channel	$\leq$1 Mbps	144 kbps
Low Rate Channel	72 kbps	72 kbps
Modulation/Access	QPSK/Phase Quadrature	PSK/TDMA
Coding	R = 1/3; K=7 Convolutional (High Rate Channel Only)	TBD
Power Division (High Rate/Low Rate)	80%/20%	
PN Code Rate	14.5 Megachips/sec	11.234 Megachips/sec

3.2 CCIR POWER FLUX DENSITY

A power flux density limitation at the earth's surface produced by emissions from any satellite, has been imposed by international agreement and is controlled by NASA specifications [1].

At Ku-band the power flux density at the earth's surface produced by emissions from a TDRS, for all methods of modulation, are not to exceed the following values:

a) -152 dBW/m^2 in any 4-kHz band for angles of arrival between 0 and 5 degrees above the horizontal plane.

b) $-152 + (\theta-5)/2$ dBW/m^2 in any 4-kHz band for angles of arrival θ (in degrees) between 5 and 25 degrees above the horizontal plane.

c) -142 dBW/m^2 in any 4-kHz band for angles of arrival between 25 and 90 degrees above the horizontal plane.

The required minimum spread bandwidth is defined as that bandwidth required to meet these flux density restrictions, assuming the peak signal EIRP is distributed evenly over that bandwidth. It can be assumed that the flux density restrictions are met if the RF bandwidth defined by the frequency separation between the first nulls of the envelope of the transmitted spectrum equals the required minimum spread bandwidth.

The PN code used to spread the uplink signal has an autocorrelation given by

$$R_{PN}(\tau) = \begin{cases} 1-\left(\frac{1+1/p}{\tau_c}\right)|\tau| & |\tau| \le \tau_c \\ -1/p & \tau_c \le |\tau| \le p\tau_c \end{cases} \qquad (3\text{-}1)$$

where p = period of the sequence (2047 chips)

τ_c = chip period ($1/11.232\times10^6$ sec)

and has a line power spectrum given by

$$S_{PN}(\omega) = \left[\left(\frac{p+1}{p^2}\right)\left(\frac{\sin \omega\tau_c/2}{\omega\tau_c/2}\right)^2 \sum_{\substack{n=-\infty \\ \neq 0}}^{\infty} S\left(\omega - \frac{2\pi n}{p\tau_c}\right)\right] + \frac{1}{p^2} S(\omega) \qquad (3\text{-}2)$$

In the present case the line spectrum of (3-2) may be approximated by the continuous power spectral density curve of Figure 3-1. The loss tabulation included in Figure 3-1 has proven useful in estimating filter bandlimiting degradations. The equivalent rectangular bandwidth of the filter should be used to properly estimate the loss from Figure 3-1. A similar spectrum plus bandlimiting loss table is provided in Figure 3-2 for manchester code.

Note that the uplink signal revision will impact the maximum EIRP allowable from the TDRS. A reduction in the PN spread spectrum code from 14.5 Megachips/sec to 11.232 Megachips/sec implies that the TDRS EIRP must be reduced by 1.11 dBW to ~48.0 dBW to maintain equivalent power flux density at the surface of the earth.

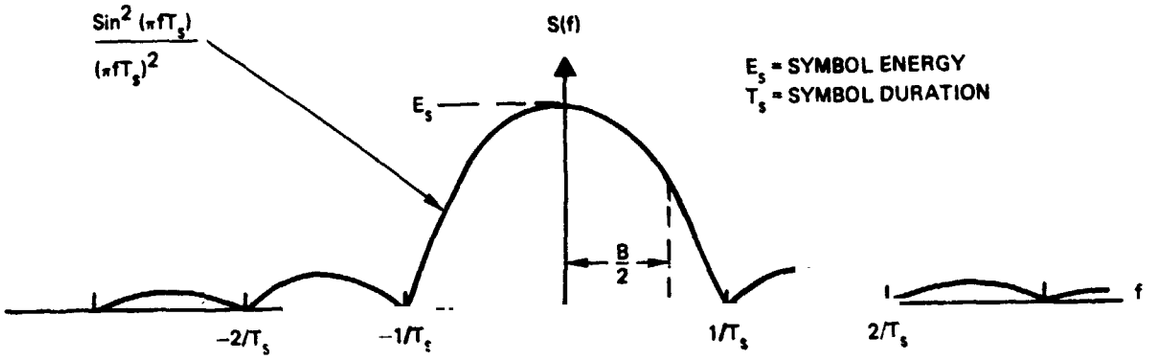

B/2 [1/T_S Hz]	0	1	2	3	4	5	6	7	8	9
0.0		57.84	48.81	43.53	39.78	36.88	34.51	32.51	30.77	29.25
0.1	27.88	26.65	25.52	24.49	23.54	22.65	21.82	21.05	20.32	19.63
0.2	18.98	18.36	17.77	17.21	16.68	16.17	15.68	15.21	14.76	14.33
0.3	13.91	13.51	13.12	12.75	12.39	12.04	11.70	11.38	11.06	10.75
0.4	10.46	10.17	9.89	9.62	9.36	9.10	8.86	8.61	8.38	8.15
0.5	7.93	7.71	7.51	7.30	7.10	6.91	6.72	6.54	6.36	6.18
0.6	6.01	5.85	5.69	5.53	5.38	5.23	5.09	4.94	4.81	4.67
0.7	4.54	4.41	4.29	4.17	4.05	3.94	3.83	3.72	3.61	3.51
0.8	3.41	3.31	3.22	3.13	3.04	2.95	2.86	2.78	2.70	2.62
0.9	2.55	2.48	2.40	2.34	2.27	2.20	2.14	2.08	2.02	1.96
1.0	1.91	1.85	1.80	1.75	1.70	1.66	1.61	1.57	1.52	1.48
1.1	1.44	1.41	1.37	1.33	1.30	1.27	1.24	1.21	1.18	1.15
1.2	1.12	1.10	1.07	1.05	1.03	1.01	0.99	0.97	0.95	0.93
1.3	0.92	0.90	0.89	0.87	0.86	0.84	0.83	0.82	0.81	0.80
1.4	0.79	0.78	0.77	0.77	0.76	0.75	0.74	0.74	0.73	0.73
1.5	0.72	0.72	0.71	0.71	0.71	0.70	0.70	0.70	0.70	0.69
1.6	0.69	0.69	0.69	0.69	0.69	0.68	0.68	0.68	0.68	0.68
1.7	0.68	0.68	0.68	0.68	0.68	0.68	0.68	0.68	0.68	0.68
1.8	0.68	0.68	0.68	0.68	0.68	0.68	0.68	0.68	0.68	0.68
1.9	0.68	0.68	0.68	0.68	0.68	0.68	0.68	0.68	0.68	0.68
2.0	0.68	0.68	0.68	0.68	0.68	0.68	0.68	0.68	0.68	0.68
2.1	0.68	0.68	0.68	0.68	0.68	0.68	0.68	0.68	0.68	0.68
2.2	0.68	0.68	0.68	0.68	0.68	0.68	0.68	0.68	0.68	0.67
2.3	0.67	0.67	0.67	0.67	0.67	0.67	0.67	0.67	0.67	0.67
2.4	0.67	0.67	0.67	0.67	0.66	0.66	0.66	0.66	0.66	0.66
2.5	0.66	0.65	0.65	0.65	0.65	0.65	0.65	0.64	0.64	0.64
2.6	0.64	0.63	0.63	0.63	0.62	0.62	0.62	0.62	0.61	0.61
2.7	0.61	0.60	0.60	0.59	0.59	0.59	0.58	0.58	0.57	0.57
2.8	0.57	0.56	0.56	0.55	0.55	0.54	0.54	0.54	0.53	0.53
2.9	0.52	0.52	0.51	0.51	0.50	0.50	0.50	0.49	0.49	0.48
3.0	0.48	0.47	0.47	0.47	0.46	0.46	0.45	0.45	0.44	0.44

Figure 3-1. Tabulation of Loss (in dB) Versus One-Sided Rectangular Bandwidth B/2 (1/T_S Hz) for Binary, NRZ Spectrum Encoding (NEP)

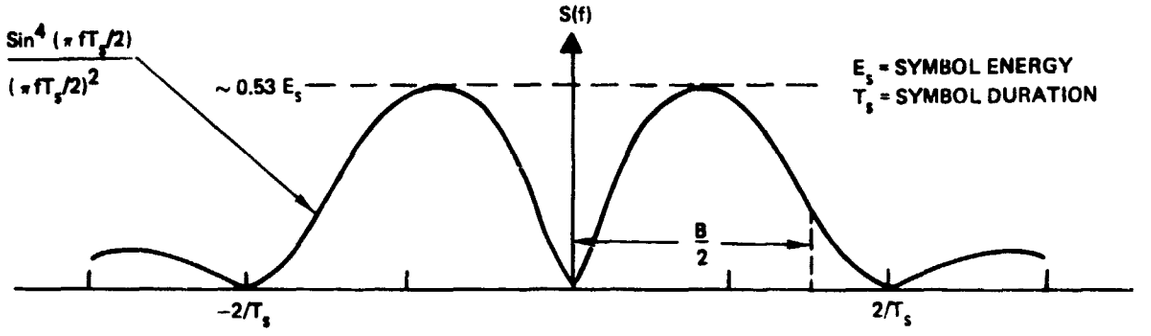

B/2 [$1/T_S$ Hz]	0	1	2	3	4	5	6	7	8	9
0.0		16.99	13.98	12.22	10.98	10.01	9.23	8.56	7.99	7.49
0.1	7.04	6.63	6.27	5.93	5.62	5.34	5.07	4.82	4.59	4.37
0.2	4.17	3.98	3.79	3.62	3.46	3.30	3.16	3.02	2.88	2.76
0.3	2.64	2.52	2.41	2.31	2.21	2.11	2.02	1.94	1.85	1.78
0.4	1.70	1.63	1.56	1.49	1.43	1.37	1.32	1.26	1.21	1.16
0.5	1.11	1.07	1.03	0.99	0.95	0.91	0.88	0.85	0.82	0.79
0.6	0.76	0.74	0.71	0.69	0.67	0.65	0.63	0.61	0.60	0.58
0.7	0.57	0.55	0.54	0.53	0.52	0.51	0.50	0.50	0.49	0.48
0.8	0.48	0.47	0.47	0.46	0.46	0.46	0.45	0.45	0.45	0.45
0.9	0.45	0.45	0.45	0.45	0.44	0.44	0.44	0.44	0.44	0.44
1.0	0.44	0.44	0.44	0.44	0.44	0.44	0.44	0.44	0.44	0.44
1.1	0.44	0.44	0.44	0.44	0.44	0.44	0.43	0.43	0.43	0.43
1.2	0.43	0.42	0.42	0.42	0.42	0.41	0.41	0.41	0.40	0.40
1.3	0.40	0.39	0.39	0.38	0.38	0.38	0.37	0.37	0.36	0.36
1.4	0.35	0.35	0.34	0.34	0.34	0.33	0.33	0.32	0.32	0.31
1.5	0.31	0.31	0.30	0.30	0.29	0.29	0.29	0.28	0.28	0.28
1.6	0.27	0.27	0.27	0.26	0.26	0.26	0.25	0.25	0.25	0.25
1.7	0.24	0.24	0.24	0.24	0.24	0.24	0.23	0.23	0.23	0.23
1.8	0.23	0.23	0.23	0.23	0.23	0.23	0.23	0.22	0.22	0.22
1.9	0.22	0.22	0.22	0.22	0.22	0.22	0.22	0.22	0.22	0.22
2.0	0.22	0.22	0.22	0.22	0.22	0.22	0.22	0.22	0.22	0.22
2.1	0.22	0.22	0.22	0.22	0.22	0.22	0.22	0.22	0.22	0.22
2.2	0.22	0.22	0.22	0.22	0.22	0.21	0.21	0.21	0.21	0.21
2.3	0.21	0.21	0.21	0.21	0.20	0.20	0.20	0.20	0.20	0.20
2.4	0.20	0.19	0.19	0.19	0.19	0.19	0.19	0.19	0.18	0.18
2.5	0.18	0.18	0.18	0.18	0.18	0.17	0.17	0.17	0.17	0.17
2.6	0.17	0.17	0.17	0.16	0.16	0.16	0.16	0.16	0.16	0.16
2.7	0.16	0.16	0.16	0.15	0.15	0.15	0.15	0.15	0.15	0.15
2.8	0.15	0.15	0.15	0.15	0.15	0.15	0.15	0.15	0.15	0.15
2.9	0.15	0.15	0.15	0.15	0.15	0.15	0.15	0.15	0.15	0.15
3.0	0.15	0.15	0.15	0.15	0.15	0.15	0.15	0.15	0.15	0.15

Figure 3-2. Tabulation of Loss (in dB) Versus One-Sided Rectangular Bandwidth B/2 ($1/T_S$ Hz) for Binary, Diphase Spectrum Encoding (NEP)

3.3 UPLINK POWER BUDGET

This section consists of a line-by-line discussion of the uplink power budget. A brief derivation together with the pertinent data source is given for each item.

CALCULATION OF SYSTEM NOISE TEMPERATURE, UPLINK POWER BUDGET, AND CIRCUIT MARGIN

- TDRSS EIRP . . . . . 48.0 dBW

  The TDRSS EIRP is based on a transmitter power of 0.87W (29.5 dBm), a transmission circuit loss of 2 dB, a transmit antenna gain of 52.0 dB, a 0.5 dB antenna pointing error loss, and a TDRSS satellite transponder loss of 1 dB. (Turnaround Noise)

  Source(s): Reference [2]
  STDN No. 101.2, Rev. 2 (TDRS Users Guide)
  Section 3.2

- SPACE LOSS . . . . . 207.7 dB

  f_o = 13.775 GHz; R = 22,786 nautical miles. The loss is calculated using

  $$L_{space} = (\lambda/4\pi R)^2 \cdot \begin{cases} \lambda = \dfrac{3 \times 10^8 \text{ meters/sec}}{13.775 \times 10^9 \text{ Hz}} = 0.021779\text{M} \\ R = 22{,}786 \times 1852 = 42199672\text{M} \end{cases}$$

  $$L_{space} = 20\,[\log \lambda - \log (4\pi R)] = -207.7 \text{ dB}$$

  Source(s): Reference [2]
  Above Calculation

- RECEIVE ANTENNA LOSSES . . . . . 0.2 dB

  This assumes antenna pointing and polarization losses of 0.1 dB and 0.1 dB, respectively.

  Source(s): Reference [3]

- TOTAL RECEIVED SIGNAL POWER . . . . -159.9 dBW
  (referenced to omni)

  Calculation - Sum of the above.

- RF CIRCUIT LOSSES (RECEIVER) . . . . 1.3 dB

COMPONENT	RECEIVE LOSSES (dB)
COMPARATOR	0.30
COUPLER (RCV TEST)	0.05
WAVEGUIDE (5 IN)	0.02
DIPLEXER	0.40
CIRCULATOR	-
GATED SWITCH LIMITED	0.30
WAVEGUIDE (18 IN)	0.08
BPF	-
WAVEGUIDE SWITCH	-
WAVEGUIDE (WB ANT)	-
COUPLER (TLM)	-
WAVEGUIDE (36 IN)	-
ISOLATOR (TWT)	-
VSWR	0.16
LOSS	1.3

Source(s): Reference [3]

• ORBITER G/T . . . . 7.8 dB/K

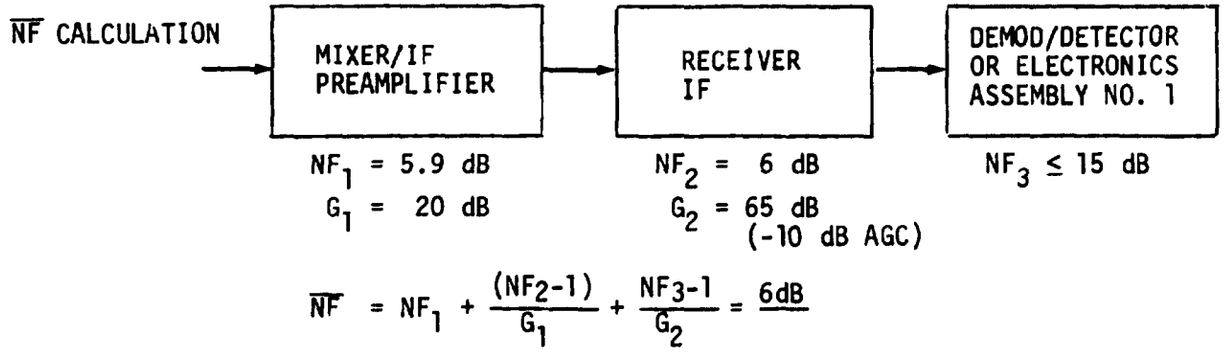

$$\overline{NF} = NF_1 + \frac{(NF_2-1)}{G_1} + \frac{NF_3-1}{G_2} = \underline{6dB}$$

PARAMETER	VALUE	COMMENTS
ANTENNA GAIN G	39.7 dBi	PEAK GAIN AT 13.775 MHz
EFFECTIVE RECEIVER SYSTEM NOISE TEMPERATURE (Te)		Te = $\overline{NF}$ · T_o ·(INTERNAL NOISE DOMINANCE)
$\overline{NF}$	6.0 dB	SEE RECEIVE SYSTEM NOISE FIGURE ($\overline{NF}$) CALCULATION ABOVE
T_o	24.6 dB-°K	290°K STANDARD TEMPERATURE
L	1.3 dB	SEE CIRCUIT LOSSES ABOVE
Te	31.9 dB-°K	1549°K
G/Te	7.8 dB/°K	

Source(s): Reference [3]

- CARRIER-TO-NOISE C/N_0 . . . . . 76.5 dB-Hz

  This is the received signal power (referenced to an omnidirectional antenna) = -129.9 dBm compared to Boltzmann's constant -198.6 dBm/Hz - °K, plus G/T.

- BER DEGRADATION BUDGET (RECEIVER) . . . . . 4.2 dB

  Based on the following estimates:

DESPREADER	.....	1.5 dB
CARRIER REC/DEMOD	.....	0.7 dB
BIT SYNCHRONIZER	.....	1.5 dB
FILTER LOSSES	.....	0.5 dB

  Source(s): Reference [2]

- INFORMATION BIT RATE (216 kbps) . . 53.3 dB

- SNR . . . . . 19.0 dB

- THEORETICAL E_b/N_0 REQUIRED FOR 10^{-6} BER PSK (UNCODED) . . . . . 10.5 dB

- CIRCUIT MARGIN . . . . . 8.5 dB

  [Note that margin $\approx$ G/T]

Table 3-2. Shuttle/TDRSS Uplink Power Budget

FREQUENCY	13.775 GHz
TDRS EIRP	48.0 dBW
SPACE LOSS (22,786 nmi)	207.7 dB
RAIN/ATMOSPHERIC LOSS	0.0 dB
RECEIVE ANTENNA LOSSES	0.2 dB
RECEIVED CARRIER POWER (REFERENCED TO OMNI)	-129.9 dBm
ORBITER KU-BAND ANTENNA GAIN	39.7 dBi
RECEIVER RF LOSSES, L_{RF}	1.3 dB
ORBITER G/T	7.8 dB/K
BOLTZMANN'S CONSTANT	-228.6 dBW/Hz - °K
RECEIVED CARRIER POWER-TO NOISE DENSITY RATIO C/N_o	76.5 dB-Hz
BER DEGRADATION (ESTIMATE)	4.2 dB
INFORMATION BIT RATE (216 kbps)	53.3 dB
SNR	19.0 dB
THEORETICAL E_b/N_o REQUIRED FOR 10^{-6} BER (UNCODED PSK)	10.5 dB
CIRCUIT MARGIN	8.5 dB

Table 3-2 shows a comfortable 8.5 dB margin without the use of a front-end paramp or error-correction coding. Section 3.3 will now investigate the BER degradation more realistically by using the "LINK" computer simulation program developed and successfully applied by TRW on past programs - most recently on TDRSS.

3.4 COMPUTER SIMULATION OF UPLINK SIGNAL

The interaction of the various degradation sources affecting BER in a link with a complex modulation structure limits the usefulness of conventional analytic techniques. In order to obtain accurate estimates of BER degradations for such links TRW has developed a simulation in which time waveforms are successively distorted by transfer functions representing each significant distortion element in the channel. This simulation has been run for numerous links with the resulting BER degradation confirmed by BER measurements on high data rate links [4,5]. Features of the simulation include:

- Allows performance evaluation of complex, flexible models
- Is particularly well-suited for evaluating the effect of each link component on the overall transponder performance and isolating major degradation contributors
- Evaluates the transient response of the link at any point desired.

The TRW "LINK" Simulation program was adapted to determine signal degradation for the Ku-band Shuttle uplink. The Western Union/TRW proposed TDRSS configuration was used in modeling the ground and TDRS portions of the link.

3.4.1 Model Description

Figure 3-3 is a basic system that can be analyzed using "LINK". The program allows the user to specify the type of input waveform (PSK, Manchester, or MSK), data rate, and input sequence parameters. Input sequences are maximal length shift register sequences of length 15, 31, or 63 bits. Filters are modeled as being ideal (Chebyshev or Butterworth), by specifying phase and magnitude as power series, or by specifying the amplitude and frequency of sinusoidal phase and gain ripples. Amplifiers are modeled as linear, hard or soft limiters or TWTA-type amplifiers. For TWTAs, the amplitude response is fit analytically in two portions - a linear region and a cosine region. Phase shift through the device is represented by a constant AM-to-PM conversion factor, a truncated power series or the Berman-Mahle model. The simulation also allows specification of a rms phase noise and a rms bit sync jitter.

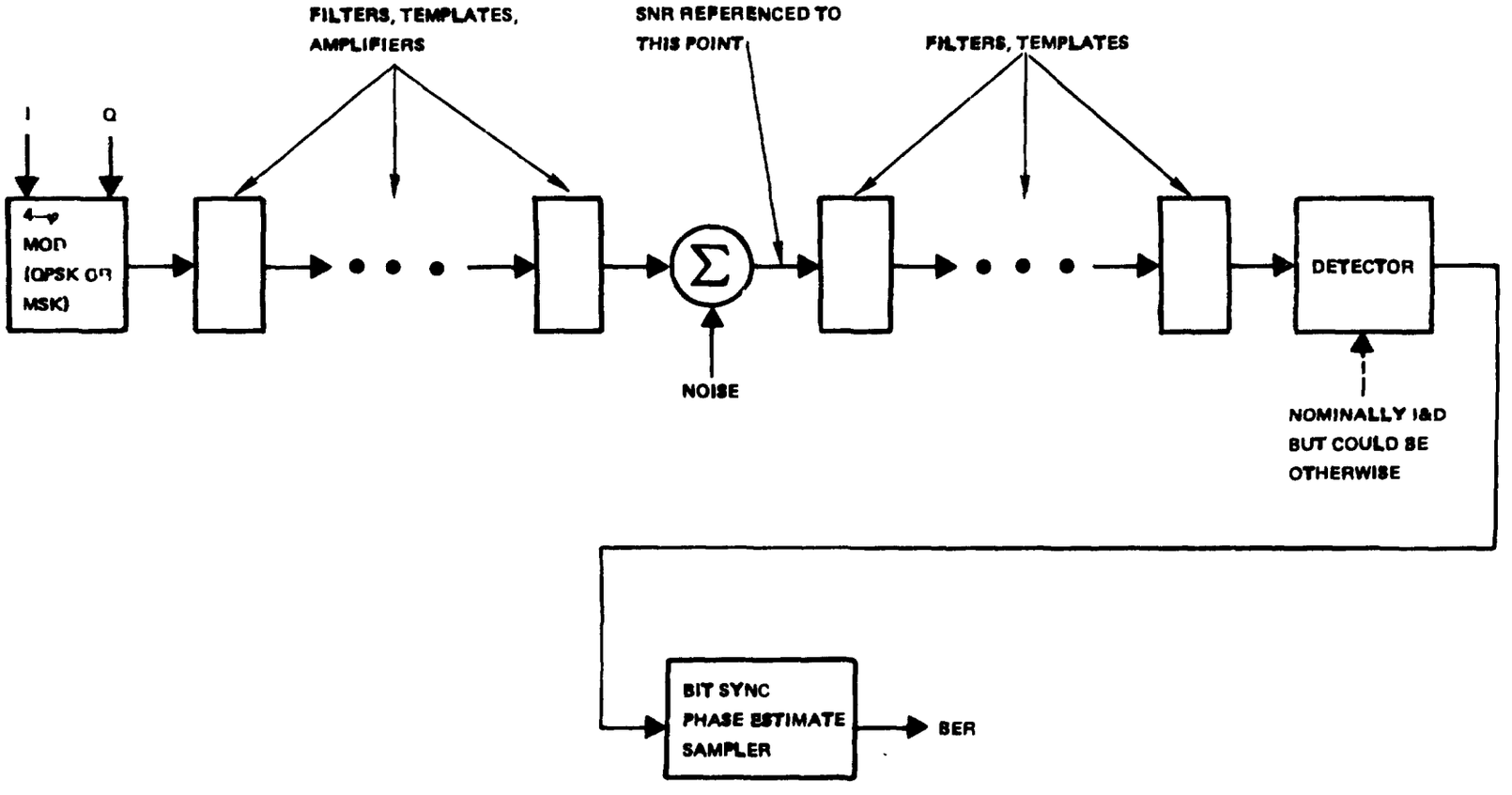

Figure 3-3. Basic Simulation Model

Bit synchronization and phase rotation are obtained by correlating the signal coming out of the channel with an undistorted signal. The bit error rate is determined for each bit in the sequence and then an average BER over all bits in each channel is calculated. The final output is a table of bit error rate and signal degradation versus signal-to-noise ratio. Plots of the signal waveform at various points in the system can also be obtained.

A recent modification to the program simulates the effects of a spread spectrum channel on the signal. This is done by spreading two data bits with a PN sequence, passing this signal through the channel up to the despreader and then despreading the signal by multiplying by the PN sequence. The resulting signal is a distorted two bit sequence caused by the spreading/despreading process. The resulting distorted bits are repeated until a data sequence of 31 bits is obtained and this signal is then passed through the part of the channel after the despreader.

Figure 3-4 is a block diagram of the elements modeled in for the simulation.

The ground station and TDRS are the models used for the Western Union/TRW proposed TDRS system. The model for the RF front end, IF/AGC, Shuttle spectrum despreader, demodulator carrier recovery loop and bit synchronizer were developed during this study with reference to [3].

3.4.2 Results of the Uplink Simulation

The results of the uplink computer simulation may be quickly stated. At the 10^{-6} BER design point a total BER degradation of 2.4 dB was observed by the computer model previously described in Section 3.4.1.

By varying the value of each of the parameters in the simulation model individually the sensitivity of the forward link performance to variation in that parameter can be found. The results of the parameter sensitivity analysis for the forward link are shown in Figure 3-5. Variation in parameters of devices prior to the spread spectrum processor over a

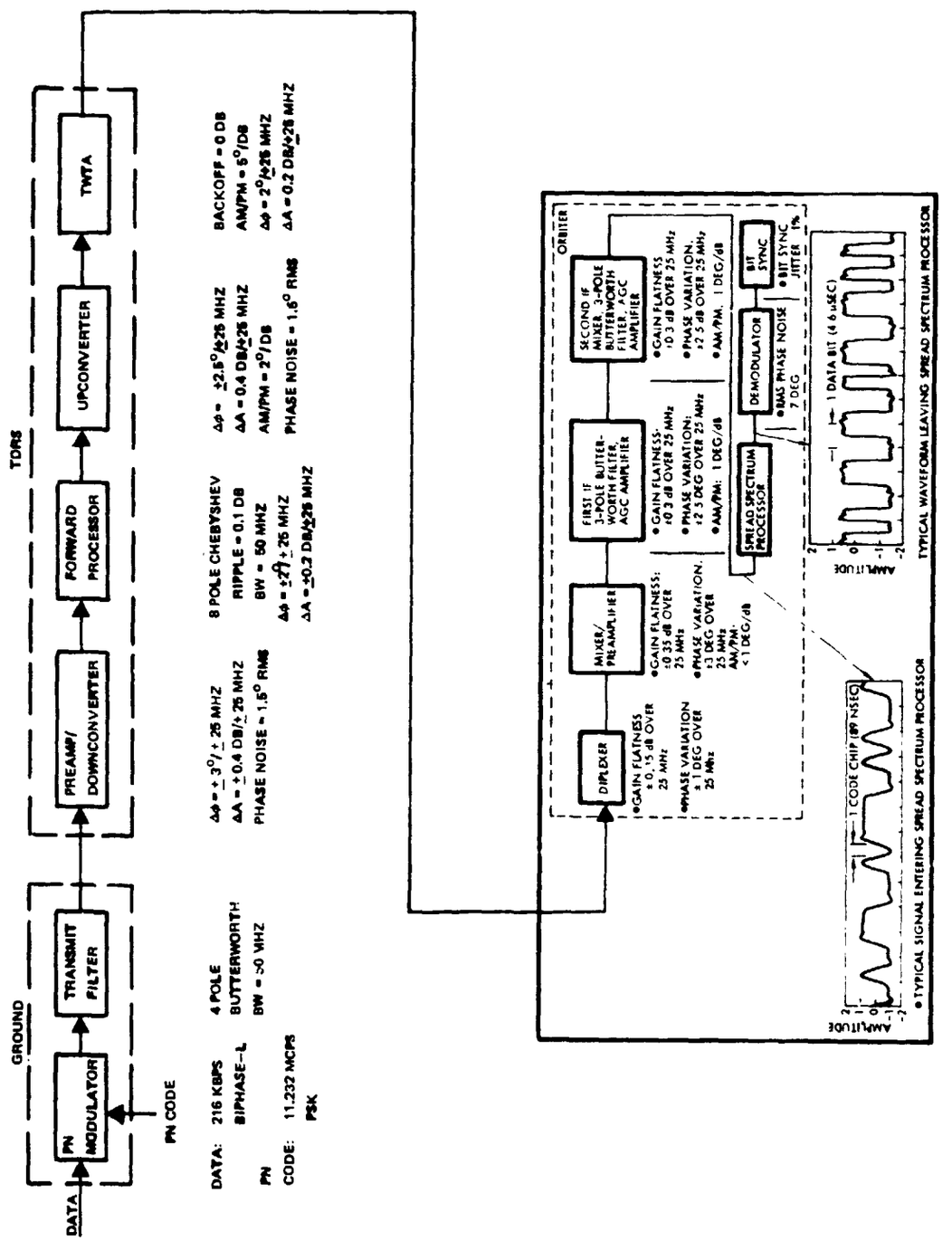

Figure 3-4. TDRSS/Shuttle Ku-Band Uplink Simulation Model

PARAMETER SENSITIVITY ANALYSIS

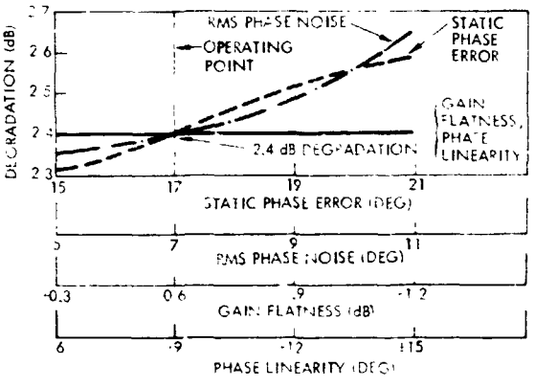

BER DEGRADATION BUDGET	DEGRADATION (dB)
FILTER ENERGY LOSS	0.4
SPREAD SPECTRUM WAVEFORM DISTORTION	0.2
SPREAD SPECTRUM PROCESSOR CODE MISALIGNMENT	0.6
PHASE NOISE	0.1
DEMODULATOR STATIC PHASE ERROR	0.6
BIT SYNC JITTER	0.5
	2.4

Figure 3-5. Parameter Sensitivity Analysis Results and BER Degradation Budget Summary for Forward Link

wide range were found to have little effect on the overall link performance. Variations in demodulator phase noise over a large range produce variation in performance of less than 0.3 dB which will not have a significant impact on the link performance.

In summary the previous estimate of receiver degradation of 4.2 dB is high. An additional 1.8 dB of link margin can be added to the uplink power budget of Table 3-2 for a total uplink margin of 10.3 dB.

3.5 RECEIVER PERFORMANCE

This brief section is a summary qualitative description of the major effects on the despreader, carrier recovery loop, and bit synchronizer performance resulting from the uplink signal revision. A detailed discussion of these components will follow in Section 5.

3.5.1 RF Components

The uplink signal design assessment incorporates the best estimates presently available for the calculation of the Shuttle/TDRSS Ku-band uplink power budget, Orbiter G/T, system noise temperature, and link margin for the revised uplink signal (216 kbps PSK). These calculations indicate that the overall uplink circuit margin is approximately equal to the value of G/T. Ultimate results were obtained parametrically for different values of RF line loss and for two values of preamp gain and noise figure typical of those with and without a paramp. The basic conclusion of these calculations indicate that the paramp is not required to obtain high values of G/T. Error correction coding, similarly, is not required.

3.5.2 PN Despreader

Greatly improved performance of the PN despreader, treated in detail in Section 5.2, was obtained for the revised uplink signal structure. Specifically, the improvements are in the areas of a faster code acquisition, allowed by the lower dwell times, and better threshold identification between signal plus noise and noise only. These results are given parametrically for different design values of C/N_0.

3.5.3 Carrier Recovery Loop

As expected, the revised signal allows a great degree of commonality with the S-band receiver. Preliminary results (see Section 5.3) indicate that the same carrier recovery/demodulator approach (Costas loop) yields good performance, having a relatively fast acquisition time and low tracking error.

3.5.4 Bit Synchronizer

A primary advantage of the revised uplink signal (216 kbps PSK) is that it allows the use of the SCTE NSP bit synchronizer without modification for the Ku-band orbiter receiver bit synchronizer. The time required for bit synchronization for the higher SNR values in the Ku-band application is well within one second (see Section 5.4).

4. DEVELOPMENT OF PERFORMANCE SPECIFICATIONS (TASK 2)

Task 2 of the Signal Design Study for Shuttle/TDRSS Ku-Band Uplink is the development of performance specifications. Specifically, Task 2 calls for the development of a detailed set of RF and signal processing performance specifications for the Orbiter hardware associated with the TDRSS/Orbiter Uplink. In addition, any changes to existing TDRSS performance specifications are supplied by NASA, which appear reasonable and desirable, are to be recommended.

Results of the Task 2 study effort is documented in this section. The TDRSS/Orbiter Ku-band uplink communication system requirements are reviewed and a detailed Orbiter receiver specification is presented. Specifications relating to the antenna acquisition are excluded. A list of TDRSS performance specification revisions recommended by this study conclude this section.

4.1 TDRSS/SHUTTLE KU-BAND UPLINK COMMUNICATION SYSTEM REQUIREMENTS

The Ku-band receiver, hereafter referred to as the receiver, must be capable of receiving a spread spectrum signal, removing the PN spreading code at IF to produce a despread PSK signal which is then demodulated to yield output data channels of 72 kbps and 144 kbps. The specifications contained herein describe a receiver design which provides the above functiors.

The specifications and design requirements in Section 5 is the culmination of analyses and hardware tradeoff studies which are oriented towards the optimization of performance with cost-effective hardware implementation. The factors influencing the receiver design are the receiver requirements summarized in Table 4-1. These requirements are based on the best available knowledge of operational and performance constraints.

Table 4-1. Receiver Requirements

Input Frequency	13.775 GHz
Input Bandwidth	30 MHz
AGC Dynamic Range:	
On Orbit	-90 to -103 dBm
Acquisition	-101 to -118 dBm
IF Frequency Uncertainty	±1.0 MHz + RCVR LO VAR
PN Code Modulation	NRZ - L PSK
PN Code Rate	11.232 Megachips/sec
PN Code Length	2047 Chips
PN Code Doppler	±400 Chips/sec
Data Modulation	Manchester II, Biphase L
Data Rate	216 kbps
Primary Mode Link Acquisition Time	<1 minute
BER	10^{-6}
BER Degradation	4.5 dB

4.2 SPECIFICATION OVERVIEW

In the overall receiver design program, the various analyses tasks and hardware implementation studies resulted in a top level block diagram of the receiver which incorporates five functional modules as shown in Figure 4-1. Specified design parameters for each of these modes are contained in Section 4.3.3.1.2.

The receiver specification is organized into three basic sections, namely, scope, applicable documents, and requirements. Scope, for this program, refers to the "reason for and extent of" the document, applicable documents are those references such as drawings, environmental specifications, next level specifications, parts requirements, etc., which are necessary for the design, fabrication, assembly, and test of the item being procured. This is generally a "boilerplate" which outlines the overall program requirements. For the procurement of a breadboard receiver, this entire section may contain a series of TBS or "To be specified" by NASA/JSC.

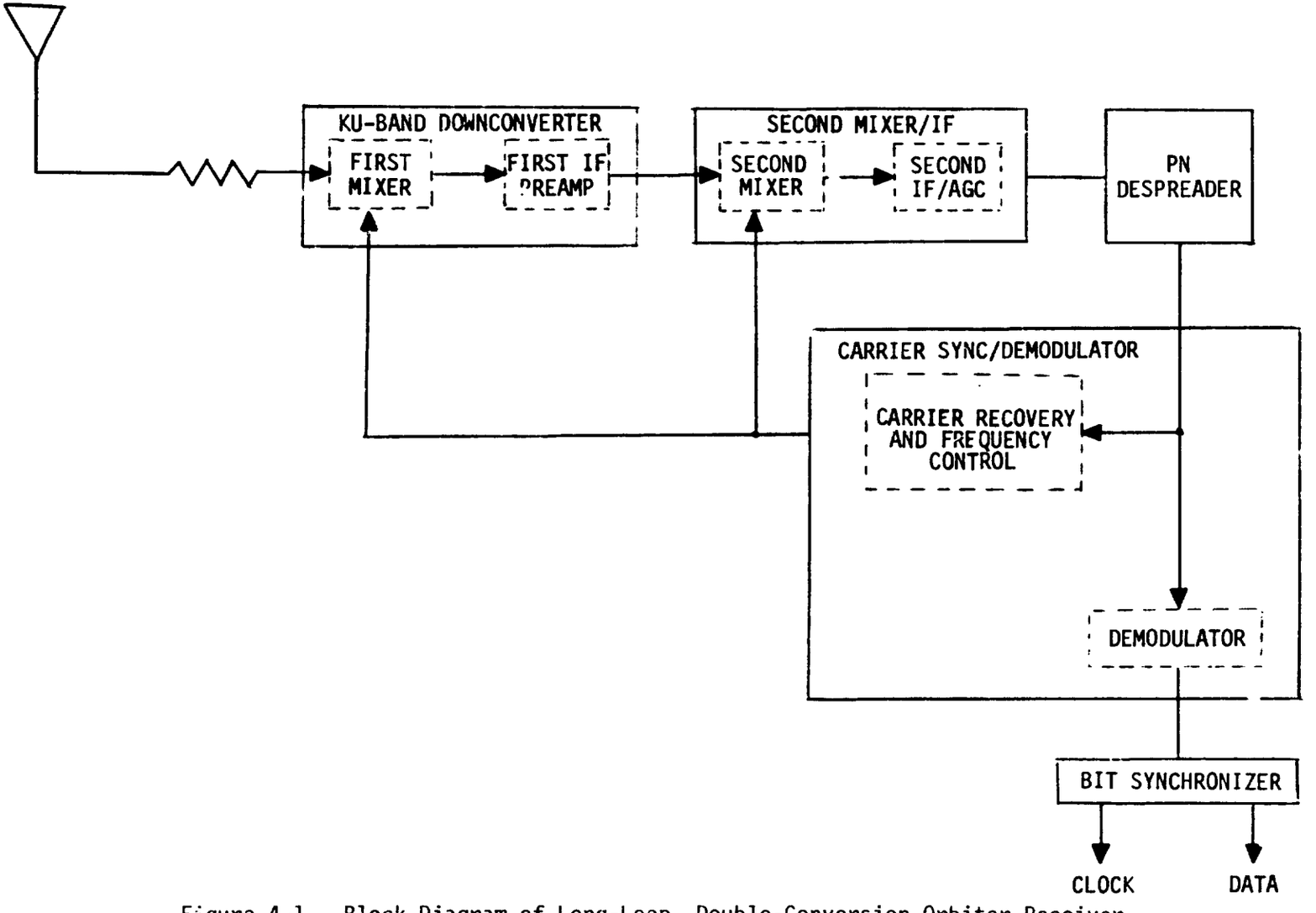

Figure 4-1. Block Diagram of Long-Loop, Double-Conversion Orbiter Receiver (Solid Boxes are Modules)

In the various module sections, the specifications augment those in the general receiver specifications and the interface are defined. The third section contains all pertinent information relative to electrical performance, size, weight, and thermal conditions.

The requirements section is structured to provide sufficient detailed information of the desired receiver characteristics such that a design may be implemented. Consequently, the requirements described in Section 4.3 include several parameters which cannot be determined from the information of Section 4.1, but nevertheless, have been included for completeness. The requirements section is divided into four broad categories of performance, interface requirements, environmental conditions, and design and construction.

In this study program, there are several analyses and hardware implementation study tasks which were performed to arrive at a candidate receiver design. These include:

- Configuration Study - Long versus short loop, single versus multiple frequency conversion
- Frequency Plan - Spurious frequency generation detrimental to the operation of the receiver
- Gain Distribution - Gain and noise figure allocation
- Receiver Interfaces - Levels, control

The module design requirements of Section 4.3.3.1.2 are predicated on the following assumptions.

- All requirements and specifications represent beginning of life values and do not account for measurement tolerance.
- Gain and noise figure allocations generated earlier and currently incorporated in the module specifications do not include mismatch losses; i.e., VSWR effects.
- Some minor impedance adjustment for phase and/or amplitude compensation may be required for the successful integration of the modules.
- RF and dc connectors are to be specified independently.
- EMC requirements for each module must be established prior to finalizing the specification.

- The packaging concept, though currently unspecified, may require modifications to the specifications; i.e., additional interconnect cables.

4.3 RECEIVER REQUIREMENTS AND SPECIFICATIONS

4.3.1 Scope

This specification defines the performance, design, construction, and testing requirements for the Ku-Band Orbiter Receiver.

4.3.2 Applicable Documents

4.3.2.1 Government Documents

The following government documents, of the exact issue shown, form a part of this specification to the extent specified herein.

SPECIFICATIONS	
Military	TBS
NASA	TBS
STANDARDS	
Military	TBS
Other	TBS
OTHER PUBLICATIONS	
NASA	TBS

4.3.2.2 Nongovernment Documents

The following nongovernment documents, of the exact issue shown, form a part of this specification to the extent specified herein.

SPECIFICATIONS	TBS
DRAWINGS	TBS

4.3.3 Requirements

4.3.3.1 Performance

The Ku-band receiver, hereafter referred to as the receiver, shall consist of RF devices and control circuits necessary for:

1) Receiving a spread spectrum signal

2) Removing the PN spreading code at IF to produce a despread PSK signal

3) Demodulating the PSK signal to provide an output data stream of 216 kbps.

4.3.3.1.1 Functional Characteristics

4.3.3.1.1.1 RF Signal Characteristics. The receiver shall perform within the limits of this specification when RF signals with characteristics specified herein are applied to the input connector.

4.3.3.1.1.1.1 Frequency. The nominal RF signal center frequency shall be 13775 MHz with an uncertainty of ±1 MHz maximum, which includes doppler frequency shift.

4.3.3.1.1.1.2 Level. The RF signal power level applied to the input connector shall be -90 to -118 dBm.

4.3.3.1.1.1.3 Modulation. The RF signal shall consist of a data signal spread by a PN signal.

4.3.3.1.1.1.3.1 Data. The data signal shall be Manchester II, biphase L, 216 kbps PSK.

4.3.3.1.1.1.3.2 PN Signal. The PN spreading signal shall consist of a psuedo-noise code generated by an 11-stage maximum length shift register generator. The PN code is NRZ-L, has a length of 2047 bits, and a rate of 11.232 Megachips/sec.

4.3.3.1.1.2 G/T. The receiver G/T shall be a minimum 4.6 dB/°K.

4.3.3.1.1.3 Acquisition. RF signal acquisition for the designated center frequency ±1 MHz shall be automatic. Allowance shall be made for receiver LO variation not to exceed ±100 kHz. Phaselock shall occur to the center frequency; sideband, spurious, or internal signal lock shall not occur.

4.3.3.1.1.3.1 Acquisition Time and Probability. The receiver shall acquire data after antenna acquisition in one minute or less with a probability of at least 0.99. The acquisition time is defined as the sum total of time required to achieve PN code acquisition, carrier phaselock, and bit synchronization.

4.3.3.1.1.3.2 Code Acquisition Time. The spectrum despreader shall achieve PN code acquisition with an average acquisition time of 10 seconds or less with a probability of acquisition of at least 0.99 at a received signal level of -102 dBm.

4.3.3.1.1.3.3 Acquisition Threshold. The receiver shall be capable of acquiring and phase tracking the RF signal at the minimum signal level of -118 dBm. Acquisition threshold is defined as the minimum signal level at which the receiver will acquire the RF signal and maintain lock.

4.3.3.1.1.4 In-Lock Tracking. The receiver, after acquiring lock, shall be capable of phase tracking and maintaining lock of PSK modulated signals with the characteristics described in Paragraph 4.3.3.1.1.1.3.1.

4.3.3.1.1.4.1 Tracking Performance Limit. Tracking performance limit is defined as the RF signal level below which phase track accuracy cannot be maintained to within the specified phase variance. The tracking performance limit shall be -102 dBm.

4.3.3.1.1.4.2 Tracking Phase Error. The maximum phase error under any specified condition, including static and dynamic phase error, shall not exceed 7 degrees. The static phase error shall not exceed 17 degrees.

4.3.3.1.1.5. Image Rejection. The receiver shall reject image frequencies and interfering signals to the extent specified herein.

4.3.3.1.1.6 Received Signal Transients. The receiver shall tolerate received signal transients (signal dropout) of up to TBS msec in duration after data acquisition occurring less than once per second. Automatic signal acquisition circuits shall not be unabled by the transient condition.

4.3.3.1.1.7 Telemetry Outputs. The receiver shall provide the following telemetry outputs.

4.3.3.1.1.7.1 Discrete Outputs. The receiver shall provide the following bilevel telemetry signal outputs.

4.3.3.1.1.7.1.1 Code Synchronization. The receiver shall provide a "true" indication when PN code synchronization is achieved, and a "false" indication when the PN codes are not synchronized.

4.3.3.1.1.7.1.2 Carrier Phaselock. The receiver shall provide a bilevel signal output indicating the status of receiver carrier tracking loop. The signal shall provide a "true" indication when phaselock is achieved and a "false" indication when the loop is unlocked.

4.3.3.1.1.7.2 Analog Output. The receiver shall provide the following analog telemetry signal output.

4.3.3.1.1.7.2.1 AGC. The receiver shall provide an analog telemetry output whose amplitude is proportional to the total receive power. The output shall be derived from the AGC control voltage and shall have the following characteristics:

a) Output voltage: 0 to 5 volts

b) Scale factor: 30 millivolts per dB of RF signal voltage change

c) Scaling range: The output voltage shall be in the range specified in a) for input power levels from -118 to -90 dBm.

4.3.3.1.1.8 Frequency Response. The receiver shall have an amplitude versus frequency response as follows.

a) 1 dB bandwidth: 25 MHz

b) Gain slope: 0.1 dB per MHz over a 25 MHz frequency band centered on the nominal center frequency.

4.3.3.1.1.9 Phase Linearity. The departure from linear phase response shall not exceed ±9 degrees over a 25 MHz frequency band centered on the nominal center frequency, as measured from the receiver input connector to the demodulator input.

4.3.3.1.1.10 DC Power. The total dc power input to the receiver shall be less than TBS watts.

4.3.3.1.2 Design Specifications. The receiver shall be designed to the additional requirements shown below.

4.3.3.1.2.1 Ku-Band Downconverter. The Ku-band downconverter shall be in accordance with the design specifications given below.

4.3.3.1.2.1.1 Performance. The Ku-band downconverter unit shall consist of a Ku-band mixer, IF amplifier, LO multiplier chain, appropriate filters, and shielding for the down-conversion of Ku-band signals to the IF frequency range.

4.3.3.1.2.1.2 RF Signal Characteristics. The unit shall perform within the limits of this specification for RF signals with the characteristics specified below applied to the input connector.

4.3.3.1.2.1.2.1 Frequency. The nominal RF signal center frequency shall be 13775 MHz.

4.3.3.1.2.1.2.2 Level. The RF signal power level applied to the input connector shall be -84 dBm to -104 dBm.

4.3.3.1.2.1.2.3 Bandwidth. The RF bandwidth shall be 30 MHz, centered on 13775 MHz.

4.3.3.1.2.1.2.4 Modulation. The RF signal shall consist of an PSK data signal spread by a PN signal.

4.3.3.1.2.1.3 Noise Figure. The unit noise figure shall be less than or equal to 6 dB referred to the first mixer input.

4.3.3.1.2.1.4 Gain. The unit shall have a net RF to IF conversion gain of 20 dB ± 1 dB.

4.3.3.1.2.1.4.1 Gain Variation. The gain variation versus frequency over the specified bandwidth shall not exceed ±0.5 dB referenced to the gain of Paragraph 4.2.3.1.2.1.4.

4.3.3.1.2.1.4.2 Gain Slope. The maximum gain slope over the specified bandwidth shall not exceed 0.02 dB per MHz.

4.3.3.1.2.1.5 Gain Compression. The output power at the 1.0 dB gain compression point shall be greater than 0 dBm.

4.3.3.1.2.1.6 RF Input VSWR. The RF input VSWR shall not exceed 1.2:1.

4.3.3.1.2.1.7 IF Signal Characteristics

4.3.3.1.2.1.7.1 Frequency. The nominal output frequency shall be 305.88 MHz.

4.3.3.1.2.1.7.2 Level. The output level shall be commensurate with the specified input level and gain.

4.3.3.1.2.1.8 Spurious Outputs. All spurious outputs generated in the unit within the specified bandwidth shall be greater than or equal to 50 dB below the desired output for a single carrier applied at any frequency within the specified bandwidth. Spurious outputs outside the specified bandwidth shall be greater than or equal to 35 dB below the desired output signal.

4.3.3.1.2.1.9 Spurious Frequency Rejection. The unit shall provide the following rejection at the input connector.

4.3.3.1.2.1.9.1 LO Frequency Rejection. The unit shall provide 30 dB minimum of LO frequency rejection.

4.3.3.1.2.1.9.2 Image Frequency Rejection. The unit shall provide 65 dB minimum of image frequency rejection including diplexer rejection.

4.3.3.1.2.1.9.3 Transmitter Frequency Rejection. The unit shall provide 70 dB minimum of rejection at 14908.5 MHz.

4.3.3.1.2.1.10 LO Signal Characteristics. The unit shall perform within the limits of this specification when LO signals with characteristics specified herein are applied to the LO connector.

4.3.3.1.2.1.10.1 Frequency. The nominal LO frequency shall be 13469.12 $\pm$0.1 MHz.

4.3.3.1.2.1.10.2 Level. The LO power level applied to the LO connector shall be 10 dBm $\pm$1 dB.

4.3.3.1.2.1.10.3 Spurious Frequencies. Discrete spurious frequencies within $\pm$15 MHz of the LO signal shall be greater than 93 dBc. All other spurious frequencies shall be greater than 50 dBc.

4.3.3.1.2.1.11 DC Power. The total dc power into the unit shall be less than TBS watts.

4.3.3.1.2.2 Second Mixer/IF. The second mixer/IF shall be in accordance with the design specifications given below.

4.3.3.1.2.2.1 Performance. The second mixer/IF unit shall consist of a mixer, AGC level control, appropriate filters, and shielding for the down-conversion to the second IF.

4.3.3.1.2.2.2 RF Signal Characteristics. The unit shall perform within the limits of this specification for RF signals with the characteristics specified below applied to the input connector.

4.3.3.1.2.2.2.1 Frequency. The nominal RF signal center frequency shall be 305.88 MHz.

4.3.3.1.2.2.2.2 Bandwidth. The RF signal shall occupy a 3 dB bandwidth of 25 MHz, centered on 305.88 ±1.1 MHz.

4.3.3.1.2.2.2.3 Modulation. The RF signal shall consist of an PSK data signal spread by a PN signal.

4.3.3.1.2.2.3 IF Signal Characteristics

4.3.3.1.2.2.3.1 Frequency. The nominal output frequency shall be 31 MHz.

4.3.3.1.2.2.3.2 Bandwidth. The IF bandwidth shall be 25 MHz, centered on 31 ±1.1 MHz including doppler and static frequency uncertainty.

4.3.3.1.2.2.3.3 AGC Loop. The IF shall incorporate AGC to maintain a constant ±1 dB signal plus noise power to the despreader. The loop shall have a maximum bandwidth of 10 Hz.

4.3.3.1.2.2.4 Spurious Outputs. All spurious outputs generated in the unit within the specified bandwidth shall be greater than or equal to 50 dB below the desired output for a single carrier applied at any frequency within the specified bandwidth. Spurious outputs outside the specified bandwidth shall be greater than or equal to 35 dB below the desired output signal.

4.3.3.1.2.2.5 Spurious Frequency Rejection. The unit shall provide the following rejection at the input connector.

4.3.3.1.2.2.5.1 LO Frequency Rejection. The unit shall provide 30 dB minimum of LO frequency rejection.

4.3.3.1.2.2.5.2 Image Frequency Rejection. The unit shall provide 65 dB minimum of image frequency rejection.

4.3.3.1.2.2.6 LO Signal Characteristics. The unit shall perform within the limits of this specification when LO signals with characteristics specified herein are applied to the LO connector.

4.3.3.1.2.2.6.1 Frequency. The nominal LO frequency shall be 274.88 MHz.

4.3.3.1.2.2.6.2 Level. The LO power level applied to the LO connector shall be 2 dBm ±4 dB.

4.3.3.1.2.2.6.3 Spurious Frequency. Discrete spurious frequencies within ±15 MHz of the LO signal shall be greater than 75 dBc. All other spurious frequencies shall be greater than 50 dBc.

4.3.3.1.2.2.7 DC Power. Not applicable.

4.3.3.1.2.3 PN Despreader. The PN despreader shall be in accordance with the design specifications given below.

4.3.3.1.2.3.1 Performance. The PN despreader unit shall consist of RF and digital devices required to perform the operational and control functions necessary for removing the PN code and produce the despread PSK signal.

4.3.3.1.2.3.2 RF Signal Characteristics. The unit shall perform within the limits of this specification for RF signals with characteristics specified below applied to the input connector.

4.3.3.1.2.3.2.1 Frequency. The nominal center frequency shall be 31 MHz.

4.3.3.1.2.3.2.2 Level. The RF signal power level applied to the input connector shall be -15 dBm ±1 dB.

4.3.3.1.2.3.2.3 Modulation. The RF signal shall consist of a data signal spread by a PN signal.

4.3.3.1.2.3.2.3.1 Data. The data signal shall be a noncoherent, unbalanced PSK characterized as specified in Paragraph 4.3.3.1.1.1.3.1.

4.3.3.1.2.3.2.3.2 PN Signal. The PN spreading signal shall be as specified in Paragraph 4.3.3.1.1.1.3.2.

4.3.3.1.2.3.2.4 Bandwidth. The nominal 1 dB bandwidth of the RF signal shall be 25 MHz.

4.3.3.1.2.3.3 Acquisition. Code acquisition for the designated center frequency ±1.1 MHz shall be automatic.

4.3.3.1.2.3.3.1 Acquisition Time and Probability. The unit shall achieve code synchronization in an average time of 10 seconds or less with a probability of at least 0.99.

4.3.3.1.2.3.3.2 Acquisition Threshold. The unit shall be capable of acquiring and tracking the code for an input signal-to-noise ratio (SNR) of -5 dB. Acquisition threshold is defined as the minimum SNR at which the unit will acquire and maintain code synchronization at the design parameters given below.

4.3.3.1.2.3.4 Signal Transients. The unit shall tolerate signal transient (signal dropouts) of up to TBS msec in duration, occurring less than once per second. Automatic code acquisition circuits shall not be enabled by the transient condition.

4.3.3.1.2.3.5 Telemetry Output. The unit shall provide a bilevel telemetry signal output indicating the status of the code tracking loop. The unit shall provide a "true" indication when PN code synchronization is achieved, and a "false" indication when the PN codes are not synchronized.

4.3.3.1.2.3.6 Mode Logic. The unit shall provide a discrete output indicating the status of the code tracking loop. The unit shall provide a true indication when PN code synchronization is achieved, and a "false" indication when the codes are not synchronized.

4.3.3.1.2.3.7 Output Characteristics. The unit shall provide an output with the following characteristics.

4.3.3.1.2.3.7.1 Frequency. The nominal center frequency shall be 31 MHz.

4.3.3.1.2.3.7.2 Modulation. The output signal shall consist of an PSK data signal as specified in Paragraph 4.3.3.1.1.1.3.1.

4.3.3.1.2.3.7.3 Bandwidth. The RF bandwidth shall be 12.5 ±1.1 MHz.

4.3.3.1.2.3.8 DC Power. The total dc power input to the unit shall be TBS watts.

4.3.3.1.2.3.9 PN Despreader Design Parameters. The PN despreader shall be designed to have the following additional design characteristics.

a) Acquisition loop bandwidth: 400 Hz

b) Tracking loop bandwidth: 6 Hz

c) Pull-in time: ≤ 20 msec

d) Damping factor: 0.707

e) Tracking loop lag: ≤ 0.007 chip

f) RMS tracking error: 0.04 chip

g) BER degradation: 1.5 dB.

4.3.3.1.2.4 Carrier Sync/Demodulator. The carrier sync/demodulator shall be in accordance with the design specifications given below.

4.3.3.1.2.4.1 Performance. The carrier recovery and frequency control unit shall consist of RF devices and control circuits necessary for:

1) Recovering the carrier component of PSK signal

2) Providing a variable frequency source for phasetracking of the recovered carrier

3) Providing the reference source to the demodulator

4) Providing a phaselock indicator

5) Demodulation of the 216 kbps PSK signal.

4.3.3.1.2.4.2 RF Signal Characteristics. The unit shall perform within the limits of the specification for RF signals with the characteristics specified below applied to the input connector.

4.3.3.1.2.4.2.1 Bandwidth. The nominal RF center frequency shall be 31 MHz.

4.3.3.1.2.4.2.2 Level. The RF signal bandwidth applied to the unit input shall be 12.5 MHz bandwidth centered on 31 ±1.1 MHz.

4.3.3.1.2.4.2.3 Modulation. The RF signal shall consist of an PSK data signal with characteristics as specified in Paragraph 4.3.3.1.1.1.3.1.

4.3.3.1.2.4.3 Acquisition. RF signal acquisition for the designated center frequency ±1.1 MHz shall be automatic. Phaselock shall occur to the center frequency; sideband, spurious, or internal signal lock shall not occur.

4.3.3.1.2.4.3.1 Acquisition Time and Probability. The unit shall achieve phaselock in an average time of TBS seconds or less with a probability of at least 0.99.

4.3.3.1.2.4.3.2 Acquisition Threshold. The unit shall be capable of acquiring and phasetracking the RF signal at a signal-to-noise ratio (SNR) of -3 dB, measured in a 12.5 MHz bandwidth. Acquisition threshold is defined as the minimum SNR at which the unit will acquire the signal and maintain the lock in accordance within the design specifications of Paragraph 4.3.3.1.2.4.

4.3.3.1.2.4.4 In-Lock Tracking. The unit, after acquiring lock shall be capable of phasetracking and maintaining lock of signals with the characteristics described in Paragraph 4.3.3.1.2.4.2.

4.3.3.1.2.4.4.1 Tracking Performance Limit. Tracking performance limit is defined as the SNR below which phasetracking accuracy cannot be maintained to within the required phase variance. The tracking performance limit shall be -3 dB.

4.3.3.1.2.4.4.2 Tracking Phase Error. The maximum phase error under any condition specified, including static and rms dynamic phase error, shall not exceed 24 degrees.

4.3.3.1.2.4.5 Received Signal Transients. The unit shall tolerate signal transients (signal dropout) up to TBS msec in duration, occurring less than once per second. Automatic signal acquisition circuits shall not be enabled by the transient condition.

4.3.3.1.2.4.6 Telemetry Outputs. The unit shall provide the following telemetry outputs.

4.3.3.1.2.4.6.1 Discrete Outputs. The receiver shall provide a bilevel signal output indicating the states of the carrier tracking loop. The signal shall provide a "true" indication when phaselock is achieved and a "false" indication when the loop is unlocked.

4.3.3.1.2.4.6.2 Analog Output. The unit shall provide an analog telemetry output whose amplitude is proportional to the signal power. The output shall be derived from the AGC control voltage.

4.3.3.1.2.4.7 Local Oscillator. The unit shall provide local oscillator outputs for the Ku-band downconverter and the UHF downconverter derived from the carrier tracking VCXO.

a) Ku-band downconverter: 13469.12 MHz

b) UHF downconverter: 274.88 MHz

4.3.3.1.2.4.8 Reference Oscillator. The unit shall provide a reference oscillator output frequency of 31 MHz.

4.3.3.1.2.4.9 Signal Output. The unit shall provide a data output of 216 kbps.

4.3.3.1.2.4.10 DC Power. The total dc power input to the unit shall be less than TBS watts.

4.3.3.1.2.4.11 Design Parameters. The unit shall be designed to the additional requirements shown below.

4.3.3.1.2.4.11.1 VCO. The unit shall incorporate a VCXO which shall be used to close the phaselock loop. The VCXO shall have the following characteristics:

a) Center frequency: 274.88 MHz

b) Stability: ±2 PPM, ±1 PPM goal

c) Pulling range: ±40 PPM

4.3.3.1.2.4.11.2 Carrier Tracking Phaselock Loop Parameters. The carrier tracking phaselock shall be designed to have the following properties:

a) Loop bandwidth: 5 kHz

b) Dynamic phase error: <7 degrees rms

c) Static phase error: <17 degrees

d) Damping factor: 0.707

e) Loop order: Second

f) Loop configuration: Costas

g) BER degradation: <1 dB

4.3.3.1.2.5 Bit Synchronizer. The bit synchronizer shall be in accordance with the design specifications given below.

4.3.3.1.2.5.1 Performance. The bit synchronizer unit shall consist of the analog and digital circuitry required to provide a bit-synchronized data stream of 216 kbps with NRZ-L format and frame synchronization.

4.3.3.1.2.5.2 Input Signal Characteristics. The unit shall perform within the limits of this specification for input signals having the following characteristics.

a) Waveform: Manchester II, biphase L

b) Data rate: 216 kbps

c) Voltage amplitude: 100 mV rms (+20 dB, -8 dB)

d) Terminating impedance: 71 Ω (±10%)

e) Signal termination: Differential direct coupled

4.3.3.1.2.5.3 Outputs. The unit shall provide the following outputs.

4.3.3.1.2.5.3.1 Data. The unit shall provide bit-synchronized 216 kbps output data in an NRZ-L format.

4.3.3.1.2.5.3.2 Clock. The unit shall provide as an output a phase coherent clock for frame synchronization.

4.3.3.1.2.5.3.3 Lock Status. The unit shall provide a bit sync flag to the mode status control board as an indication of the establishment of lock.

4.3.3.1.2.5.4 DC Power. The total dc power dissipated by the unit shall be <7 watts.

4.3.3.1.2.5.5 Bit Synchronization Design Parameters. The bit synchronizer shall be designed to have the following additional design characteristics.

a) Threshold SNR: 0 dB

b) Mean acquisition time: <1 sec (including frame sync)

c) Loop bandwidth: 80 Hz, at E_b/N_o = 0 dB and a 50 percent transition density

d) Sync jitter: <1 percent

e) BER degradation: <1 dB

4.3.3.2 Interface Requirements

4.3.3.2.1 RF Input Characteristics. The receiver RF input port shall have the following characeristics.

a) Nominal impedance: 50 ohms ±10 percent

b) Input VSWR: 1.6 or better

c) Source VSWR: TBS

d) Protection: The receiver shall be stable and shall not be damaged when operated with the RF input short of open circuited or with RF input signal levels of 5 dB.

e) Isolation: The receiver input port shall be isolated from the transmitter port such that the transmitter to receiver frequency band isolation is a minimum of TBS dB.

4.3.3.2.2 Data Output. The receiver shall provide demodulated baseband signals with the following characteristics.

a) Signal type: Baseband data

b) Data rate: 216 kbps biphase-L

c) Voltage level: TBS

d) Output polarity: Binary zero (1,0); negative phase transition
Binary one (0,1); positive phase transition

e) Output impedance: TBS ohms ±10 percent

f) Termination: TBS

4.3.3.2.3 Telemetry Interface. The receiver shall provide telemetry output signals with the following characteristics.

4.3.3.2.3.1 Discrete Output

a) True state: 5 volts ±1 volt

b) False state: 0 volt ±0.5 volt

c) Load impedance: TBS ohms

d) True current: TBS ma

e) False current: TBS ma

f) Power off impedance: TBS ohms

g) Discretes per return: TBS

4.3.3.2.3.2 Analog Output.

a) Voltage range: 0 to plus 5 volts

b) Source impedance: TBS ohms

c) Load impedance: TBS ohms

d) Analogs per return: TBS

4.3.3.2.4 DC Power Interface. TBS

4.3.3.2.5 Command Interface. TBS

4.3.3.3 Environmental Conditions

4.3.3.3.1 Temperature. The receiver shall be designed to operate over the temperature range specified herein.

a) Deployed assembly: TBS

b) Electronic assembly: TBS

4.3.3.4 Design and Construction

4.3.3.4.1 Dimensions. The receiver shall be designed to the following form factor and dimensions.

a) Deployed assembly: TBS

b) Electronic assembly: TBS

4.3.3.4.2 Weight. The receiver shall be designed to the following weight.

a) Deployed assembly: TBS pounds maximum

b) Electronic assembly: TBS pounds maximum

4.4 REVIEW OF TDRSS SPECIFICATION

This section is composed of a brief series of comments on the TDRSS Specification [27]. These comments are basically concerned with

1) The compatibility of the TDRSS Specification and the Ku-Band Shuttle Communications Specifications taken from [28]

2) Potential problem areas which interface with the Ku-band communication functions apparently uncontrolled by specification.

Obviously, the scope of the Uplink Signal Design Study precludes an exhaustive TDRSS/Orbiter "systems" critique. Extensive changes to procurement specifications would probably, in fact, be inappropriate at this time. Therefore, the revisions recommended by the study are limited to the very brief list presented in the remainder of this section.

4.4.1 Return Link Frequency

According to the Orbiter communications specification (Reference [28]) Paragraph 3.2.1.2.3.2, the return link center frequency should be 15.0085 GHz. However, the TDRSS specification (Reference [27]) in Table 2-2, page 7 under "Return Link Signal Parameters" shows the carrier frequency for KSA users to be equal to the forward link frequency times the ratio 1600/1469,

$$13.775 \text{ GHz} \times 1600/1469 = 15.0034 \text{ GHz}$$

It is, therefore, recommended that the TDRSS specification be changed to show a 5.1 MHz increase in the return link carrier frequency.

4.4.2 Definition of Mode 2 Return Link

Specifications [27] and [28] differ in three respects in the definition of the Mode 2 return link.

8.5 MHz Subcarrier

The TDRSS specification [27] states, in Section 8.2.1.2, that the signal format into the FM modulator shall be an analog modulated carrier and an 8.5 MHz QPSK modulated squarewave subcarrier. The Shuttle Orbiter specification [28], under Paragraph 3.2.1.2.3.4.2 treating "Mode 2

Modulation," does not state that the 8.5 MHz subcarrier is squarewave. It is noted that the TRW proposal (Reference [3]) in response to [28] assumed a sinusoidal subcarrier.

Channel 3 Data

The Shuttle Orbiter specification [28], under Paragraph 3.2.1.2.3.3 treating "Mode Description," states that "Channel 3 shall consist of 4.5 megahertz TV, or up to 4 Mbps digital NRZ format data, or 4.5 megahertz analog data or other data that are compatible with the response characteristics of this channel." The TDRSS specification [27] makes no provision for digital data in this channel.

Two-Channel Configuration

The Shuttle Orbiter specification [28], under Paragraph 3.2.1.2.3.3b states that the return link Mode 2 may also consist of "two channels of simultaneous data." No mention of this two-channel configuration is found in the TDRSS specification [27].

4.4.3 Forward Link TDRS EIRP

In light of the power flux density considerations of Section 3.2, it is recommended that the TDRSS specification [27] show a maximum signal EIRP of 48 dBw in Table 2-3 rather than a minimum of 48.5 dBw.

4.4.4 Rejection of Shuttle S-Band Harmonics

At present no known applicable specification controls the Ku-band Shuttle Orbiter receiver filter rejection of harmonic interference from the SCTE.

The 6th, 7th, and 8th harmonics of the Shuttle and payload S-band transmit signals are potential interference for the Ku-receive band at 13775 $\pm$120 MHz. Figure 4-2 shows the S-band transmit bands and the required bands for the 6th, 7th, and 8th harmonics to occur within the Ku-band receive band.

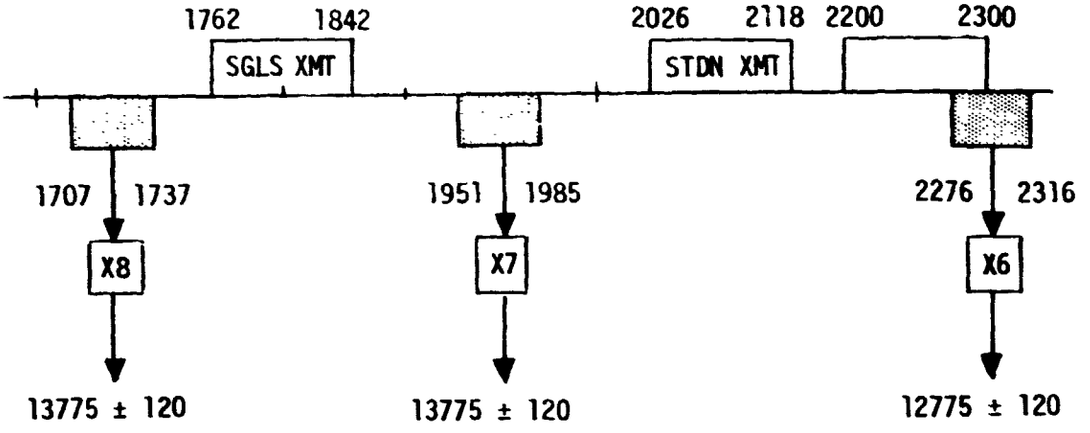

Figure 4-2. SCTE Generated In-Band Interference

As evident from the figure only the 6th harmonic of signals in the 2276-2300 MHz transmit band fall in the Ku-receive band. The following frequencies are, therefore, of interest:

	XMT Signals	S-Band Frequency	6th Harmonic at Ku-Band
1)	STDN/SGLS (Ch. 18)	2287.5 MHz	13725 MHz
2)	Payload-to-Shuttle XMT	2275-2300 MHz	13650-13800 MHz

The two cases investigated below [29] were based on the best information available during the uplink study time frame. It is recommended that SCTE interference rejection requirements be incorporated into the Ku-Band Shuttle Orbiter receiver specification.

Case 1: S-Band Transmitter Generates the 6th Harmonic.

From Tables 4-2, 4-3, and 4-..

Maximum S-Band Transmitter Output Power: (TDRS Mode at 2287.5 MHz)	51 dBm
Transmitter 6th Harmonic Spur Level Rejection:	-76 dB
Preamp Assembly Diplexer Rejection:	-115 dB
Maximum Spur Level into S-Band Antenna:	-140 dBm
Estimated Quad Antenna Gain (Ku-Band)	10 dB
Space Loss (20 Feet, 13775 MHz)	-71 dB
Maximum Ku-Band Receive Antenna Gain:	40 dB
6th Harmonic Spur Level at Receiver (Negligible)	-161 dBm

Case 2: Ku-Band Receive Mixer Generates 6th Harmonic and Resulting IF Spur

Maximum S-Band Transmitter Output Power:	51 dBm
Estimated Quad Antenna Gain (S-Band):	10 dB
Space Loss (20 Feet, 2287.5 MHz):	-55 dB
Ku-Band Antenna Gain at 2287.5 MHz:	<24 dB
Received S-band signal level at Ku-band waveguide feed assembly:	+30 dBm
Waveguide, BPF, and mixer rejection at S-band to reject 6th harmonic to 20 dB below -106 dBm (minimum acquisition level):	156 dB

Table 4-2. Present Filter Requirements

SYSTEM	FILTER REQUIREMENTS	COMMENTS
1. Shuttle Ku-Band Comm. (NASA Breadboard RFP)	3.2.8 Signal Rejection 3.2.8.1 Image: ≥80 dB for signals applied to antenna port 3.2.8.2 IF: ≥80 dB for IF signals applied to antenna port 3.2.8.3 Internal Spurs: Coherently related signals below acquisition level (∿-110 dBm at antenna port) 3.2.8.4 AM Rejection: 9 dB p-p AM at 50 Hz shall not make receiver perform out-of-spec	For use in laboratory environment. (Potentially more severe than in space for spurious signals)
2. Shuttle S-Band Comm. (Receiver Concept Review)	3.1.1.6.1 Spurious Signal Rejection Such that receiver performance degradation ≤0.2 dB for signals up to -50 dBm and greater than ±40 MHz away from receive frequency	Apparently derived from signals being transmitted from a payload to the Shuttle at frequencies within the overall receive band
3. Shuttle Ku-Band Despreader Receiver Design	Spurious Outputs (Internal Spurs) a) In-band spurs: 50 dB below desired signal b) Out-of-band spurs: 35 dB below desired signal	Module specs
	Image Rejection ≥65 dB	Ku-band downconverter module
	Transmitter Frequency Rejection ≥70 dB at 14.9085 GHz	Ku-band downconverter module
4. Shuttle S-Band Comm. (Reference [28])	10.3.2.1.2.1.4.1.5a. Image Rejection: >60 dB	

Table 4-3. S-Band Shuttle Diplexer/Triplexer Transmit Rejection Requirements

UNIT	FILTER REJECTION REQUIREMENTS
• S-BAND TRANSPONDER ASSEMBLY TRIPLEXER	1 dB at ±2.5 MHz 20 dB at +17 MHz 60 dB at ±50 MHz
• S-BAND PREAMP ASSEMBLY DIPLEXER	1.2 dB at ±2.5 MHz 65 dB at ±50 MHz 115 dB at -175 MHz

Table 4-4. Known Interference Signals (All Modulated)

BAND	ORIGIN	FREQUENCY (GHz)	POWER LEVEL (dBm)	COMMENT
Ku-Band	Shuttle Radar	13.775	43 ave 60 peak	• 20 watts 1 kw (output noise determined by gain, ∿40 dB, NF, ∿30 dB)
	Shuttle Comm	15.0085	45	• 30 watts (noise as above)
S-Band	Shuttle-to-Payload	1.762-1.842 (20 Channels SGLS)	38.5	• 7 watts max. (for triplexer rejection
		2.026-2.118 (20 channels STDN)		Antenna gain unknown. XMTR spurious 85 dB below carrier
	Shuttle-to-Ground	2.2175 (Ch.4) 2.2875 (Ch.18) (STDN & SGLS)	38.5	• (For triplexer rejection, Hemi and quad antenna gains unknown
			Triplexer Rej. puts to -63 dB	Spurs: <-63dB 2nd Harm:<-25dB >3 Harm:<-35dB
	Shuttle-to-TDRS	2.2175 2.2875	51 (125W)	• Harm Spurs: <-10 dB 2nd <-20 dB 3rd <-76 dB>3rd
	Shuttle-to-Ground	2.250	42	• 15 watts, FM mode All spurs: <-65 dB

5. DETAILED DESIGN AND PARAMETER OPTIMIZATION (TASK 3)

Task 3 of the Signal Design Study for Shuttle/TDRSS Ku-Band Uplink covers detailed design and parameter optimization of a detailed design of the PN despreader, the PSK carrier synchronization loop, and the symbol synchronizer. All critical parameters are to be identified and optimized. This section documents the work performed during the Ku-Band Uplink Signal Study in response to the above task definition. The noncoherent AGC analysis is presented in Appendix A.

5.1 ORBITER RECEIVER BLOCK DIAGRAM

Before proceeding to the analysis and detailed design of the PN despreader, PSK carrier synchronization loop, and the symbol synchronizer it is first convenient to briefly discuss an overall receiver configuration derived in the study and to identify the operational units of interest.

The receiver functions required to receive and convert the Ku-band uplink signal into the two data streams of 72 and 128 kbps must be provided. These include

- Provision of adequate G/T
- Spread spectrum processing
- Provision of coherent demodulation references
- Provision of synchronous timing for matched filter data detection
- Local correlation with frame sync pattern, phase ambiguity resolution, and demultiplexing
- Data quality screening.

These functions are illustrated in the receiver block diagram of Figure 5-1.

A 7.8 dB recommended system G/T, 3.2 dB more than required, is provided by a 39.7 dB antenna, 6 dB receiver noise figure and 1.3 dB of circuit losses for the autotrack comparator, transmit receive isolation diplexer, and signal presence calibration components. Double downconversion to 31 MHz is used to obtain stable spur-free performance, as well as cost effective design commonality with SCTE spread spectrum processing, Costas detection, and reference oscillator equipment.

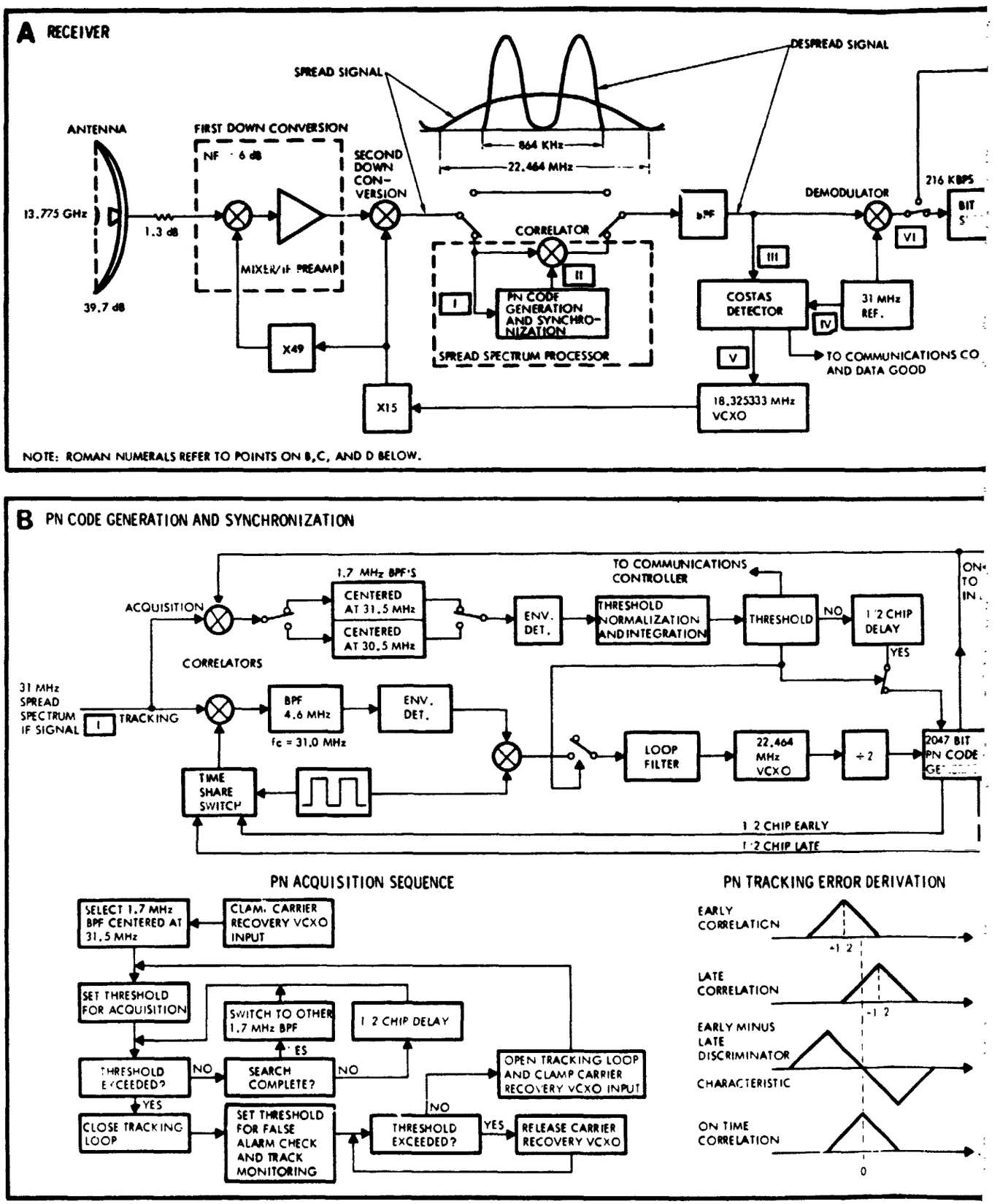

PRECEDING PAGE BLANK NOT FILMED

FOLDOUT FRAME /

ORIGINAL PAGE IS OF POOR QUALITY

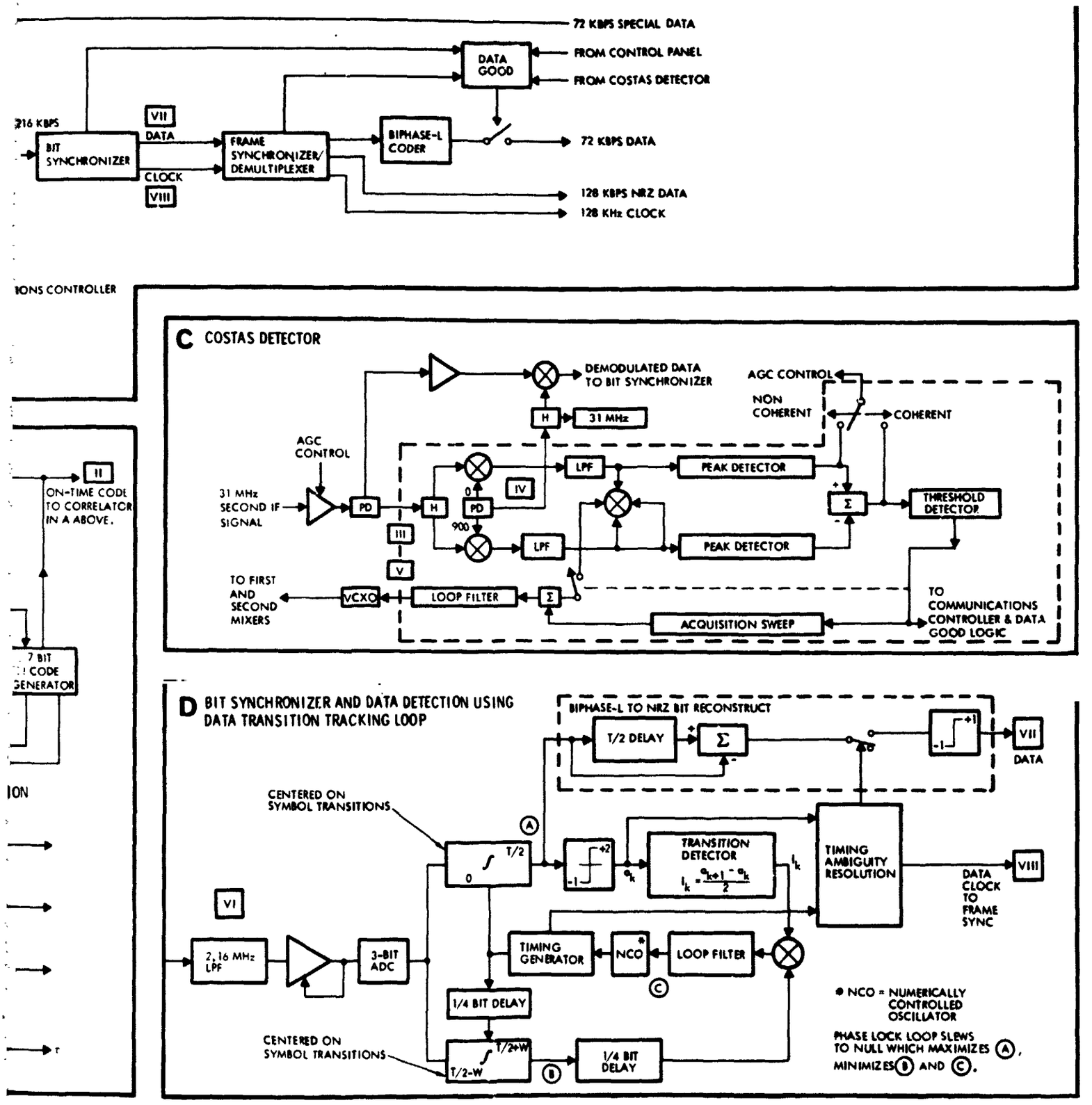

Figure 5-1. Ku-Band Orbiter Receiver

(REVERSE OF THIS PAGE LEFT BLANK)

Spread spectrum processing is accomplished with TRW's SCTE design with only simple modifications to the filter bandwidths and acquisition sequence made necessary by greater carrier frequency uncertainty and shorter acquisition time requirements. Synchronization of the local and received PN codes is achieved by systematic correlation with each possible code phase until the correct phase is found. Positive carrier doppler is assumed for the first search then negative doppler if the first search is unsuccessful. If neither search is successful, the sequence is repeated until acquisition is accomplished. Synchronization is maintained by a standar' timeshare early-late tracking loop. The predetection filter bandwidth of this loop has been made wide enough to accommodate the subsequent carrier acquisition frequency sweep.

The received carrier is made coherent with the 31-MHz demodulator reference using a standard Costas loop to derive local oscillators for the downconversions. Phase error signals for the VCXO are generated using TRW's SCTE design, again with only some modifications to tracking loop bandwidth and acquisition sweep rate made necessary by greater carrier frequency uncertainty and shorter acquisition time requirements. A recent problem identified on SCTE was false lock on data sidebands. This resulted from operating with weak signals, at negative SNRs. The KRCE will not have this problem because the post-despreader SNR is several dB positive. Phase ambiguity is resolved in the frame synchronizer and, if necessary, an inverter is commanded.

TRW's SCTE bit synchronizer is directly applicable to synchronizing the demodulated biphase-L encoded 216 kbps data. This synchronizer uses a data transition tracking loop (DTTL) which is essentially a digital version of a Costas loop. Prior to synchronization, the demodulated data passes through a 2.16-MHz filter selected to minimize noise and aliasing, is A/D converted at a 32-sample/bit rate and fed to the DTTL. Integration intervals are centered on or between symbol transitions corresponding to the I or Q phase detectors of a Costas loop. The synchronizer includes provisions to resolve bit or symbol transition ambiguities based on relative probabilities, and also contains a biphase-L to NRZ bit reconstruct circuit.

Frame synchronization for demultiplexing is accomplished by bit correlation with the local 32-bit pattern. Greater than 29 or less than three agreements correspond to positive and negative correlation and establish the frame time. Negative correlation results in the invert command being sent to the bit synchronizer. The data quality screening circuit is based on simultaneous lock detection indications from the Costas detector, bit synchronizer, frame synchronizer, and an enable from the control panel.

The PN despreader, carrier synchronization loop, and bit synchronization is now discussed in greater detail.

5.2 DESPREADER

The evolution of a detailed design for the K-band Orbiter receiver despreader is presented in this section. The key specifications used during the study are stated and a general design approach is described. A groundwork of analysis leads to a systematic selection of design parameters by means of an analysis-based computer program which allows the selection of the pertinent parameters for optimum performance. Finally, a description of the recommended despreader implementation and associated hardware completes the content of this section.

5.2.1 Basic Configuration and Analysis

At the offset certain key specifications were used for purposes of this study. Every effort was made to make these as realistic as possible based on the best information available. These specifications are listed in Table 5-1.

Because of the presence of data modulation at the input to the despreader, a noncoherent detection of Figure 5-2 is used for timing alignment of the local PN code. After correlating with the local PN signal, the received signal is passed through an IF bandpass filter prior to the square-law device. The output of the square-law device is then integrated over time interval T. Since the signal to integrator is bandlimited to the IF bandwidth B_{IF}, the sampling theorem is applied to approximate the output of the integrator as the discrete sum of M ($=B_{IF}T$) samples. This integrator output is then used as a test statistic of the acquisition detection for timing alignment of the PN code.

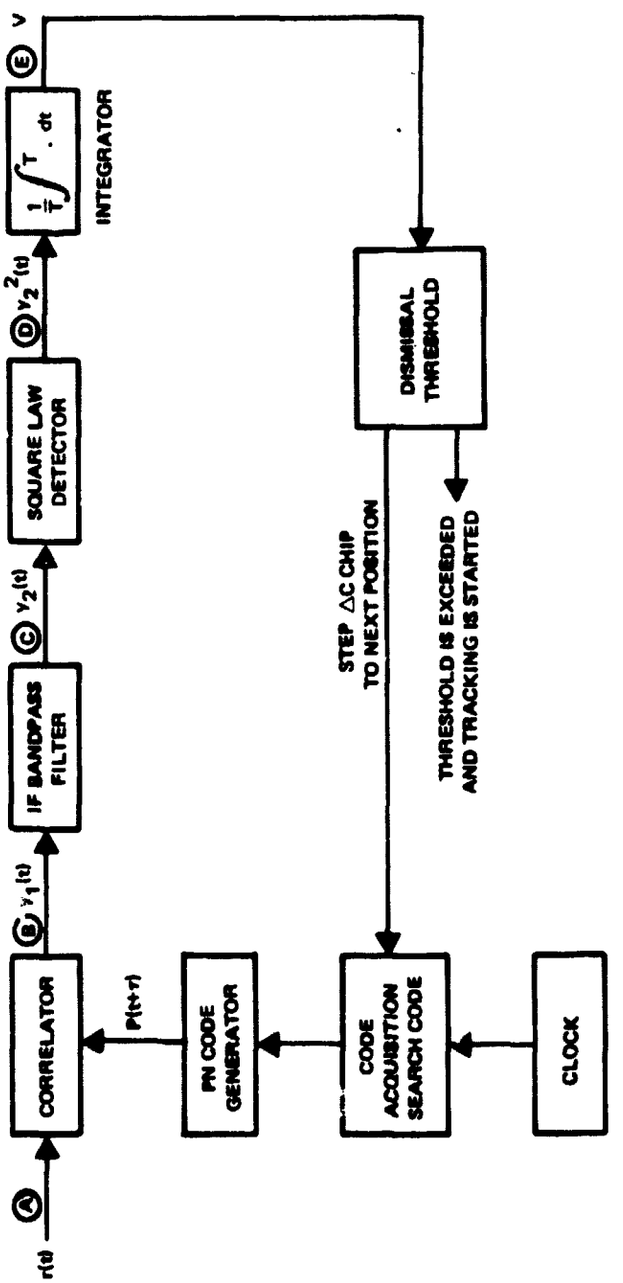

Figure 5-2. PN Code Acquisition

Table 5-1. Key Specifications for K-Band Despreader

PN CODE RATE	11.232 MEGACHIPS/SEC
PN CODE LENGTH	2047
PN CODE MODULATION	NRZ-L PSK
DATA RATE	216 KBPS
DATA MODULATION	MANCHESTER II, BIPHASE L
PN CODE ACQUISITION TIME	$\leq$10 SEC
SPECIFIED SIGNAL LEVEL	-102 dBm*
DETECTION PROBABILITY	0.99
FALSE ALARM PROBABILITY	10^{-6}
CODE DOPPLER	$\pm$400 Hz
IF FREQUENCY UNCERTAINTY	$\pm$1.0 MHz + RCVR LO VAR**
BER DEGRADATION	$\leq$1.5 dB

*Referred to 34.6 dB; receive antenna.
**Receiver LO variation is assumed to be $\pm$100 kHz.

The objective of the acquisition strategy is to adjust the phase of the locally generated code until it approaches alignment with the phase of the code on the received signal. At that time, the bandwidth of the spectrum at point B narrows and more energy is allowed through the bandpass filter, thus producing a larger signal at the output of the square law detector. When this occurs, the output of the lowpass filter will increase in an exponential fashion until it exceeds a threshold voltage, at which time the threshold detector triggers and the system changes from the acquisition mode to the code tracking mode. At that time the tracking loop pulls the code generator into synchronization with the code on the received signal. If the threshold detector is not triggered after a

specified dwell time, the acquisition logic shifts the phase of the PN code generator by a fraction of a chip and the process is repeated. Because of the channel noises, there exists some probability that the acquisition detector misses the in-sync chance and continues to search for the timing. This case, called missed detection, is undesirable. On the other hand, during out-of-sync conditions, the acquisition detector may falsely pronounce the in-sync because of the channel noises. This case, called false alarm, should be minimized.

In a probabilistic sense, the output of the lowpass filter has a probability distribution function that varies as a function of the degree of correlation of the received and local PN codes. When the codes are not aligned, the voltage pdf at point C is essentially gaussian. When the codes approach alignment, the voltage at point C will include a narrow-band phase-modulated signal, plus a gaussian noise term generated by receiver noise and a fraction of uncorrelated signal. The square law detector will respond to the phase modulated signal as if there were no phase reversals, if the signal envelope is essentially undistorted by the bandpass filter (i.e., if the BPF is wider than the signal spectrum). Under these two conditions the square law detector output pdf at point D will be either Rayleigh or Ricean, and given by

$$P(v) = \frac{v}{\sigma^2} e^{-\frac{v^2}{2\sigma^2}} \tag{5-1}$$

or by

$$P(v) = \frac{v}{\sigma^2} e^{-\frac{v^2 + 2P_s}{2\sigma^2}} I_0\left(\frac{v\sqrt{2P_s}}{\sigma^2}\right) \tag{5-2}$$

where

σ is the standard deviation. σ^2 corresponds to the total noise power into the square law detector, which corresponds to the total energy input, less the energy in the correlated signal.

P_s is the power in the undistorted signal

I_0 is a modified Bessel function of the first kind of zero order

v is the envelope of the combined signal

In order to achieve reasonable probabilities of false alarm and of detection, a decision threshold must be established, as illustrated in Figure 5-3a such that the integrated areas under the two pdf's and above the threshold is small for the noise alone case and large for the signal plus noise case.

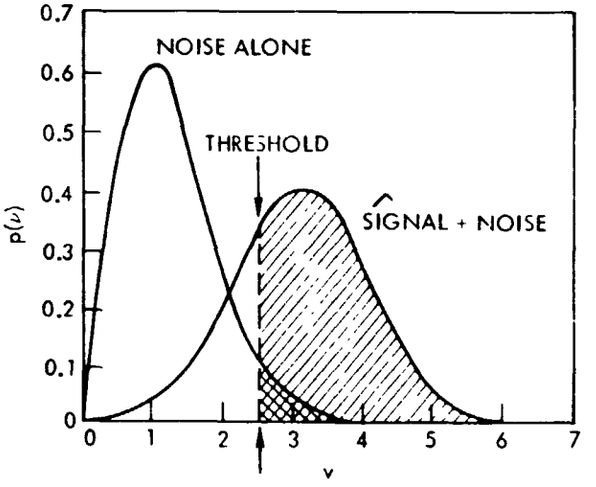

Figure 5-3a. Probability-Density Functions for Noise Alone and for Signal-Plus-Noise, Illustrating the Process of Threshold Detection

As a practical matter, it is necessary to provide additional filtering after the square law detector to improve false alarm and detection probabilities. Depending on one's point of view, the filter can be viewed as performing a filtering operation, or as providing integration gain. In the former context, the lowpass filter reduces the time variations or ac components at the output of the square law detector. This is equivalent to reducing σ^2, and to peaking up and narrowing the

two distributions about the mean value which in turn is the steady state dc value. Inasmuch as lowpass filters have a time constant, their output voltage response to a step change in the input is an exponential ramp (corresponding to integrating a charge on a capacitor). In this sense the lowpass filter may be regarded as an integrator that improves SNR with time.

Figure 5-3b is a plot of the steady-state dc voltage at the output of the lowpass filter as a function of $\rho = \tau_\varepsilon/\tau_c$ where τ_ε is the error in code alignments. The ordinate is normalized with respect to the construction due to thermal noise alone, $v_N = k\ Teq\ B$. It is assumed that:

1) The receiver has an ideal AGC system which maintains total energy into the despreader constant

2) An ideal PN code with no minor correlation peaks

3) Data modulation effects are minor, but data and doppler bandwidths are important

4) The bandpass filter's bandwidth is 1.7 MHz with an ideal response

5) All spectral densities near the center of the band are relatively flat.

The sidelobe peaks evident in Figure 5-3b occur if ρ is an integer and are caused by the energy in the uncorrelated carrier that passes through the bandpass filter to the square-law detector.

The despreader designer is required to establish a threshold voltage for the threshold detector which is used to indicate that the received and locally generated codes are sufficiently close to alignment that the code tracking loop can pull in. This is equivalent to choosing a voltage higher than the peaks that occur when ρ is an integer other than zero, and lower than the peak that occurs when $\rho = 0$. This seems to be reasonably straightforward for any single value of signal strength, C. Note, however, that it is not possible to select a single voltage that is acceptable for all possible values of signal strength. Also, the ratio of the main peak to sidelobe peaks becomes very small for the weaker signal approaching 1.60/1.10 = 1.455 at C = -98 dBm. Inasmuch as the threshold trigger must operate reliably for changes of voltage within a few percent of the threshold level, it would be desirable to improve this ratio - a matter which will be discussed further.

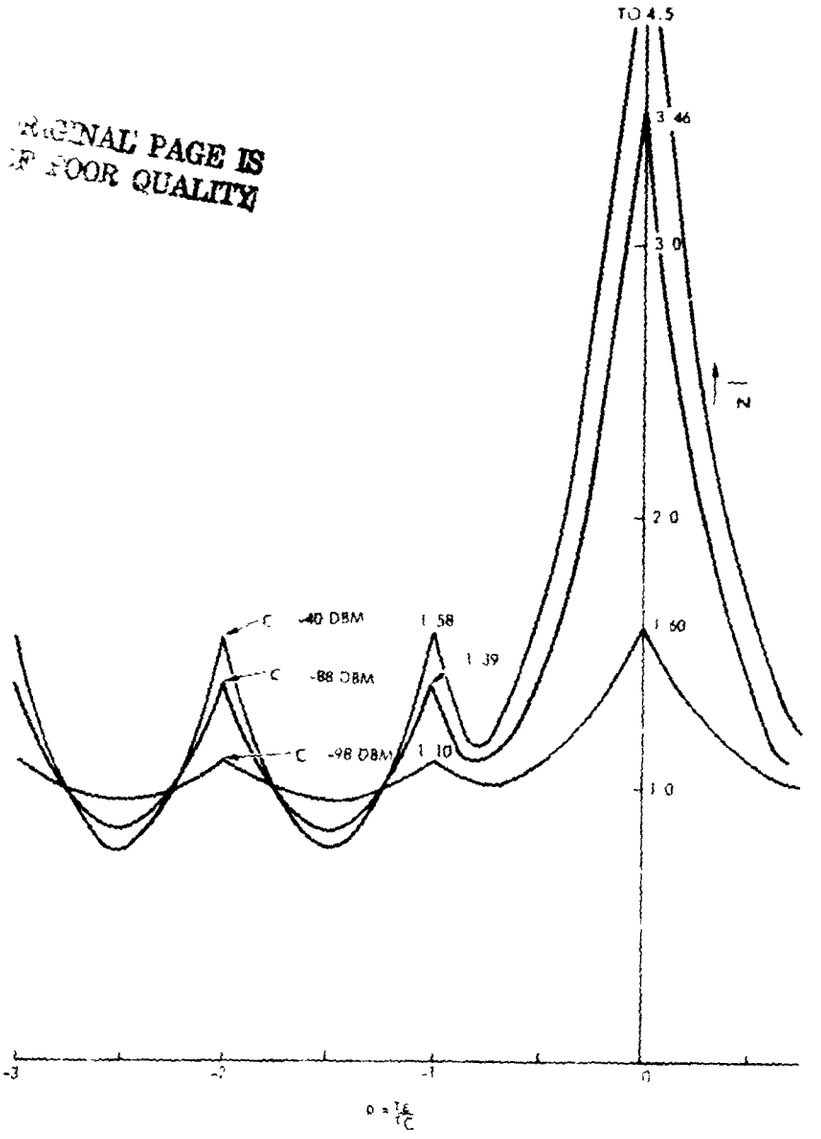

Figure 5-3b. Detector DC Output Voltage

5.2.1.1 Level Compensated Acquisition Subsystem

From the foregoing, it is desired to revise the acquisition strategy to permit setting a decision threshold for the weak signal case that will not cause a false trigger with a strong signal. The trick lies in normalizing with a voltage proportional to the peaks of the sidelobes of the correlation function of Figure 5-3b. Figure 5-4 is based on the data of Figure 5-3b, and corresponds to normalizing by the value of the sidelobe peaks. It is apparent that a single threshold can be established that is valid for all signal levels, although it would be triggered sooner by the stronger signals. Even so, ρ would be within one-half chip of alignment, and the tracking loop would pull the local PN code generator into synchronism with the received code.

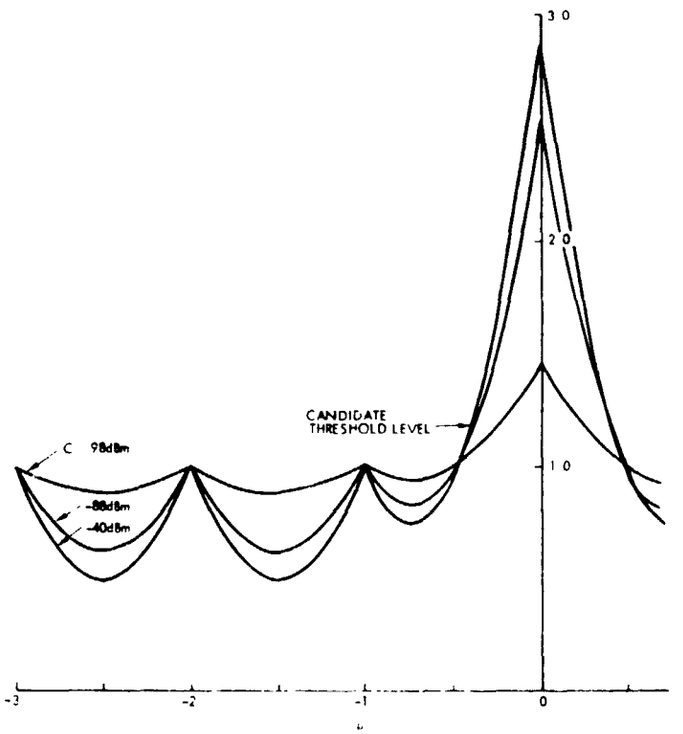

Figure 5-4. Normalized Correlation Voltage

The ratio of the peak of the correlation curve to the peaks of the sidelobe can be improved by subtracting a voltage from the output of the square law detector that equals the sidelobes peak. This is easily achieved with the circuit of Figure 5-5 which samples the received signal ahead of the correlator, generates a dc voltage at the output of the lowpass filter, and subtracts it from the lower lowpass filter output before presenting a voltage to the threshold detector. The output of the summing junction is always negative, except when $|\rho| < 1$.

The output of the upper channel is proportional to the sidelobe peaks because these peaks correspond to multiplying the received signal by a PN code whose crossings are in synchronism with the crossings of the received code, i.e., where ρ is an integer. But this corresponds to multiplying by a 1, since the product of a PN code with another code, or with a 1 yields a signal with equivalent spectra. Multiplying by 1 is equivalent to not multiplying at all, as illustrated in Figure 5-5. A level set attenuator is used, however, to compensate for the insertion loss of the balanced mixer (correlator).

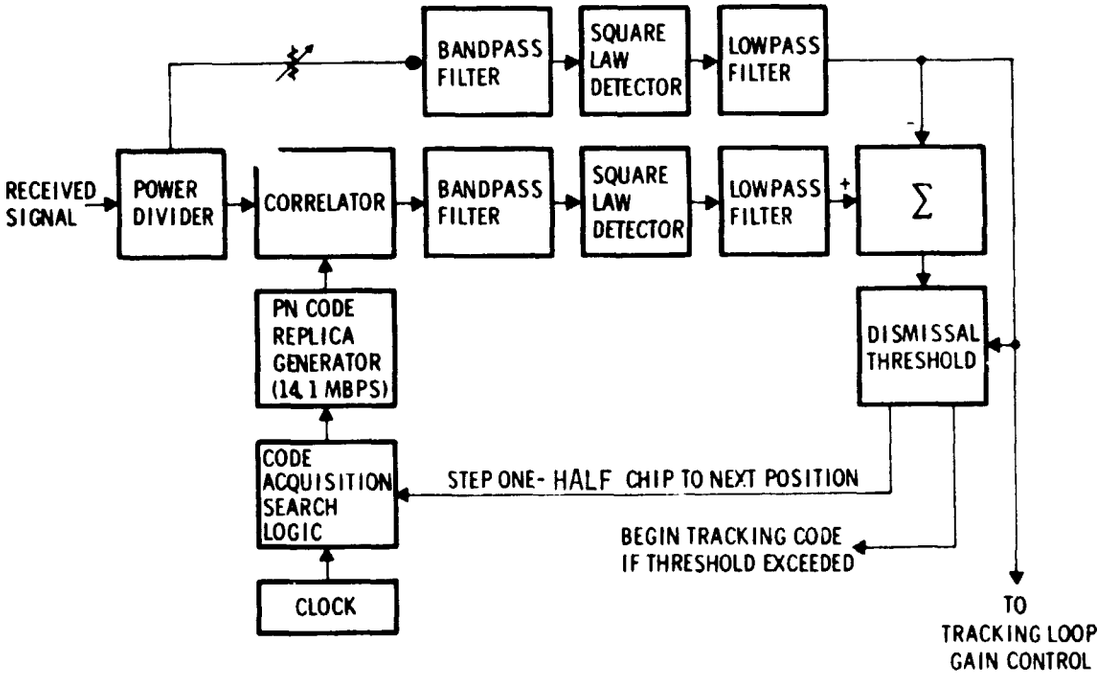

Figure 5-5. Block Elements of PN Code Acquisition Strategy

Normalization is obtained by making the dismissal threshold proportional to the signal level derived from the upper compensating channel.

Note that the dc voltage from the upper lowpass filter would not change with signal strength if the receiver has a perfect AGC. In reality, the upper channel simply provides a dc voltage that is proportional to the total energy from the power divider on the left. Inasmuch as an ideal receiver AGC would keep the total energy (signal + noise) constant, the despreader circuit has no way of knowing whether the SNR is high or low. Nevertheless, the parallel compensating circuit is quite useful in that it compensates for an imperfect AGC which would allow the total energy to vary by 1 dB, or $\pm$20 percent. Further, it provides a means of suppressing the voltage level into the threshold detector to improve the ratio of maximum-to-minimum voltage, and thereby to ease circuit sensitivity requirements.

To evaluate the accuracy of the curves in Figures 5-3 and 5-4, a series of laboratory measurements were made using one PN generator to simulate the data source, and a second PN generator to PN modulate the data. The second PN generator was hardwired through a controllable delay to a balanced demodulator. The results are shown in Figures 5-6 and 5-7. Data was taken for three levels of AGC performance, with variations of $\pm$1 dB. Figures 5-6b and 5-7b correspond to a -98 dBm signal level, and Figures 5-6c and 5-7c correspond to a -88 dBm signal level. The reader will be able to compare results by adding 1.0 to the ordinate of Figure 5-7 and comparing with Figure 5-4.

5.2.1.2 Statistical Characteristics of Signals for Acquisition Detection

For evaluating the performance of an acquisition detector, we shall examine the statistical parameters of the output signals of the IF bandpass filter for the in-sync and out-of-sync conditions. Let the received signal input to the despreader be represented by

$$r(t) = \sqrt{2P_\ell}\, P(t)\, d(t)\, \sin(\omega_{IF}t + \phi) + n(t) \qquad (5\text{-}5)$$

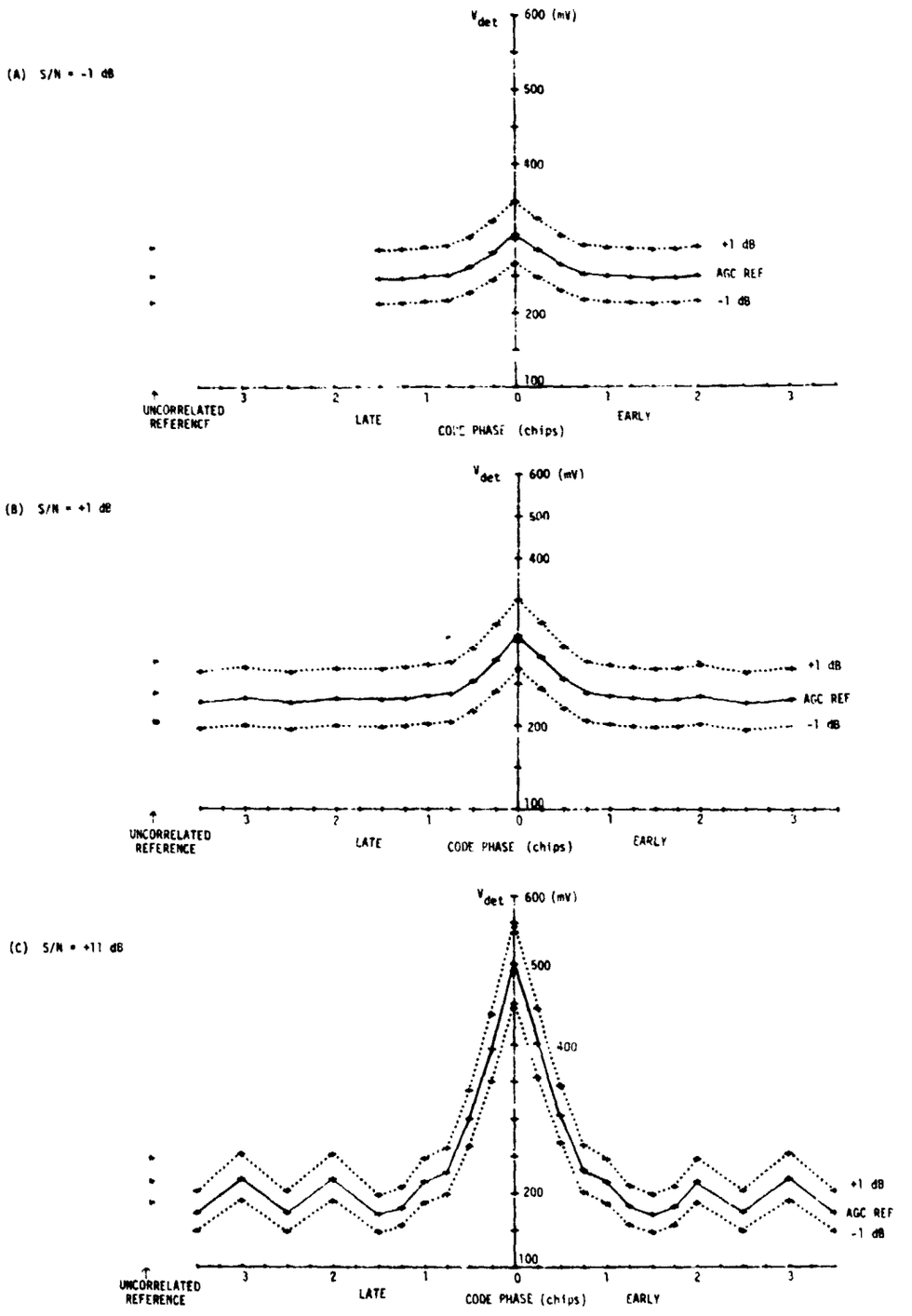

Figure 5-6. Detector Output Versus Code Phase for Low Data Rate

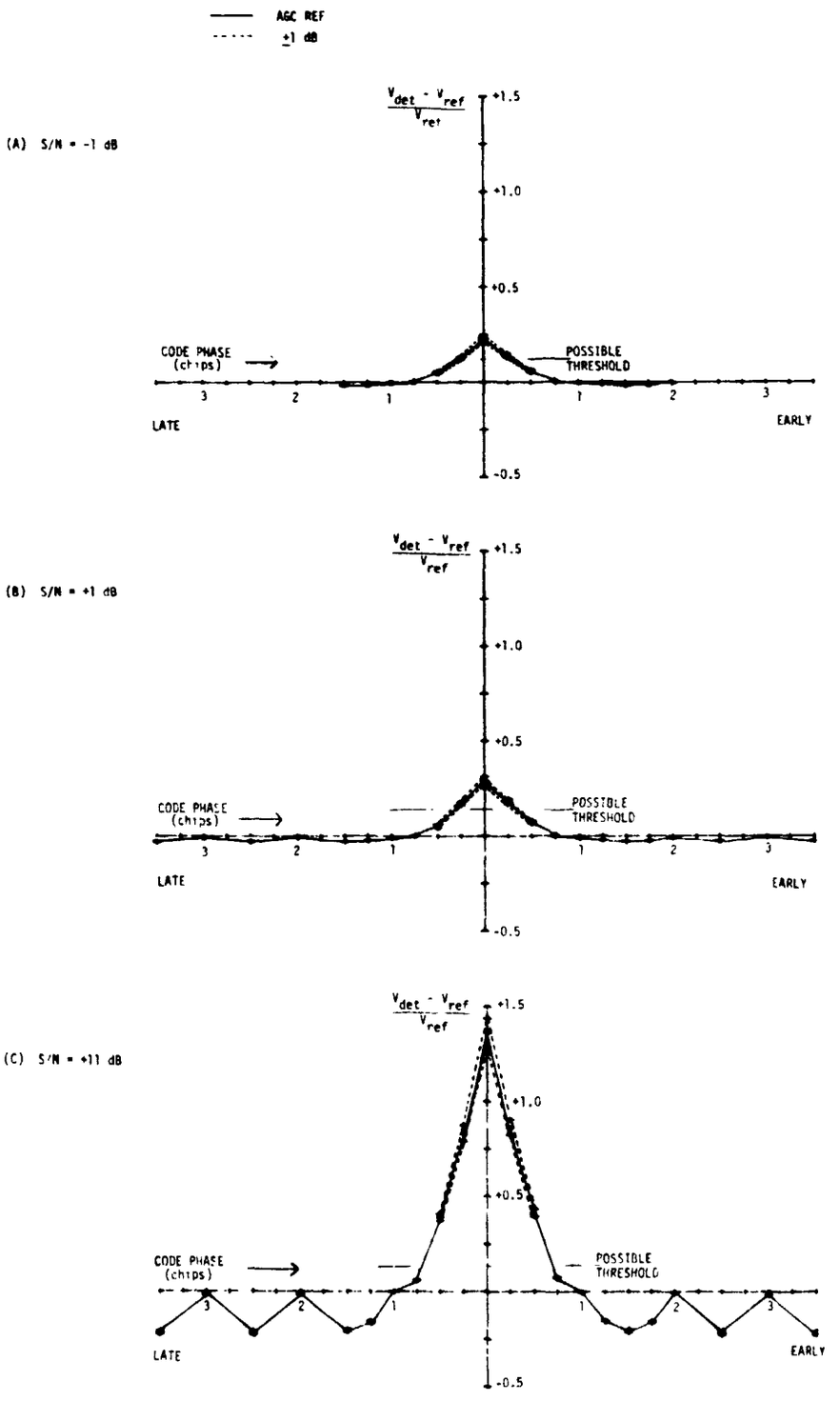

Figure 5-7. Normalized Outputs Versus Code Phase for Low Data Rate

where

P_ℓ = the signal power

$P(t)$ = the PN sequence waveform of $\{\pm 1\}$ with code length M

$d(t)$ = Manchester coded message $\{\pm 1\}$

$\frac{\omega_{IF}}{2\pi}$ = IF carrier frequency

ϕ = the carrier phase

$n(t)$ = bandpass Gaussian noise process with zero mean and spectral power density

$\frac{N_0}{2}$ (Two-sided)

$= \sqrt{2}N_c(t) \cos(\omega_{IF}t+\phi) - \sqrt{2}N_s(t) \sin(\omega_{IF}t+\phi)$

$N_c(t)$ and $N_s(t)$ = low pass Gaussian noise processes with the same mean and spectral power density as $n(t)$

The correlating signal resulted from multiplying $r(t)$ by the local PN sequence $P(t+\tau)$ is

$$y_1(t) = \sqrt{2P_\ell}\, c(t,\tau)d(t) \sin(\omega_{IF}t+\phi) + n(t)\, p(t+\tau) \qquad (5\text{-}6)$$

where

$c(t,\tau) = p(t)\, p(t+\tau)$

τ = time misalignment from the received sequence

This signal is filtered by the IF bandpass filter. Assuming that the data bandwidth is smaller than the IF bandwidth B_{IF} and that the data $d(t)$ may be further neglected for the simplicity of analysis, one may express the output of the IF filter as shown in Equation (5-7).

$$y_2(t) = y_1(t) \; * \; h_{IF}(t)$$

$$= \sqrt{2P_\ell} \; \{[c(t,\tau) \sin(\omega_{IF}t+\theta)] \; * \; h_{IF}(t)\}$$

$$+ \{[n(t)\, p(t+\tau)] \; * \; h_{IF}(t)\} \qquad (5\text{-}7)$$

where

$h_{IF}(t)$ = the impulse response of the IF filter

$*$ denotes the convolution operation

One may examine the properties of $y_2(t)$ from its power spectrum:

$$|Y_2(\omega)|^2 = \frac{P_\ell}{2} [S_p(\omega+\omega_{IF},\tau) + S_p(\omega-\omega_{IF},\tau)] \; |H_{IF}(\omega)|^2$$

$$+ [|S_n(\omega)|^2 \; * \; S_{pn}(\omega)] \; |H_{IF}(\omega)|^2 \qquad (5\text{-}8)$$

where

$S_p(\omega,\tau)$ = the power spectrum of $c(t,\tau)$

$S_{pn}(\omega)$ = the power spectrum of $p(t)$

$|S_n(\omega)|^2$ = the power spectrum of $n(t)$

$$= \begin{cases} \frac{N_o}{2} & \text{for } |\omega-\omega_{IF}| < B_n \quad \text{(Noise bandwidth)} \\ 0 & \text{elsewhere} \end{cases}$$

and

$H_{IF}(\omega)$ = the transfer function of the IF filter

Here it has been assumed that the p(t) and n(t) are statistically independent.

It is known that the spectra of a PN code p(t) and its correlating signal P(t) P(t+τ) for a large code length can be approximately expressed as: [6]

$$S_{pn}(\omega) = T_c \operatorname{sinc}^2 \left(\frac{\omega T_c}{2}\right) \tag{5-9a}$$

and

$$S_p(\omega,\tau) = \begin{cases} T_c \left|\frac{\tau}{T_c}\right|^2 \operatorname{sinc}^2 \left(\frac{|\tau|}{T_c}\frac{\omega T_c}{2}\right) \\ \quad + \left(1 - \frac{|\tau|}{T_c}\right)^2 \operatorname{sinc}^2 \left[\left(1 - \frac{|\tau|}{T_c}\right)\frac{\omega T_c}{2}\right] S_\delta(\omega) \\ \qquad\qquad \text{for } |\tau| < T_c \\ T_c \left[\left(\frac{|\tilde{\tau}|}{T_c}\right)^2 \operatorname{sinc}^2 \left(\frac{|\tilde{\tau}|}{T_c}\frac{\omega T_c}{2}\right)\right. \\ \quad \left. + \left(1 - \frac{|\tilde{\tau}|}{T_c}\right)^2 \operatorname{sinc}^2\left(\left(1 - \frac{|\tilde{\tau}|}{T_c}\right)\frac{\omega T_c}{2}\right)\right] \\ \qquad\qquad \text{for } |\tau| > T_c \end{cases} \tag{5-9b}$$

where

$\tilde{\tau} \equiv \tau$ in reduced modulo in $(0, T_c)$

$$S_\delta(\omega) = 2\pi \sum_{n=-\infty}^{\infty} \delta\left(\omega - \frac{2\pi n}{T_c}\right)$$

$\delta(\omega)$ = a delta function

$$\operatorname{sinc} x = \frac{\sin x}{x}$$

Two conditions - in-sync and out-of-sync will be discussed separately. First for $\tau > T_c$, the out-of-sync condition, the signal $c(t,\tau)$ remains a wide spread spectrum. The first term in the expression (5-8) shows that

the modulated signal $c(t,\tau)\sin(\omega_{IF}t + \theta)$ may be approximated as a noise-like signal since its power spectrum, a frequency shifted spectrum of $c(t,\tau)$, is filtered by $|H_{IF}(\omega)|^2$ and remains nearly flat in the bandwidth of the IF filter. In the sequel, it is, therefore, reasonable to assume that, for the out-of-sync condition, the first term in $y_2(t)$ behaves like a bandpass Gaussian random process with a zero mean (in fact, one can show that its mean is proportional to $\frac{-1}{M}$) and with an equivalent variance σ_1^2 as defined by

$$\sigma_1^2 = P_\ell \int_{-\infty}^{\infty} S_p(\omega-\omega_{IF},\tau)\ |H_{IF}(\omega)|^2\ \frac{d\omega}{2\pi} \tag{5-10}$$

$$= [\tilde{\rho}^2\ C_1 + (1 - \tilde{\rho})^2\ C_2]\ P_\ell$$

where

$$C_1 = \frac{T_c}{2\pi} \int_{-\infty}^{\infty} \text{sinc}^2\left(\tilde{\rho}\ \frac{(\omega-\omega_{IF})T_c}{2}\right)\ |H_{IF}(\omega)|^2\ d\omega \tag{5-11a}$$

$$C_2 = \frac{T_c}{2\pi} \int_{-\infty}^{\infty} \text{sinc}^2\left((1-\tilde{\rho})\ \frac{(\omega-\omega_{IF})T_c}{2}\right)|H_{IF}(\omega)|^2\ d\omega \tag{5-11b}$$

$\tilde{\rho}$ = the normalized variable of $\tilde{\tau}\left(= \frac{\tau}{T_c}\right)$

The value of the parameter $\tilde{\rho}$ is defined to be in the interval [0,1]. For an ideal IF filter, i.e., $H_{IF}(\omega) = 1$ for $|\omega-\omega_{IF}| < \frac{B_{IF}}{2}$ and 0 elsewhere, the expression C_1 and C_2 can be simplified as

$$C_1 = \frac{T_c}{2\pi} \int_{-B_{IF}/2}^{B_{IF}/2} \text{sinc}^2\left(\tilde{\rho}\ \frac{\omega T_c}{2}\right)\ d\omega \tag{5-12a}$$

$$C_2 = \frac{T_c}{2\pi} \int_{-B_{IF}/2}^{B_{IF}/2} \text{sinc}^2\left((1-\tilde{\rho})\ \frac{\omega T_c}{2}\right)\ d\omega \tag{5-12b}$$

Thus, we may conclude that, for out-of-sync condition, the signal $y_2(t)$ can be approximately represented as a bandpass Gaussian random process and denoted by

$$y_0(t) = \sqrt{2}\, N_{oc}(t) \cos \omega_{IF} t - \sqrt{2}\, N_{os}(t) \sin \omega_{IF} t \qquad (5\text{-}13)$$

where $N_{oc}(t)$ and $N_{os}(t)$ are two lowpass Gaussian random processes with zero mean and with the same variance $\sigma^2_{NOC} = \sigma^2_{NOS}$. The sum of these two variances is

$$\sigma^2_{NO} = \sigma^2_{NOC} \quad \sigma^2_{NOS} = \sigma^2_1 + N_o B_{IF} \qquad (5\text{-}14)$$

where

$N_o B_{IF}$ = the variance of the channel noise.

Here is has been assumed that the noise bandwidth B_n is much larger than $\frac{1}{T_c}$. Substituting the expression (5-10) into Equation (5-14), one has the variance of $y_0(t)$ as follows:

$$\sigma^2_{NO} = N_o B_{IF} (1 + k_1) \qquad (5\text{-}15)$$

where

$$k_1 = [\tilde{\rho}^2 C_1 + (1-\tilde{\rho})^2 C_2] (SNR)_{IF} \qquad (5\text{-}16)$$

$(SNR)_{IF}$ = the IF signal-to-noise ratio

$$= \frac{P_\ell}{N_o B_{IF}}$$

This shows that the variance of the equivalent random process $y_0(t)$ for the out-of-sync is not only a function of channel noises, but also a function of the IF signal-to-noise ratio, system parameters C_1 and C_2, and the position of the timing misalignment β. Next, we shall examine the signal $y_2(t)$ for the in-sync condition. As indicated in Equation (5-9b), the signal $c(t,\tau) \sin(\omega_{IF} t+\theta)$ consists of two types of components - one in spread and the other despread. The component with spreading spectrum will also be treated as a part of noises while the despread part, a

stream of delta functions, is filtered by $H_{IF}(\omega)$ so that only the dc component remains in the output of the IF filter. One may express the signal $y_2(t)$ for the in-sync case as follows:

$$y_1(t) = \sqrt{2}\,(1-|\rho|)\,\sqrt{P_\ell}\,\sin(\omega_{IF}t-\theta) + N_I(t) \qquad (5\text{-}17)$$

where

ρ = the normalized time misalignment $(\frac{\tau}{T_c})$

θ = phase angle of the despread signal

$$N_I(t) = \sqrt{2}N_{IC}(t)\cos\omega_{IF}t - \sqrt{2}N_{IS}(t)\sin\omega_{IF}t \qquad (5\text{-}18)$$

$N_{IC}(t)$ or $N_{IS}(t)$ = a lowpass Gaussian random process with zero mean and variance $\sigma_{NI}^2/2$

$$\sigma_{NI}^2 = N_0 B_{IF} + \rho^2 C_3 P_\ell \qquad (5\text{-}19)$$

$$C_3 = \frac{T_c}{2\pi}\int_{-\infty}^{\infty}\mathrm{sinc}^2\left(\rho\,\frac{(\omega-\omega_{IF})T_c}{2}\right)|H_{IF}(\omega)|^2\,d\omega \qquad (5\text{-}20)$$

Similarly, the variance σ_{NI}^2 can be expressed as

$$\sigma_{NI}^2 = N_c B_{IF}\,(1 + k_2) \qquad (5\ 21)$$

where

$$k_2 = (SNR)_{IF}\,\rho^2\,C_3$$

The parameter k_2 is functions of IF signal-to-noise ratio and timing misalignment ρ. The signal $y_I(t)$ is also bandlimited to $(\omega_{IF} - \frac{B_{IF}}{2}, + \frac{B_{IF}}{2})$.

The in-sync and out-of-sync signals, $y_I(t)$ and $y_o(t)$, formulated above, are inputted to the square law detector then integrated. Based on a test statistic, the output of the integrator, the acquisition detector decides whether the PN code is in-sync. Sampling approach will be used for the formulation of the test statistic of the acquisition detection.

Finally, the timing misalignment ρ used in the above must be specified for the following study. Here, we shall assume that the ρ for the in-sync case is in average equal to $\frac{\Delta c}{2}$, half of acquisition steps adopted in the acquisition scheme. The Δc is the step size of the local PN code timing to advance (or to retard) whenever the acquisition detection declares "out-of-sync." When the local PN code is completely misaligned with the received code (out-of-sync case $\rho > 1$), the correlating signal remains in spread. Hence, it is treated as a part of noises. Although the amount of power contributed by this spread signal depends on the relative misalignment to the received signal, as indicated by (5-15), we shall consider this noise power in the worst case by assuming $\tilde{\rho} = 0$.

Effect of Doppler

As discussed previously, it is clear that the output of the integrator is proportional to the total signal and noise power passing through the IF bandpass filter within the integration time (or dwell time). However, in the practical case, the relative alignment of the local and received codes does not remain constant throughout the dwell time, because of the doppler effect on the received signal. Therefore, it is necessary to take into account the effect of doppler slippage on the signal and noise power input to the integrator.

For the out-of-sync case, no correction is needed to include the doppler effect since the worst case was considered. However, for the in-sync case, the factor $|\rho|^2$ in equation (5-21) must be modified accordingly.

Let f_{cd} be the doppler code rate and ρ_o be the initial misalignment at t=0, then the variation of $\rho(t)$ is

$$\rho(t) = \rho_o + f_{cd}t$$

When $f_{cd}=0$, the factors $(1 - |\rho|)^2$ and ρ^2 should be $(1 - |\rho_o|)^2$ and ρ_o^2, respectively. But, when $f_{cd}\neq 0$, the correction factor for the factor $(1 - |\rho|)^2$ is

$$L_{DD1} = \frac{1}{(1 - |\rho_o|)^2 T} \int_0^T (1 - |\rho(t)|)^2 \, dt$$

Assume that the dwell time is so small that $f_{cd}T_D$ is only a fraction of ρ_o. In general this should be true, otherwise it would be very difficult in aligning the local and received codes. It is assumed for the worst case consideration that the doppler code rate f_{cd} is positive. Then, substituting $\rho(t)$ into the integral, one has

$$L_{DD1} = 1 - \frac{|f_{cd}| T}{1-|\rho_o|} + \frac{(f_{cd}T)^2}{3(1-|\rho_o|)^2} \qquad (5\text{-}22)$$

Similarly, one can compute the correction factor for $|\rho|^2$ as follows:

$$L_{DD} = 1 + \left|\frac{f_{cd}T}{\rho_o}\right| + \frac{(f_{cd}T)^2}{3\,\rho_o^2} \qquad (5\text{-}23)$$

In addition to the consideration of doppler effect, filtering and circuit loss prior to the despreader L_c and IF bandpass filter loss L_f are also taken into account in the evaluation of the operating characteristics of the acquisition detection.

In summary, the system parameter σ_{NI}^2 becomes

$$\sigma_{NI}^2 = N_o B_{IF} (1 - k'^2) \qquad (5\text{-}24)$$

where $k'^2 = (SNR)_{IF} \rho_o^2 C_3 L_{DD2}$.

During acquisition the worst-case predetection SNR is given by

$$X = \frac{P_L L_c L_f L_{\rho o} L_{DD}}{N_o(IN)\, B_{IF}} \tag{5-25}$$

where

L_c = all circuit losses prior to despreader

L_f = despreader BPF loss

An interesting result here is that the ratio of out-of-sync noise power density $N_o(OUT)$ to the in-sync noise power density $N_o(IN)$ is always greater than unity. The ratio of the in- and out-of-phase noise densities will be useful later and is given by

$$R = \frac{N_o(OUT)}{N_o(IN)} \tag{5-26}$$

5.2.1.3 Determining the Dwell Time and the Threshold For P_D and P_{Fd}

The preceding section has reduced the synchronizati .. problem to one of deciding between the two hypotheses

$$H_o: y(t) = n_{OUT}(t) \tag{5-27}$$

$$H_1: y(t) = (1 - |\rho|)\sqrt{2P_\ell}\, \ell(t) \sin(\omega_{IF} t + \phi) + n_{IN}(t)$$

This, of course, is almost identical to the classic radar detection problem described by Marcum [7], except that the spectral densities of the two noises are different. However, this difficulty can be easily overcome. Marcum shows that a nearly optimum detector consists of a square-law device followed by a post-detection integrator (PDI) and a threshold comparator. The output of the square-law device near dc is proportional to the total energy in the input signal y(t). The PDI acts to increase the SNR of its input by roughly $N = BT_D$. The output of the PDI after T_D seconds is compared to a threshold which is chosen to meet the requirements on P_d and P_{fa}.

For large N, Marcum shows that the normalized threshold voltage required to meet $P_d = 0.99$ is

$$\theta \triangleq \frac{V_{TH}}{N_o(IN)\ B} = 1 + X - 2.32\sqrt{\frac{1+2X}{N}} \qquad (5\text{-}28)$$

Furthermore, the pair N and θ yield a probability of false alarm per sync position equal to

$$P_{fa} \cong \sqrt{\frac{N}{2\pi}}\left(\frac{\theta}{R}\right)^N \frac{\exp[-N(\theta/R-1)]}{N(\theta/R-1)+1} \qquad (5\text{-}29)$$

Equations (5-25), (5-26), (5-28), and (5-29) provide the solution to the detection problem. First, a value of N is chosen and $T_D = N/B$ is used to determine X from (5-25). Equation (5-28) then yields a value for θ, and then (5-29) gives a value for P_{fa}. If $P_{fa} < 10^{-6}$, the process is complete. Otherwise, a larger N is chosen and the process repeated iteratively by a computer program.

5.2.1.4 Setting the Threshold Voltage

Consider the channel shown in Figure 5-8. This channel can be used to measure the out-of-sync noise power $N_o(OUT)\ B$, and thus can be used to set the threshold voltage. The received spread signal r(t) is passed through a BPF and a square-law device identical to that in the detection channel. The spectrum of this signal is well known (See [8]), and the portion of this spectrum in the frequency band (-B, B) is shown in Figure 5-9. If this signal is passed through a narrow lowpass filter (LPF), the output voltage will be nearly constant with magnitude equa. to the dc voltage, or

$$V_{LPF} \approx N_o(OUT)\ B \qquad (5\text{-}30)$$

where N_{OUT} is given by Equation (5-15) with $|\tilde{\rho}| = 1$ and the required threshold voltage is given by (5-28).

Figure 5-8. Channel for Setting Detection Threshold Voltage

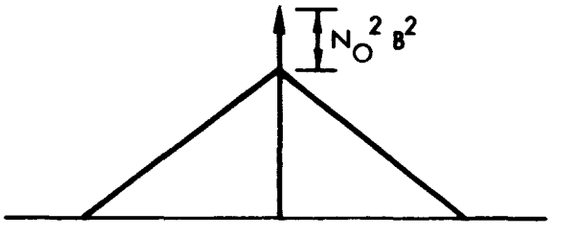

Figure 5-9. Spectrum of Squared Noise About DC

It is now necessary to determine a threshold value to assure that the system will stay in lock during code tracking. The acquisition circuit will continue to operate in the same fashion as before, but with the threshold voltage changed to ensure a reasonable probability of false dismissal throughout the duration of one pass by each TDRSS satellite. The worst case will occur near the beginning or end of each pass when the signal is weakest, thus the interval between false dismissals should be longer than the part of each pass when the signal is weakest.

The probability of false dismissal in any interval T is given by

$$P_{FD} = 1 - P_{DT}^{N}$$

where P_{DT} is the probability of detection per trial, and N is the number of dismissal opportunities, given by T/T_D. Rearranging, leads to

$$P_{DT} = (1 - P_{FD})^{\frac{T_D}{T}}$$

During the tracking mode P_{DT} is set to 0.99 for a T = 100 minute interval by appropriate lowering of the threshold voltage.

5.2.1.5 Tracking Analysis

A timeshared early late tracking loop will be used in the despreader. In such a loop the incoming signal is alternately correlated with the early and late versions of the local PN code and the error signal is obtained by alternately inverting the demodulated correlation signal and lowpass filtering the result.

The block diagram of the timeshared loop is shown in Figure 5-10. The received signal is multiplied by the local code which is alternately obtained from an early or late port of the PN code generator, in accordance with the binary squarewave, q(t). The output of the square law detector will be amplitude-modulated if the code loop is not in synchronization. The output is product-detected, with the output of the product detector used an an error signal which is applied to the VCO through the loop filter.

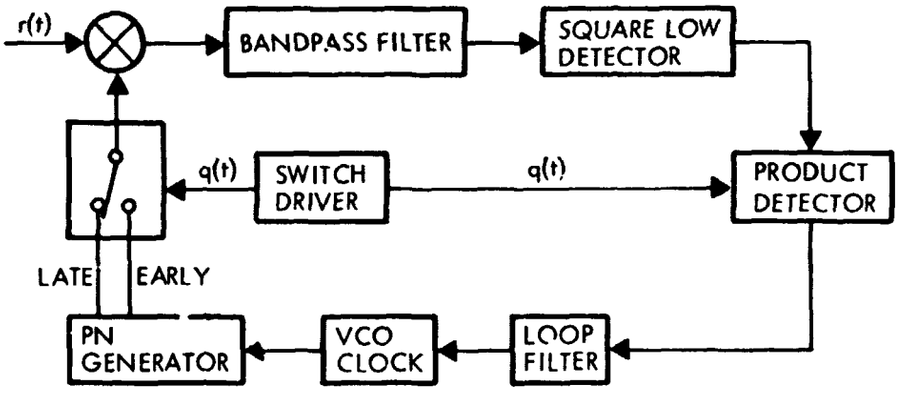

Figure 5-10. The Time-Shared Early-Late Loop for Tracking a PN Code

For the following, the assumed signal parameters are summarized in Table 5-1. Note that the tracking code doppler differs from the acquisition doppler. The reason is that when the sync acquisition circuit declares sync, the code clock may be offset by up to ±400 chips/sec, so the maximum doppler seen by the loop during acquisition is ±400 chips/sec.

5.2.1.6 Linear Loop Analysis

The mathematical model for the linear loop is shown in Figure 5-11. The constant K_d is the gain of the detector characteristic and is proportional to the signal strength. The constant K_V is the VCO gain, and the constant K_G is an arbitrary gain which will be chosen to meet some specification on performance. The requirements on this loop are that the degradation in the data detection channel due to the loop timing jitter be less than 1 dB and that the average total despreader acquisition time be less than 10 seconds.

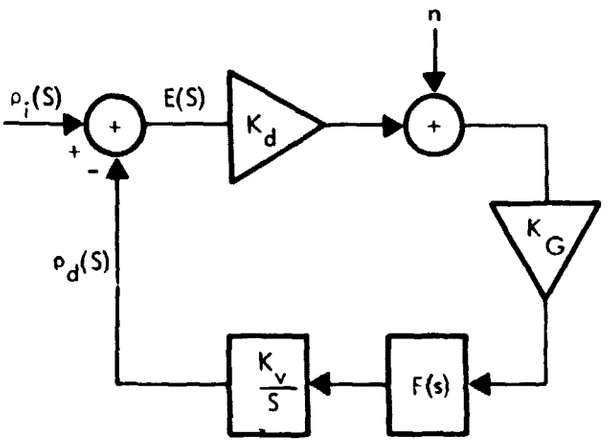

Figure 5-11. The Linear Model of the Loop

The loop input signal can be represented by

$$\rho_i(t) = \rho_{io} + \dot{\rho} \qquad (5\text{-}31)$$

where $\rho_i(t)$ is the normalized difference between the true delay and the acquisition circuit's estimate. From Figure 5-11 the closed loop transfer function is

$$H(s) \triangleq \frac{\rho_o(s)}{\rho_i(s)} = \frac{\frac{GF(s)}{s}}{1 + \frac{GF(s)}{s}} \tag{5-32}$$

where s is the LaPlace variable and

$$G = K_d\, K_V\, K_G \tag{5-33}$$

is called the loop gain.

The loop filter is assumed to be an imperfect integrator, or

$$F(s) = \frac{1 + s\,\tau_2}{1 + s\,\tau_1},\ \tau_1 >> \tau_2 \tag{5-34}$$

A circuit which closely approximates this transfer function is shown in Figure 5-12. From this figure, the filter time constants are given by

$$\tau_1 = (R_1 + R_2)C \tag{5-35}$$
$$\tau_2 = R_2\, C$$

Additionally, the circuit has a dc gain given by $G_{DC} = -R_3/R_1$.

Substituting (5-34) into (5-32) yields

$$H(s) = \frac{1 + \frac{2\zeta s}{\omega_n}}{1 + (2\zeta + \frac{\omega_n}{G})\frac{s}{\omega_n} + \frac{s^2}{\omega_n^2}} \tag{5-36}$$

where

$$\zeta \cong \frac{\tau_2}{2}\sqrt{\frac{G}{\tau_1}} \tag{5-37}$$

is called the loop damping factor, and

$$\omega_n = \sqrt{\frac{G}{\tau_1}} \tag{5-38}$$

is called the loop natural frequency. Typically ζ is chosen to be $1/\sqrt{2} = 0.707$ so that the loop is critically damped. The loop transfer function for this case is then

$$H(s) = \frac{1 + \sqrt{2}\,\frac{s}{\omega_n}}{1 + \left(\sqrt{2} + \frac{\omega_n}{G}\right)\frac{s}{\omega_n} + \frac{s^2}{\omega_n^2}} \tag{5-39}$$

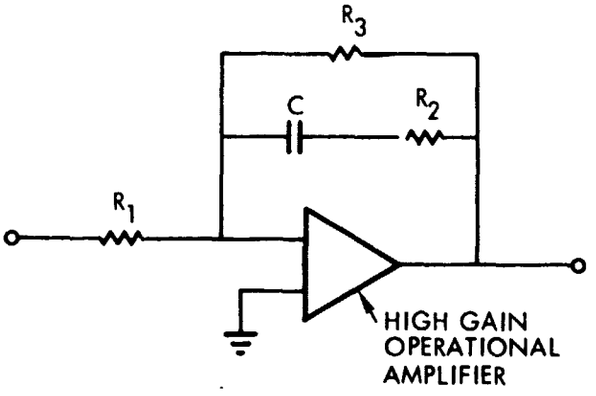

Figure 5-12. Loop Filter Circuit

One of the contributors to the final timing error can now be computed. This error is the mean steady-state tracking error due to the input signal alone. From the definition of H(s) in (5-32), the loop error signal is related to the input signal by

$$\varepsilon(s) = \rho_i(s)\,[1 - H(s)] \tag{5-40}$$

From (5-31)

$$\rho_i(s) = \frac{\rho_{io}}{s} + \frac{\dot{\rho}}{s^2} \tag{5-41}$$

The mean steady-state error signal is given by

$$\bar{\varepsilon} \triangleq \lim_{t\to\infty} \varepsilon(t) = \lim_{s\to 0} s\varepsilon(s) \tag{5-42}$$

Substituting (5-40) and (5-41) into (5-42) yields

$$\bar{\varepsilon} = \frac{\dot{\rho}}{G} \tag{5-43}$$

Equation (5-43) states that the mean steady-state error is caused by the lag in tracking the code doppler and can be made arbitrarily small by increasing the loop gain G, as would be expected.

The other final timing error contributor is due to the input noise. The standard deviation of the steady-state error signal, called the timing jitter, has been derived by Hartmann [9]

$$\sigma_\varepsilon = \sqrt{\left(\frac{B_L}{B}\right)\left(\frac{0.905}{SNR} + \frac{0.453 - \frac{1}{10\,B\,T_q}}{\left(1 - \frac{\Delta T}{\tau_c}\right)^2 (SNR)^2}\right)} \tag{5-44}$$

In (5-44) ΔT is the amount the early-late code is early or late. It is assumed to be

$$\frac{\Delta T}{\tau_c} = \pm \frac{1}{2} \tag{5-45}$$

A loop with $\Delta T = \pm \frac{1}{2} \tau_c$ is termed a "one-Δ loop" since the detector characteristic is linear over the interval $(-\tau_c/2, \tau_c/2)$ with length one chip time. Also in (5-44), $1/2\ T_q$ is the frequency of the squarewave $q(t)$, and B_L is the loop bandwidth defined by

$$B_L = \frac{1}{2\pi} \int_0^\infty |H(i\omega|^2\, d\omega \tag{5-46}$$

Substituting (5-39) into (5-46) yields, for large G

$$B_L = 0.53\ \omega_n \text{ Hz} \tag{5-47}$$

In order to choose B_L or ω_n, the acquisition trajectories of the feedback loop must be considered. Nielsen [10] shows that the loop will acquire or lock onto the code as long as $\omega_n \geq \dot{\rho}_a$. It is therefore assumed that

$$\omega_n = 2\Delta\dot{\rho}_a \tag{5-48}$$

Note that here $\dot{\rho}_a$ is the acquisition code doppler. Thus with $\dot{\rho}_a = 400$

$$\omega_n = 800 \text{ rad/sec} \tag{5-49}$$

and from (5-47)

$$B_L = 424 \text{ Hz} \tag{5-50}$$

Now substituting (5-45) and (5-50) into (5-44) and assuming that 1/10 BT_q is negligible

$$\sigma_\varepsilon = 0.039 \text{ chips} \tag{5-51}$$

The loop gain G can now be chosen to make $\bar{\varepsilon}$, as given by (5-43), smaller than σ_ε. For $\dot{\rho}$ = 900 chips/sec and

$$G = 10^5 \tag{5-52}$$

Then

$$\bar{\varepsilon} = 0.0071 \text{ chips} \tag{5-53}$$

The sum of (5-51) and (5-53) will be called the total timing jitter

$$\sigma_{TOT} = \sigma_\varepsilon + \bar{\varepsilon} = 0.04 \text{ chips} \tag{5-54}$$

5.2.2 Recommended Despreader Design

During the course of the uplink study several alternate despreader designs were considered. These included both sequential and adaptive PN acquisition techniques which promised somewhat faster acquisition times. These approaches are characterized by increased complexity and higher associated risk/cost and were also judged to be somewhat less flexible than the rather straightforward approach recommended within the available resources of this study effort.

The baseline despreader, shown in Figure 5-13, is a slight modification of the S-band approach. For an improved acquisition performance the dual-frequency search of Figure 5-14 is incorporated. Filter bandwidths are changed and code phase dwell times are reduced by a factor of 4, otherwise the approach is identical to S-band. The despreader logic flow diagram is shown in Figure 5-15.

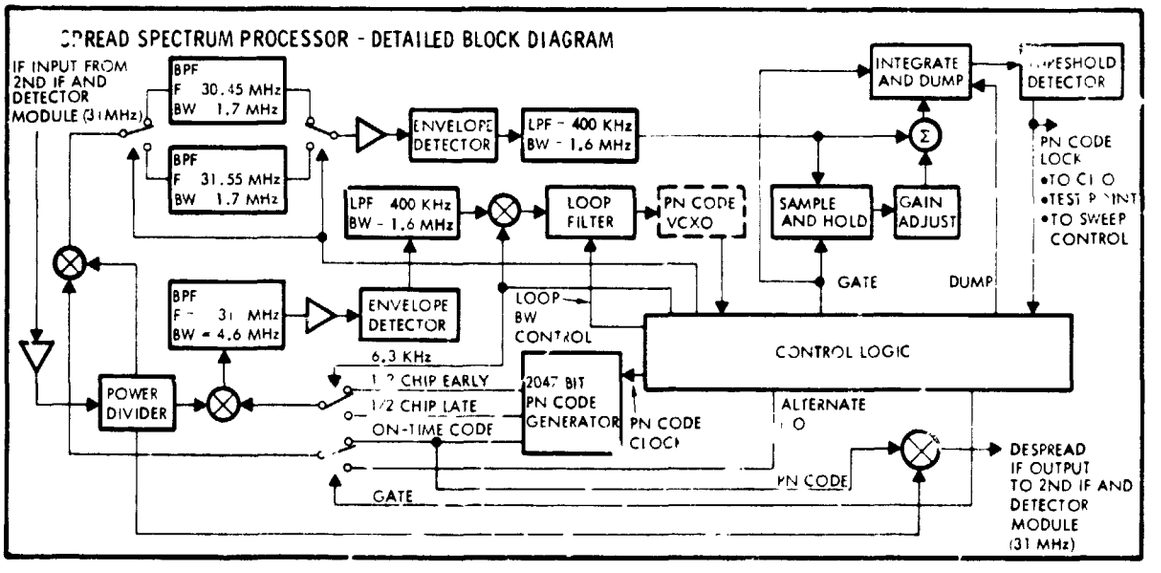

Figure 5-13. Baseline Despreader

The critical parameter having the most affect on performance is the allowable code phase dwell time, T_D. The dwell time must be consistent with $P_D = 0.99$, $P_{FA} = 10^{-6}$, and the C/N_0 into the despreader. Design point C/N_0's are derived in Table 5-2 with at least a 3 dB margin.

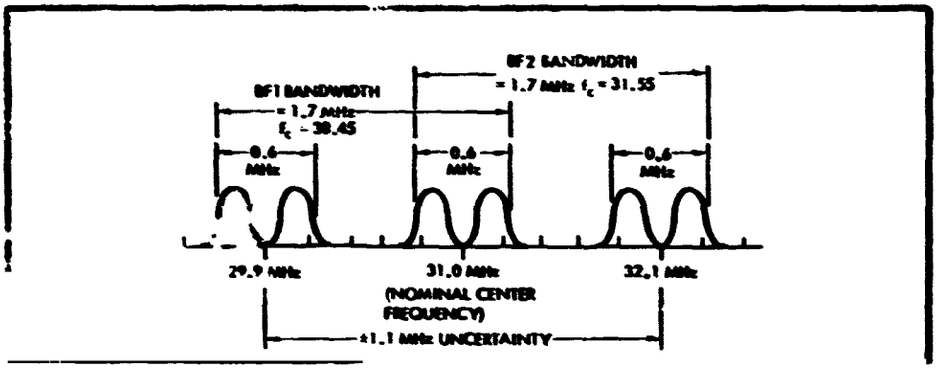

Figure 5-14. Two Bandpass Filters Used to Accommodate Total 2.2 MHz Frequency Uncertainty

Table 5-2. 3 dB Minimum Margin at Design-Point Carrier-to-Noise Densities

MINIMUM SIGNAL LEVEL FOR 10 SEC ACQUISITION (PS 3.2.1.2.2.1.2.1)	MINIMUM TDRS EIRP FOR ACQUISITION (RFP AMENDMENT NO. 1, CHANGES)
-102.0 dBm AT OUTPUT OF 34.6 dBi ANTENNA	36.6 dBw TDRS EIRP
+ 5.1 dB ΔGAIN OF 39.7 dBi ANTENNA	-207.7 dB SPACE LOSS
31.9 dB-°K SYSTEM NOISE TEMPERATURE (1549°K)	7.8 dB/°K G/T
-166.7 dBm/Hz N_o	-0.2 dB POLARIZATION AND TRACKING LOSS
69.8 dB-Hz C/N_o	65.1 dB-Hz C/N_o
66.0 dB-Hz DESIGN POINT	62.1 dB-Hz DESIGN POINT
3.8 dB MARGIN	3.0 dB MARGIN

Figure 5-16 is a plot of allowable dwell times vs P_{FA} for various values of C/N_o at a fixed detection probability of 0.991. The computer program which derives these curves accounts for all losses and degradations caused by 1) filtering prior to the despreader, 2) bandlimiting of despreader, 3) doppler code drift, 4) maximum quarter-chip offset of the half-chip increment search, and 5) increase in noise density caused by the PN code spectrum in the out-of-sync condition as discussed in Section 5.2.1. A dwell time of 155 μsec is chosen which is consistent with the P_D = 0.99; $P_{FA} = 10^{-6}$ requirement at 66.0 dB-Hz (adjusted - 102 dBm received power requirement). The time required for a complete doppler-expanded code search over two frequency bandwidths is 1.45 seconds (excluding false alarms). For P_D = 0.991, one complete search is required at 66.0 dB-Hz and five complete searches at C/N_o = 61.6 dB-Hz.

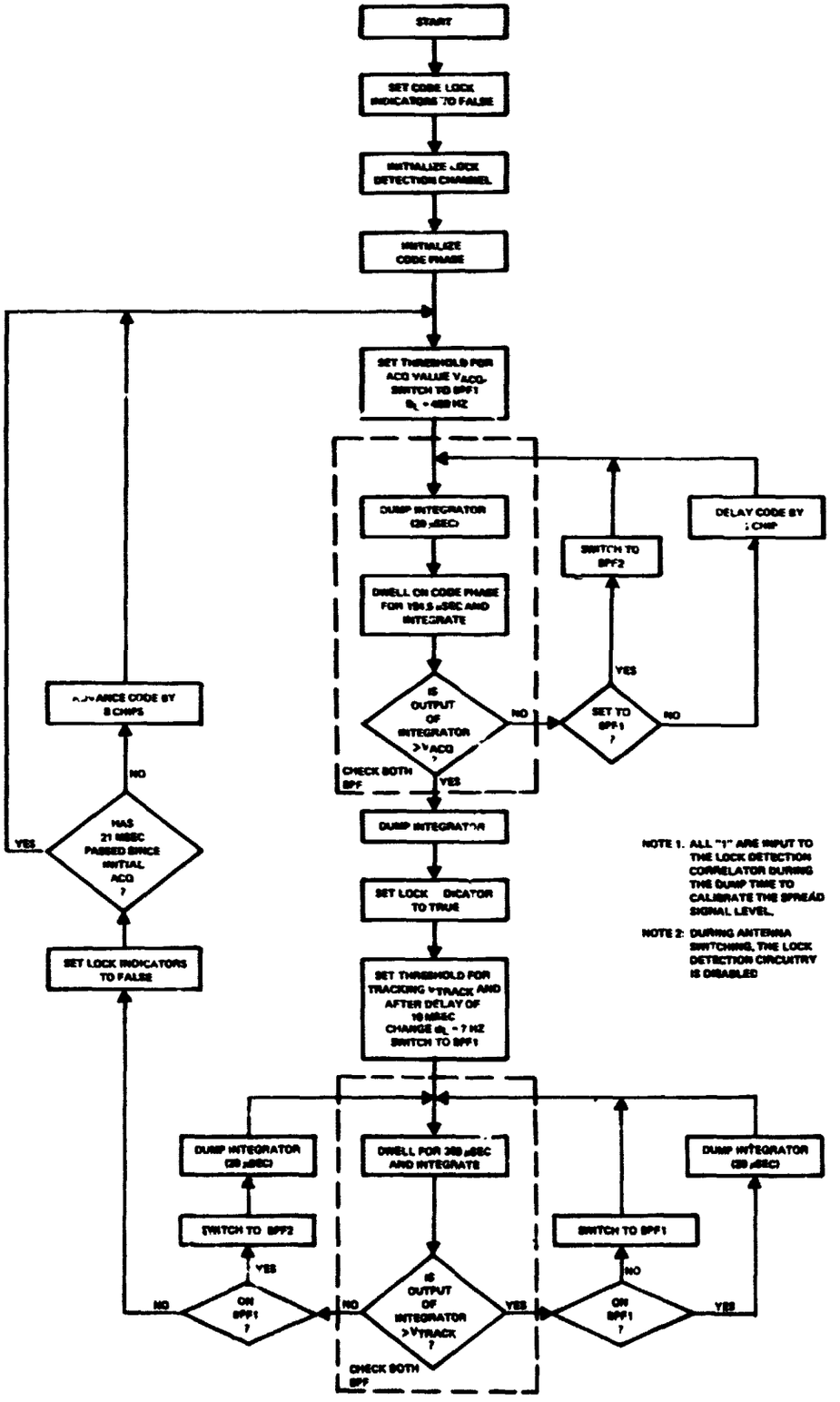

Figure 5-15. Code Acquisition and Tracking Logic Flow Diagram

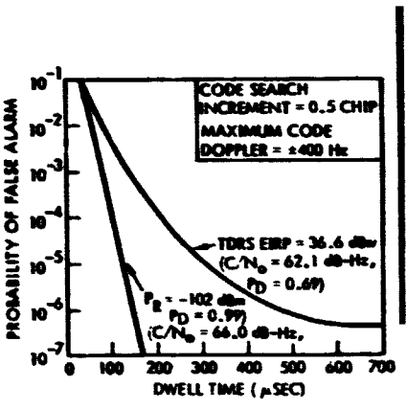

Figure 5-16. Dwell Time Versus P_{FA}

This can be seen by reference to Figure 5-16. Note that the design point dwell time corresponds to a $P_D = 0.61$, $P_{FA} = 10^{-3}$. If five sweeps are used $P_D = 1 - (.39)^5 = 0.991$. A single threshold check in tracking is sufficient to reduce false alarm probability to $\sim 10^{-10}$.

Code acquisition time is computed for an overall 99% probability. Therefore, sufficient time must be allocated for the active code search plus time penalties caused by false alarms. Hence, the quoted acquisition times are consistent with the following criteria: within time T_{ACQ} the probability of code sync is at least 0.99 and false alarms have dismissed with probability $1-10^{-6}$, i.e.,

$$P_r[\text{true sync in time } T_{ACQ}] = P_r[\text{code acquire, dismiss all false alarms}]$$

$$= (0.991)(0.999999) > 0.99$$

Analysis shows that for $C/N_0 = 66.0$ dB-Hz the number of false alarms < 1 with probability $1-10^{-6}$ and for $C/N_0 = 61.6$ dB-Hz the number of false alarms < 64 with probability $1-10^{-6}$. Reference to Figure 5-15 shows that the occurrence of a false alarm incurs a time penalty of a 10 msec delay plus 2 dwells of 309 sec each plus 2 integrator dumps of 20 μsec or a

total of 10.658 msec. Acquisition times consistent with the above criteria for the specified design points of C/N_0 = 66.0 dB-Hz and 61.6 dB-Hz are 1.64 and 8.99 seconds, respectively.

After indications of code acquisition the despreader switches to the track mode. During tracking the post detection SNR increases since degradations caused by doppler drift, quarter-chip offset, and spread spectrum contribution to noise density vanish. The threshold is lowered to increase P_D to 0.999999999 so that the probability of no false dismissal during the maximum length 98 minute transmission is greater than 0.99. The dwell time during tracking is doubled to decrease the variance of the noise density. The resulting threshold at the minimum C/N_0 = 61.6 dB-Hz yields a P_D = 0.999999999 and a $P_{FA} = 1.48 \times 10^{-10}$. The summary of key K-band despreader design parameters is listed in Table 5-3.

Table 5-3. Summary of Key SSP Design Parameters

PARAMETER	RECEIVED SIGNAL = -102 dBm	TDRS EIRP = 35.6 dBw	NOTES
CODE ACQUISITION TIME	1.6 SEC	7.2 SEC	>3 dB MARGIN
CODE PHASE ACQUISITION DWELL TIME	154.5 μSEC	154.5 μSEC	P_D = 0.99
CODE PHASE TRACKING DWELL TIME	309 μSEC	309 μSEC	$P_D \geq 0.999999999$, $P_{FA} \sim 10^{-10}$
ACQUISITION PREDETECTION BANDWIDTH	1.7 MHz	1.7 MHz	DUAL FREQUENCY SEARCH
TRACKING PREDETECTION BANDWIDTH	4.6 MHz	4.6 MHz	
PROBABILITY OF LOSS OF LOCK	<0.0001	< 0.01	DURING 100 MIN. TRANSMISSION
TRACKING LOOP BANDWIDTH (ACQUISITION)	400 Hz	400 Hz	
TRACKING LOOP BANDWIDTH (TRACKING)	6 Hz	7 Hz	
PULL-IN TIME	17 MSEC	20 MSEC	4 LOOP TIME CONSTANTS
DAMPING RATIO	0.707	0.77	
TRACKING LOOP LAG (WORST CASE)	0.007 CHIP	0.008 CHIP	
RMS TRACKING ERROR	0.04 CHIP	0.05 CHIP	
BEP DEGRADATION	<0.7 dB	<0.7 dB	WITH MAXIMUM DOPPLER

5.3 CARRIER RECOVERY LOOP

This section presents the analysis and design of the carrier synchronization loop which performs the next step in the Orbiter acquisition sequence. The revision of the uplink signal from unbalanced QPSK to 2-ary PSK is a simplifying step for the carrier recovery function and much of the earlier work to obtain satisfactory performance from the N=4 class loops with the variable high rate channel could be abandoned. The content of this section begins with a comparison of alternate approaches followed by analysis and design of the selected approach. The section concludes with a performance summary of the recommended carrier synchronization loop.

5.3.1 Costas Versus Squaring Loop Implementation [11]

It is well known that the Costas loop of Figure 5-17a and the squaring loop of Figure 5-17b have the same theoretical noise immunity in both the acquisition and tracking modes. However, in the implementation of a squaring loop, mechanization of the times two multiplier is an important consideration insofar as system performance at low signal-to-noise ratio is concerned. Considerations which must be accounted for in the choice of the "squaring" approach include a wide dynamic range with respect to the signal level, good thermal stability, and accurate square law response over the dynamic range of input signal and temperature levels of interest. Test results conducted at TRW concerning the performance of an analog multiplier, indicated degraded signal-to-noise performance relative to theoretical. In an attempt to overcome the degrading effects at low signal-to-noise ratios, an alternate approach to the implementation of a squaring circuit was considered. The alternate mechanization of the loop is illustrated in Figure 5-17c.

5.3.1.1 Preliminaries

Figure 5-17c shows the limiter/multiplier type of squaring loop under consideration. In that figure, $h_1(t)$ is a bandpass filter with center frequency ω_0 and equivalent single-sided noise bandwidth $B_i (B_i << \omega_0)$, given by

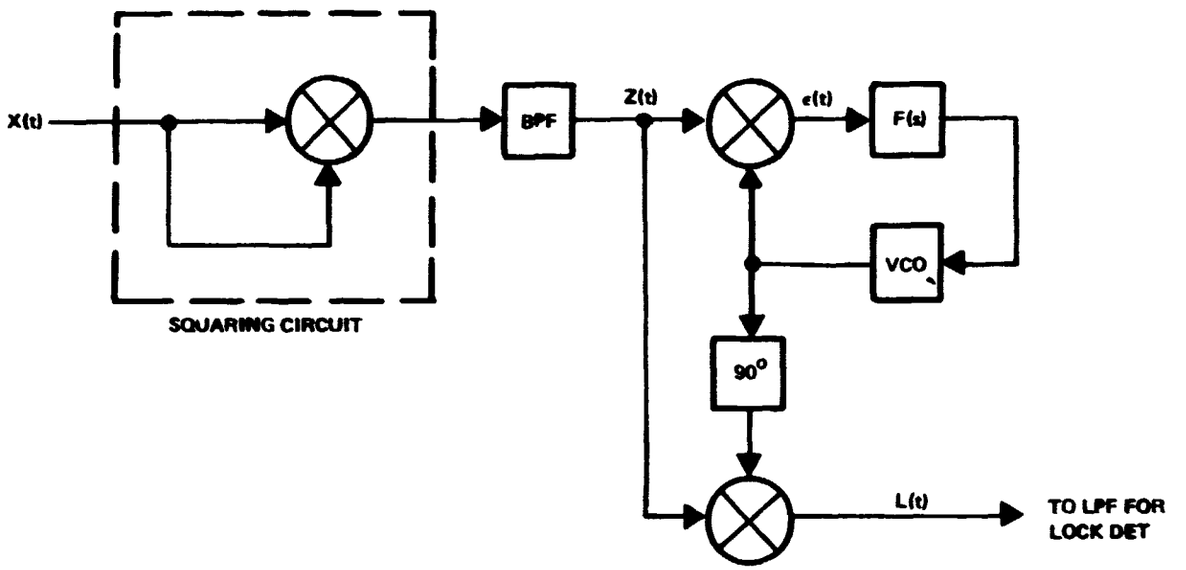

(a) BLOCK DIAGRAM OF A PERFECT SQUARING LOOP

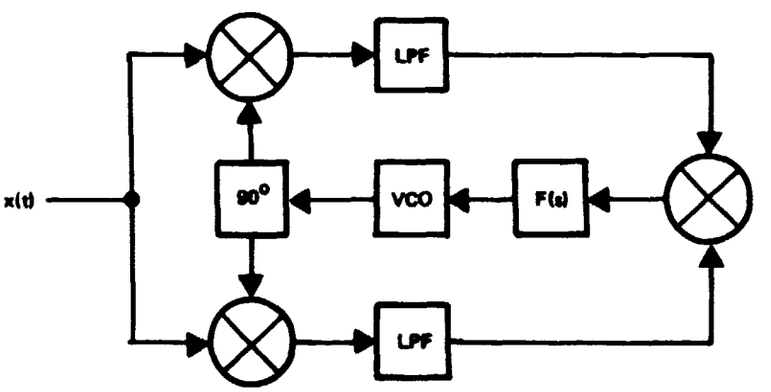

(b) BLOCK DIAGRAM OF A COSTAS LOOP

Figure 5-17. Carrier Recovery Loops

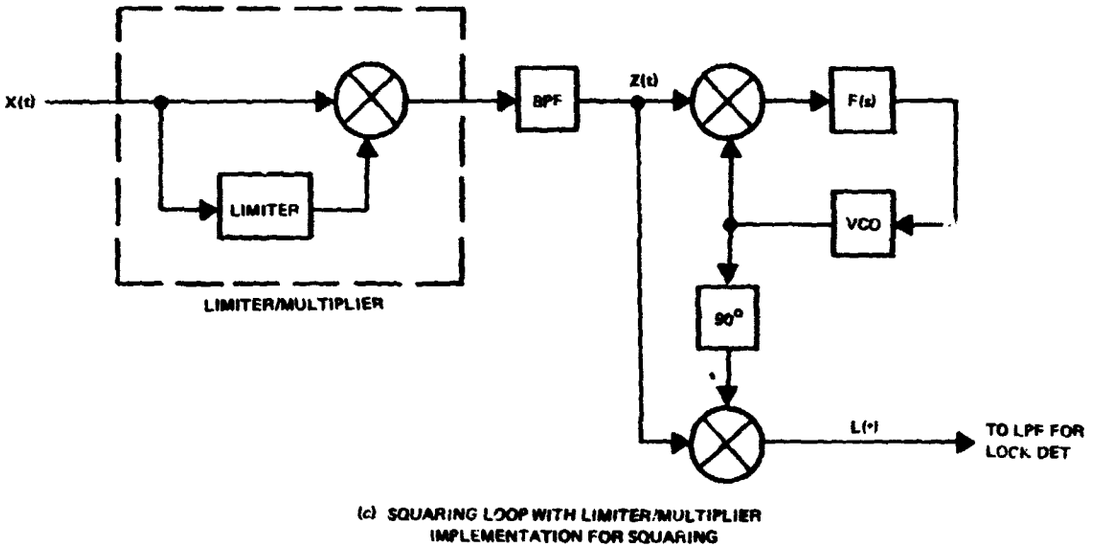

Figure 5-17. Carrier Recovery Loops

$$B_i = \frac{1}{2\pi} \int_0^{\infty} \frac{|H(j\omega)|^2}{|H(j\omega_0)|^2} \, d\omega \qquad (5\text{-}55)$$

where H is the transfer function of the filter. The input signal to the bandpass limiter is defined to be of the form

$$x(t) = s(t) + n(t)$$

with

$$S(t) = \sqrt{2}\, A \sin(\omega_0 t + \theta(t))$$

where $\theta(t)$ is the information bearing signal, and $n(t)$ is the narrowband noise represented by

$$n(t) = \sqrt{2}\,[n_c(t)\cos\omega_o t - n_s(t)\sin\omega_o t]$$

where $n_c(t)$, $n_s(t)$ are zero mean uncorrelated Gaussian processes with

$$E[n_c^2(t)] = E[n_s^2(t)] = \sigma_n^2/2$$

$$\sigma_n^2 = E[n^2(t)] = N_o B_i \qquad (5\text{-}56)$$

$$E[n_c(t)\, n_s(t+\tau)] = 0$$

In (5-56) N_o is the one sided spectral density at the input to the BPF h_1.

Through some trigonometric identities we can rewrite the input signal $x(+)$ in the form:

$$x(t) = \sqrt{2}\,[(A-N_s(t))\sin\phi(t) + N_c(t)\cos\phi(t)] \qquad (5\text{-}57)$$

where

$$\phi(t) = \omega_o t + \theta(t) \qquad (5\text{-}58)$$

$$N_c(t) = N_i(t)\cos(\theta_i(t) - \theta(t))$$

$$N_s(t) = N_i(t)\sin(\theta_i(t) - \theta(t))$$

The noise processes N_c, N_s involve the information bearing signal $\theta(t)$. To obtain the statistical properties of $N_c N_s$ we can re-write (5-58) as follows:

$$N_c(t) = n_c(t)\cos\theta(t) + n_s(t)\sin\theta(t)$$

$$N_s(t) = n_s(t)\cos\theta(t) - n_c(t)\sin\theta(t)$$

which gives directly the following, assuming the noise process and the information bearing signal are statistically independent

$$E[N_c(t)] = E[N_s(t)] = 0 \tag{5-59}$$

$$E[N_c^2] = E[N_s^2] = \sigma_n^2/2$$

$$E[N_c(t)N_s(t)] = 0$$

If in addition we define the normalized input noise autocorrelation function to be

$$R_{n_i}(\tau) = r_n(\tau) \cos \omega_0 \tau \qquad -\infty < \tau < \infty$$

where $r_n(\tau)$ is low pass and has the properties

$$r_n(0) = 1, \quad |r_n(\tau)| < 1, \int_{-\infty}^{\infty} r_n(\tau)\, d\tau = \frac{1}{B_i}$$

then the auto- and cross-correlation functions for $N_c(t)$ and $N_s(t)$ can be written in terms of $r_n(\tau)$ and σ_n^2 as:

$$E[N_c N_{c\tau}] = E[N_s N_{s\tau}] = \frac{\sigma_n^2}{2} r_n(\tau) \overline{\cos \Delta\theta_\tau} \tag{5-60}$$

$$E[N_c N_{s\tau}] = -E[N_s N_{c\tau}] = \frac{\sigma_n^2}{2} r_n(\tau) \overline{\sin \Delta\theta_\tau}$$

where

$$\Delta\theta_\tau = \theta(\tau) - \theta(\tau + \tau).$$

The ideal limiter function is defined such that

$$y(t) = \text{sgn}(x(t)) = \begin{cases} +1 & \text{if } x(t) > 0 \\ -1 & \text{if } x(t) < 0 \end{cases}$$

The input process x(t) can be written, from (5-57), as follows

$$x(t) = \sqrt{2}\, v(t) \cos(\phi(t) - \gamma(t))$$

where

$$v \equiv \sqrt{(A-N_s)^2 + N_c^2}$$

$$\gamma \equiv \tan^{-1}\left(\frac{A - N_s}{N_c}\right)$$

The limiter output y(t) can be integrated to be [13].

$$y(t) = \frac{4}{\pi} \sum_{k=0}^{\infty} \frac{(-1)^k}{2k+1} \cos\{(2k+1)[\phi(t) - \gamma(t)]\} \qquad (5\text{-}61)$$

It is clear from (5-61) that only odd harmonics are present in the limiter output.

5.3.1.2 Squarer Output

To obtain suppressed carrier tracking, the data modulation $\theta(t)$ [biphase modulation assumed] has to be removed to create a CW signal which is tracked by the PLL. This is accomplished by multiplying the limiter output (a stream of ± 1's) to the incoming signal, and then obtaining the harmonics around $2\omega_0$ by passing the multiplier output through the zonal filter h_2. The multiplier output can be written as:

$$x(t) \cdot y(t) = \sqrt{2}\, v(t) \cos(\phi(t) - \gamma(t)) \qquad (5\text{-}62)$$

$$\cdot \frac{4}{\pi} \sum_{k=0}^{\infty} \frac{(-1)^k}{2k+1} \cos\{(2k+1)[\phi(t) - \gamma(t)]\}$$

The second harmonic term can be selected from (5-62) to be the following:

$$z(t) = \frac{4\sqrt{2}}{3\pi} V(t) \cos [2 (\phi(t) - \gamma(t))] \qquad (5\text{-}63)$$

Note then that in the above discussion the filter h_2 is assumed a mathematical entity which selects only the second zone component. In reality, a physical bandpass filter can only approximate this condition since the spectrum of $\cos [2 (\phi(t) - \gamma(t)]$ extends on all ω; however, because of the assumed narrowband ($B_1 \ll \omega_0$) approximation, the error is small. Notice also from (5-63) that since biphase modulation is assumed $z(t)$ is actually a CW signal at twice the carrier frequency ω_0 when the noise effect $\gamma(t)$ is negligible.

Weak Signal Suppression

To obtain the loop error signal, the squarer output $z(t)$ is mixed with the local reference signal

$$r(t;\phi) = -\sqrt{2} \sin 2[\omega_0 t + \phi]$$

where ϕ is the phase difference between $z(t)$ and $r(t;\phi)$. Omitting $4\omega_0$ terms the error signal that the PLL tracks is then

$$\varepsilon(t) = \frac{4}{3\pi} V(t) \sin [2 (\phi + \gamma(t))] \qquad (5\text{-}64)$$

$$= \frac{4}{3\pi} \left\{ - \frac{(A-N_s)^2 - N_c^2}{\sqrt{N_c^2+(A-N_s)^2}} \sin 2\phi - \frac{2N_c \cdot (A-N_s)}{\sqrt{N_c^2+(A-N_s)^2}} \cos 2\phi \right\}$$

In the case of limiter-multiplier implementation of the squaring loop, there is signal suppression on $\varepsilon(t)$, which is a function of input SNR ρ_i. Suppression in $\varepsilon(t)$ will affect the loop bandwidth and tracking performance. The weak signal suppression factor on $E [\omega(t)]$ as a function of ρ_i can be obtained as

$$\frac{E [\varepsilon(t)]}{A} = \frac{\sqrt{\pi}}{2} \sqrt{\rho_i} e^{\frac{\rho_i}{2}} [I_0(\tfrac{\rho_i}{2}) + (1 - \tfrac{1}{\rho_i}) I_1 (\tfrac{\rho_i}{2})] \qquad (5\text{-}65)$$

This relationship is illustrated in Figure 5-18.

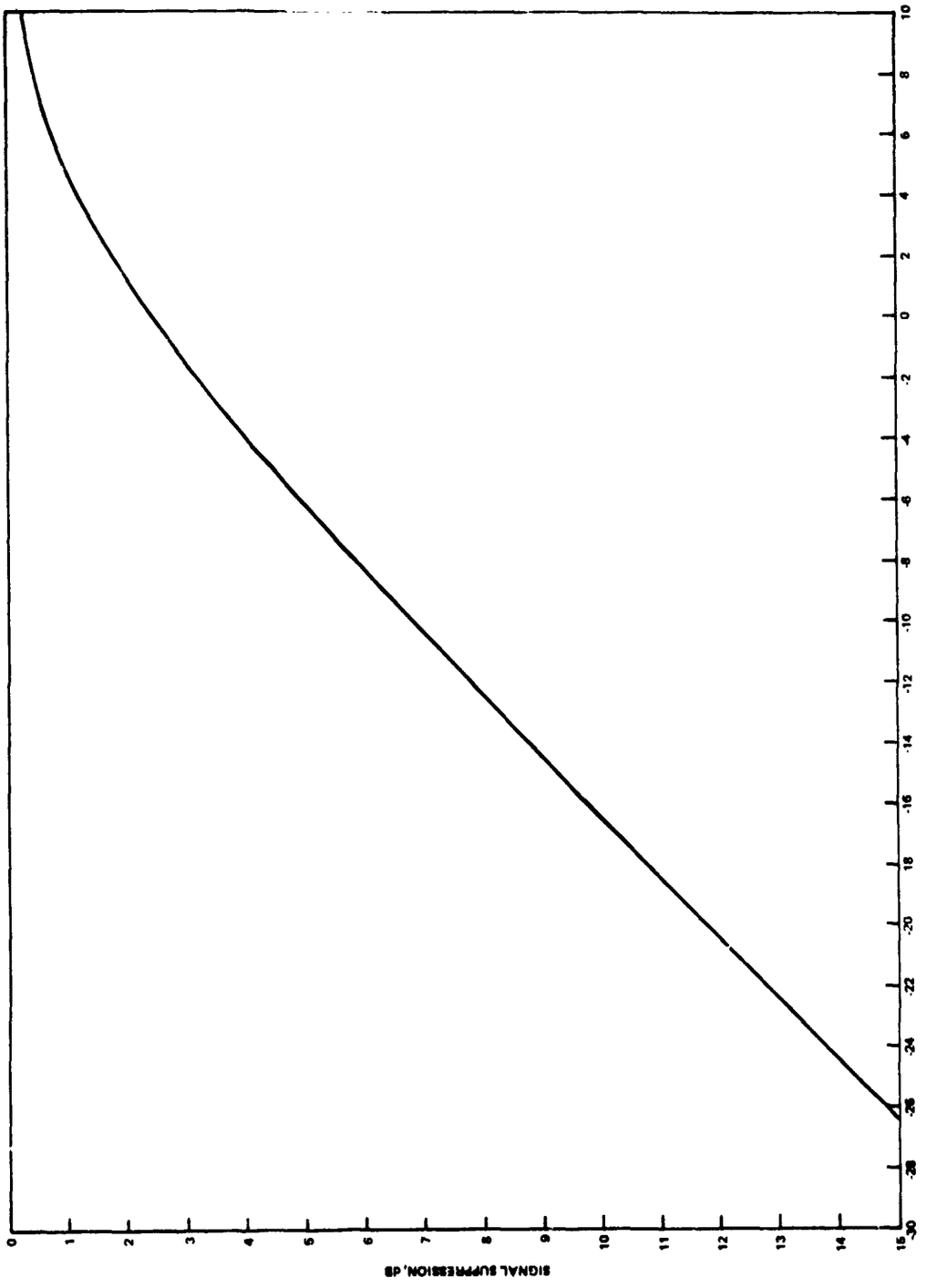

Figure 5-18. Weak Signal Suppression Factor on Loop Error Signal

5.3.1.3 Effective Loop SNR and Squaring Losses

As far as loop performance is concerned the essential factor is the effective loop SNR (See [12]) which depends on the noise power spectral density N_{eq} of the equivalent noise process in the error signal $\varepsilon(t)$, around zero frequency. N_{eq} is defined to be [13]

$$N_{eq} = 2 \int_{-\infty}^{\infty} R_{n_{eq}}(t)\, dt \tag{5-66}$$

where n_{eq} is equivalent to zero mean noise processes in $\varepsilon(t)$. For the perfect squaring loop case the auto-correlation function $R_{n_{sq}}(t)$ of the equivalent noise process has been computed by Lindsey and Simon [13] to be

$$R_{n_{sq}}(t) = 4\,[A^2 R_{n_c}(t) + R_{n_c}{}^2(t)] \tag{5-67}$$

where $R_{n_c}(t)$ is as given in (5-60). From this the equivalent noise power spectral density around zero frequency N_{sq} is computed to be

$$N_{sq} = 4\, A^2 N_o \mathcal{L}_L^{-1} \tag{5-68}$$

where N_o is the input noise spectral density and $\mathcal{L}_L$ is defined to be the circuit squaring loss

$$\mathcal{L}_L^{-1} = 1 + \frac{2}{SN_o} \int_{-\infty}^{\infty} R_{n_c}{}^2(\tau)\, d\tau \tag{5-69}$$

The effective loop SNR ρ_{eff} for the perfect squaring loop is given [13] in terms of $\mathcal{L}_L$ and the equivalent signal-to-noise ratio in the loop bandwidth (B_L) of a second order PLL $\rho = A^2/N_o B_L$ by

$$\rho_{eff}\ (\text{perfect squaring}) = \frac{\rho}{4}\mathcal{L}_L \tag{5-70}$$

To compare the two implementations it is necessary to compute the N_{eq} for the equivalent noise process in (5-64) and to define the effective squaring loss in the second implementation through Equation (5-70) by computing the effective loop SNR ρ_{eff}. To obtain N_{eq}, in this case, requires computation of the auto-correlation function of equivalent noise term in (5-64)

$$n_{eq} = 2\left(\frac{N_o.(A-N_s)}{\sqrt{N_c^2+(A-N_s)^2}}\right)\cos 2\phi$$

Assuming $\phi \approx 0$ (for tracking) the auto-correlation $R_{n_{eq}}(\tau)$ is found from

$$R_{n_{eq}}(\tau) = 4\,E\left\{\frac{N_c(A-N_s)}{\sqrt{N_c^2+(A-N_s)^2}} \cdot \frac{N_{c\tau}(A-N_{s\tau})}{\sqrt{N_{c\tau}^2+(A-N_{s\tau})^2}}\right\} \qquad (5\text{-}71)$$

The correlation times of the input noise process n(t) is much shorter than the modulation process $\theta(t)$, then the actual covariance matrix Λ of $N_c, N_s, N_{c\tau}, N_{sc}$ is given by, for all practical considerations by Equation (5-72); y_2 is given by

$$\Lambda = \frac{\sigma_n^2}{2}\begin{bmatrix} 1 & 0 & \gamma_n(\tau) & 0 \\ 0 & 1 & 0 & \gamma_n(\tau) \\ \gamma_n(\tau) & 0 & 1 & 0 \\ 0 & \gamma_n(\tau) & 0 & 1 \end{bmatrix} \qquad (5\text{-}72)$$

For simplicity in notation, define

$$x_1 = N_c,\ x_2 = N_{c\tau}$$

$$y_1 = A - N_s,\ y_2 = A - N_{s\tau}$$

Then the joint density of x_1, y_1, x_2, y_2 is given by

$$p(x_1,y_1,x_2,y_2) = \frac{1}{4\pi^2|\Lambda|^{1/2}} \exp - \frac{1}{2|\Lambda|^{1/2}} \cdot \frac{\sigma_n^2}{2} [(x_1^2+x_2^2+(y_1-A)^2+(y_2-A)^2)$$

$$- 2\,\gamma_n(\tau)\,(x_1x_2 - (y_1-A)\,(y_2-A))] \qquad (5\text{-}73)$$

Where $|\Lambda|^{1/2} = \frac{\sigma_n^4}{4}[1 - \gamma_n^2(\tau)]$. With $A \neq 0$ the computation of the expectation in (5-71) involves quite complicated four fold integrals and numerical integration seems to be the only possible method of solution. If $A = 0$ (which is a good approximation to small input SNR cases), the expectation can be evaluated exactly. In terms of the noise envelopes and random phase angles:

$$V_i = \sqrt{x_1^2 + y_1^2}\ , \ \phi_1 = \tan^{-1}\left(\frac{y_i}{x_i}\right), \ i = 1, 2 \qquad (5\text{-}74)$$

the expectation(5-71) can be computed from the following integral:

$$R_{Neg}(\tau) = \frac{1}{4\pi^2|\Lambda|^{1/2}} \int_0^\infty\int_0^\infty dv_1dv_2\ v_1^2\ V_2^2\ e\ \frac{-\sigma_n^2(v_1^2+v_2^2)}{4|\Lambda|^{1/2}} \qquad (5\text{-}75)$$

$$\int_0^{2\pi}\int_0^{2\pi} d\phi_1\ d\phi_2\ \sin 2\phi_1 \sin 2\phi_2\ e\ \frac{\sigma_n^2 r_n(\tau)v_1v_2\ \cos\ (\phi_2-\phi_1)}{2|\Lambda|^{1/2}}$$

The double integral on ϕ_1 and ϕ_2 can be evaluated directly to be

$$\int_0^{2\pi}\int_0^{2\pi} d\phi_1 d\phi_2 \sin 2\phi_1 \sin 2\phi_2 \, e^{\frac{\sigma_n^2 \gamma_n(t) v_1 v_2 \cos(\phi_2-\phi_1)}{2|\Lambda|^{1/2}}}$$

$$= 2\pi^2 I_2\left(\frac{\sigma_n^2 \gamma_n(t)}{|\Lambda|^{1/2}} v_1 v_2\right) \tag{5-76}$$

With this simplification (5-75) can be evaluated (See [14]) and the effective loop SNR can then be computed with the approximation for small SNR cases, to be

$$\rho'_{eff} = \frac{A^2 \left\{\frac{\sqrt{\pi}}{2}\sqrt{\rho_i}\, e^{-\frac{\rho_i}{2}} \left[I_0(\frac{\rho_i}{2}) + (1 - \frac{1}{\rho_i}) I_1(\frac{\rho_i}{2})\right]\right\}^2}{2N_{eq} B_L} \tag{5-77}$$

where B_L is the one sided loop bandwidth and N_{eq} is the equivalent noise spectral density computed from $R_{n_{eq}}(\tau)$.

This may be simplified to

$$\rho'_{eff} = \frac{A^2}{N_o B_L} \cdot \frac{1}{4} \cdot \mathcal{L}'_L \tag{5-78}$$

where $\mathcal{L}'_L$ is the equivalent squaring loss.

As an example, consider a bandpass filter with an RC transfer function. The equivalent low pass spectrum for $N_c(t)$ or $N_s(t)$ has correlation functions:

$$R_{Nc}(t) = R_{Ns}(t) = \frac{N_o W_i}{4} \exp(-W_i|t|) \tag{5-79}$$

Assuming signal distortion due to filtering is negligible, then the squaring loss for an ideal squaring loop for this $R_{Nc}(t)$ is computed [3] to be:

$$\mathcal{L}_L' = \frac{1}{1 + \frac{1}{4\rho_i}} \tag{5-80}$$

For the same correlation function the equivalent circuit squaring loss for the limiter/multiplier implementation can be computed numerically. This result is plotted as a function of ρ_i together with equation (5-80) on Figure 5-19. It is noted that the limiter/multiplier implementation has more squaring loss than the ideal squaring loop for low input SNR cases, which is expected. However, it is interesting to note that as $\rho_i \to 0$ the difference between the two squaring losses asymptotically approaches ≈ 0.8 dB.

As ρ_i becomes large, the $A \gtrsim 0$ approximation is no longer valid. However, it is seen from the definition of $N_{eq}(t)$ in (5-64) that

$$n_{eq} \to 2N_c(t) \qquad \text{as } \rho_i \to \infty$$

and thus

$$R_{neq}(\tau) \to 4R_{Nc}(\tau) \qquad \text{as } \rho_i \to \infty$$

$$N_{eq} \to 4N_o \qquad \text{as } \rho_i \to \infty$$

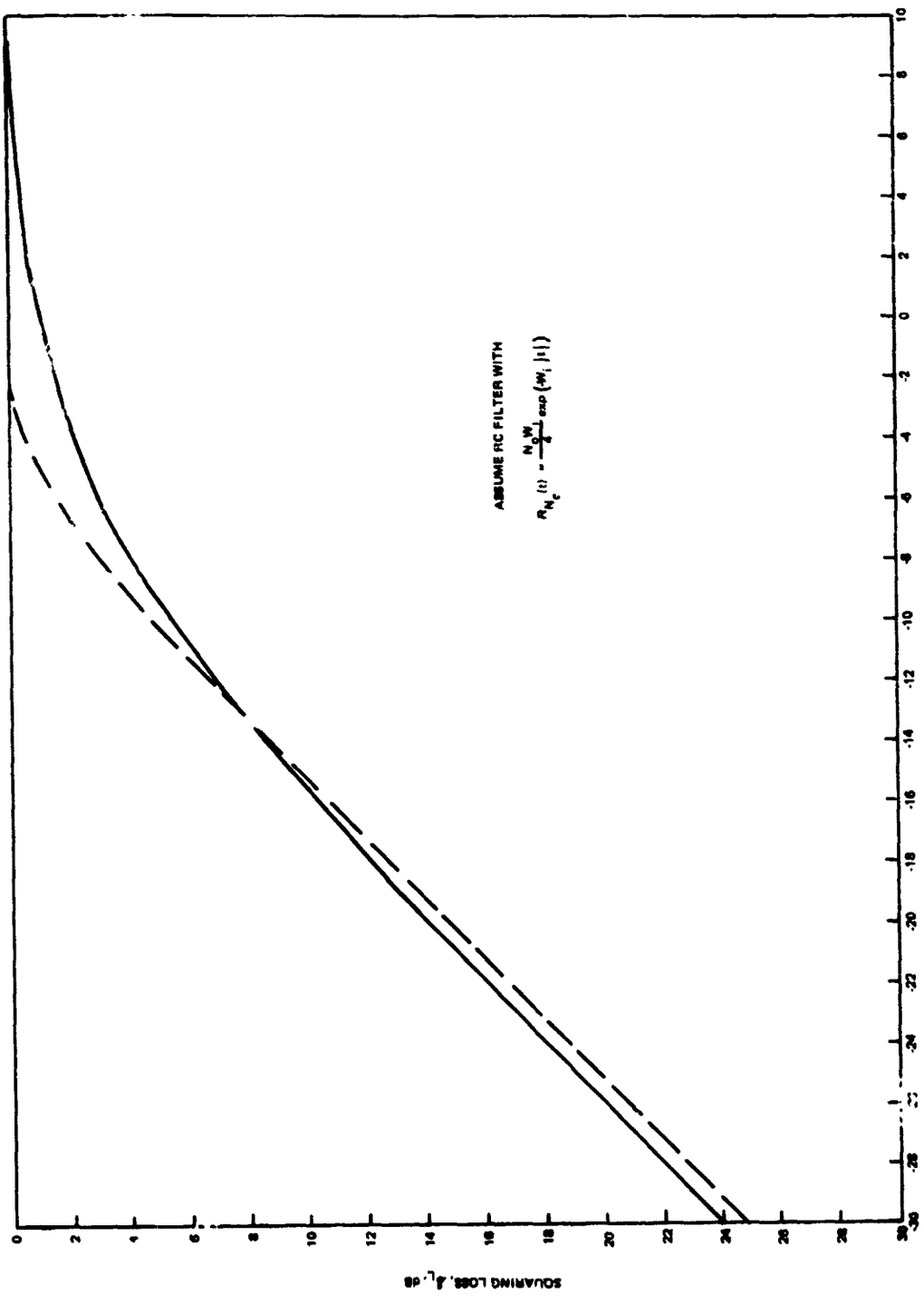

Figure 5-19. Comparison of Squaring Loss – Two Squaring Loop Implementations

On the other hand, since the signal suppression factor approaches unity as $\rho_i \to \infty$, the effective loop SNR approaches, as $\rho_i \to \infty$

$$\rho'_{eff} \to \frac{A^2}{4N_0B_L} = \frac{1}{4}\rho \qquad \text{as } \rho_i \to \infty$$

and we conclude that the loops have identical tracking performance at high signal-to-noise ratios.

5.3.1.4 Conclusions

This section has developed the tracking performance of a practical squaring loop in which the times two multiplier is mechanized as a limiter/multiplier combination; this "squaring" approach serves to produce the absolute value of the arriving signal as opposed to the perfect square law action which is required in order to render acquisition and tracking performance equivalent to that of a Costas loop. The absolute value type circuit appears to be the more practical circuit to build when such things as low signal-to-noise ratios, a wide dynamic range of signal level and temperature variations are considered. In the signal-to-noise ratio region of interest, it is shown that an absolute value type "square law" circuit degrades the input C/N_0 by 0.5 to 0.8 dB over that of an ideal squaring loop. This also says that the tracking performance of a Costas loop is better, by 0.5 to 0.8 dB, than that of a squaring loop implemented with a limiter/multiplier combination for times two multiplication. At high SNR it is shown that the tracking performance of the two mechanizations is identical. In addition, the beat note level and phase detector gain are nonlinear functions of the signal-to-noise ratio at the input to the limiter/multiplier. This is of concern as far as maintaining the design point loop bandwidth and damping as the signal level varies. The Costas loop implementation is therefore recommended.

5.3.2 Performance Analysis

The carrier recovery Costas loop is analyzed. The mean square phase error is obtained and it's individual component terms derived and analyzed separately. Tradeoff curves between mean square phase error and loop bandwidth are also presented. Acquisition time and sweep rate for 0.99 is also determined and the first mean slip time is calculated.

5.3.2.1 Stochastic Differential Equation of the Costas Loop

The Costas loop analyzed here is shown in Figure 5-20 as a short loop. This is equivalent to the phase lock IF Costas loop (long loop) implemented in the double superheterodyne PLL Ku-band receiver block diagram when the pre-Costas BPF bandwidth is wide compared to the data rate.

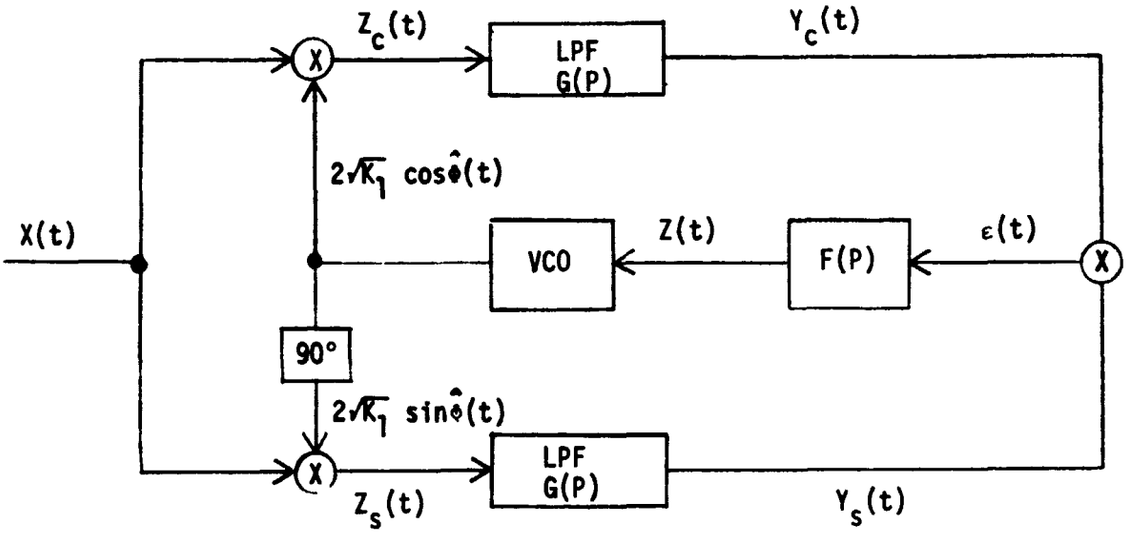

Figure 5-20. Recommended Costas Loop

Following reference [13] it is possible to show that for

$$x(t) = \sqrt{2S}\, m(t) \sin\phi(t) + n_i(t) \tag{5-81}$$

where

$m(t)$ = signal modulation, ± 1

$n_i(t)$ = narrowband noise process

$\phi(t) = \omega_o t + d(t) + \psi_1(t) = \omega_o t + \theta(t)$

($d(t)$: doppler profile; $\psi_1(t)$: transmitter oscillator instabilities)

$\hat{\phi}(t) = \omega_o t + \hat{\theta}(t) + \psi_2(t)$

$\phi(t) \triangleq \phi(t) - \hat{\phi}(t)$

then

$$\varepsilon(t) = K_1 K_m \{[\alpha S\, m^2(t) - N_c^2(t) + N_s^2(t) - 2\sqrt{S\alpha}\, m(t)\, N_s(t)] \cdot \sin 2\phi(t) + [2\sqrt{S\alpha}\, m(t)\, N_c(t) - 2 N_c(t)\, N_s(t)] \cos 2\phi(t)\} \tag{5-82}$$

where

α = is the proportion of the signal power passed by the low pass filter having noise bandwidth B_I

$$N_c(t) = \Lambda_c(t) \cos\theta(t) + \Lambda_s(t) \sin\theta(t)$$

$$N_s(t) = \Lambda_c(t) \sin\theta(t) + \Lambda_s(t) \cos\theta(t)$$

where both Λ_c and $\Lambda_s(t)$ are assumed to be statistically independent stationary W.G.N. processes of single sided spectral density N_o w/Hz and double sided bandwidth $N_o/2$ w/Hz less than $\omega_o/2\pi$.

$\sqrt{K_m}$ = gain of the upper and lower multipliers.

The instantaneous frequency at the VCO output is related to $\varepsilon(t)$ by

$$\frac{2d\hat{\phi}(t)}{dt} = Ku\, [F(P)\, \varepsilon(t)] + 2\omega_o + \frac{2d\psi_2(t)}{dt} \tag{5-83}$$

where

$$\psi_2(t) = \text{oscillator instabilities.}$$

The stochastic integro-differential equation of operation is then

$$\frac{2d\phi(t)}{dt} = \frac{2d\theta(t)}{dt} - KF(P)\{\alpha S \sin 2\phi(t) + N[t, 2\phi(t)]\} - \frac{2d\psi_2(t)}{dt}$$

where

$$N[t, 2\phi(t)] = [-N_c^2(t) + N_s^2(t) - 2\sqrt{S\alpha}\, m(t)\, N_s(t)] \sin 2\phi(t) + [2\sqrt{S}\, m(t)\, N_c(t) - 2\, N_c(t)\, N_s(t)] \cos 2\phi(t) \quad (5\text{-}84)$$

Note that $2\phi(t)$ represents the actual phase error being tracked by the loop. For P the Heaviside operator, we can rewrite (5-83) (suppressing the explicit time dependence)

$$2\phi = 2d + 2\Delta\psi - \frac{KF(P)}{P}[\alpha S \sin 2\phi + N(t, 2\phi)] \quad (5\text{-}85)$$

When the total loop phase error is small we can use the first term in a Taylor series expansion for sin 2ϕ and write $\sin 2\phi \simeq 2\phi$ [reference [15]], then from (5-85) the equation of operation becomes

$$2\phi = \frac{P}{P+\alpha SKF(P)}\, 2[dt\Delta\psi] - \frac{\alpha SKF(P)}{P+\alpha SKF(P)}\left[\frac{N(t, 2\phi)}{\alpha S}\right] \quad (5\text{-}86)$$

where

$$H\phi(P) \triangleq \frac{\alpha SKF(P)}{P+\alpha SKF(P)}$$

is the closed loop transfer function. We can rewrite then (5-86) as

$$2\phi = [1-H\phi(P)]2(d+\Delta\psi) - H\phi(P)\left[\frac{N(t, \phi 2\phi)}{\alpha S}\right] \quad (5\text{-}87)$$

5.3.2.2 Phase Error Analysis

From (5-87) it follows that the total mean square error performance, $4\sigma^2_T$*, is thus composed of

$$4\sigma^2_T = 4\sigma^2_d + 4\sigma^2_{\Delta\psi} + \sigma^2_{2\phi} \tag{5-88}$$

where σ^2_d is the mean squared tracking phase error component due to doppler effects and given by

$$\sigma^2_d \triangleq \frac{1}{2\pi i}\int_{-i\infty}^{i\infty} |1-H\phi(s)|^2 \, E\,\tilde{d}(s)|^2 ds \tag{5-89}$$

$\sigma^2_{\Delta\psi}$ is the mean squared phase error component due to transmitter and receiver oscillator instabilities and given by

$$\sigma^2_{\Delta\psi} \triangleq \frac{1}{2\pi i}\int_{-i\infty}^{i\infty} |1-H\phi(s)|^2 \, S_{\Delta\psi}(s)\, ds \tag{5-90}$$

and

$$\sigma^2_{2\phi} \triangleq \frac{1}{2\pi i}\int_{-i\infty}^{i\infty} |H\phi(s)|^2 \, \frac{S_N(s)}{(\alpha S)^2} \tag{5-91}$$

is that portion of σ^2_T due to the additive thermal noise. When the loop is locked to zero doppler, σ^2_d can be neglected and σ^2_T written as

$$\sigma^2_T = \sigma^2_{\Delta\psi} + \frac{\sigma^2_{2\phi}}{4}$$

We now study both terms on the right hand side of the above expression separately.

a) Additive noise mean squared phase error ($\sigma^2_{2\phi}$).

The one sided loop noise bandwidth is defined as

$$B_L \triangleq \frac{1}{4\pi i}\int_{-i\infty}^{i\infty} |H\phi(s)|^2 \, ds. \tag{5-92}$$

*σ_T is also known as a phase jitter.

When the loop noise bandwidth is such that $B_I >> B_L$, where B_I is the one sided noise bandwidth of the lowpass arm filters, we need only consider the noise spectral density at zero. It is not difficult to show (reference [16,17,18] that the term $N(t, 2\phi)$ in (8) have a correlation function given by

$$R_N(\tau) = 4[R_{No}(\tau)\ \alpha S + R^2_{Nc}(\tau)] \tag{5-93}$$

from where

$$S_N(o) = \frac{N'o}{2} = \int_{-\infty}^{\infty} R_N(\tau)\ d\tau. \tag{5-94}$$

When the LPF is an n pole Butterworth filter then (5-94) reduces to

$$S_N(o) = 2\ No\alpha S + 2\ No^2\ B_I\ (1 - \frac{1}{2n}) \tag{5-95}$$

so using (5-92) and (5-95) in (5-91) we get

$$\begin{aligned}\sigma^2_{2\phi} &= \frac{2B_L}{(\alpha S)^2}\left[2No\alpha S + 2No^2\ B_I\ (1 - \frac{1}{2n})\right] \\ &= 4\ \frac{B_L No}{\alpha S}\left[1 + \frac{NoB_I}{\alpha S}\ (1 - \frac{1}{2n})\right]\end{aligned} \tag{5-96}$$

For the case that the data filter is a lowpass single pole RC filter with noise bandwidth B_I, (5-96) reduces to

$$\sigma^2_{2\phi} = 4\ \frac{B_L No}{\alpha S}\left[1 + \frac{NoB_I}{2\alpha S}\right] \tag{5-97}$$

and the term

$$\mathscr{L}_L \triangleq \frac{\alpha}{1 + \frac{NoB_I}{2\alpha S}} \tag{5-98}$$

is defined as the squaring loss. When the data sequence is a Manchester bi-phase modulated signal α is given by

$$\alpha = \int_{-\infty}^{\infty} Sm(f)|G(f)|^2 \, df \tag{5-99}$$

and for the same arm filter as above the last one reduces to

$$\alpha = T_s \int_{-\infty}^{\infty} \frac{\sin^4\left(\frac{\pi f T_s}{2}\right)}{\left(\frac{\pi f T_s}{2}\right)^2} \cdot \frac{1}{1+(f/f_I)^2} \, df \tag{5-100}$$

where $B_I = \frac{\pi}{2} f_I$ and $1/T_s$ is the data rate.

b) Oscillator Instabilities Mean Square Phase Error: $(\sigma^2_{\Delta\psi})$

The VCO shown in the block diagram of the equivalent short Costas loop, Figure 5-21, is really a frequency synthesizer which we model in the following figure following reference [19].

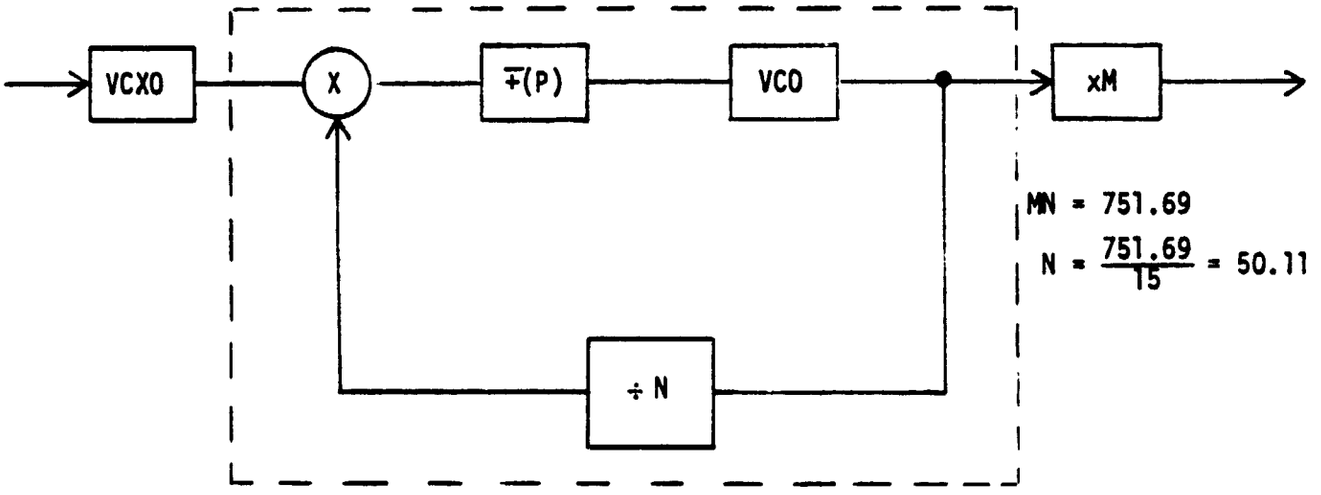

Figure 5-21. Equivalent Short Loop

The effective multiplication for the VCXO is 751.69 (=MxN) and for the VCO is 50.11(=M). These multiplication factors result as a consequence of considering an approximation to the actual, more complicated system in that in the actual system part of the signal out of the VCO is used to generate the second IF, without any further multiplication. Since the rest of the VCO output is multiplied by 49 we may just consider one IF with a multiplication factor of 50.11.

The linear model corresponding to the dashed block is the followi.

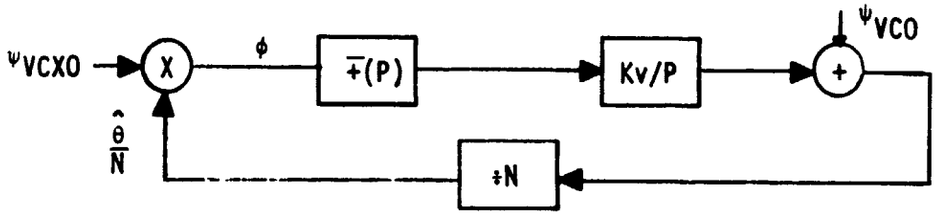

and the equation of operation is for $\phi = \psi_{VCXO} - \hat{\theta}/N$*

$$\alpha = \psi_{VCXO} - \frac{KvF(P)\phi}{NP} - \frac{\psi_{VCO}}{N} \tag{5-101}$$

The closed loop transfer function for this system is

$$\frac{\hat{\theta}/N}{\theta} = \frac{F(P)Kv}{NP + F(P)Kv} = H_{SYN}(P) \tag{5-102}$$

it follows then after solving for ϕ in (5-101) and using (5-102) that

$$\phi = [1 - H_{SYN}(P)]\left(\psi_{VCXO} - \frac{\psi_{VCO}}{N}\right) \tag{5-103}$$

Using the definition of ϕ in (5-101) and (5-103) we get

*The dummy variables used in this section are not to be confused with the ones used previously.

$$\hat{\theta} = \frac{KvF(P)\psi}{P} + \psi_{VCO}$$

$$= \frac{KvF(P)}{P}\left[1 - H_{SYN}(P)\right]\left(\psi_{VCXO} - \frac{\psi_{VCO}}{N}\right) + \psi_{VCO} \qquad (5\text{-}104)$$

$$= \frac{KvF(P)N}{NP+KvF(P)}\ \psi_{VCXO} - \frac{KvF(P)N}{NP+KvF(P)}\ \frac{\psi_{VCO}}{N} + \psi_{VCO}$$

$$= N\,H_{SYN}(P)\,\psi_{VCXO} + \left[1 - H_{SYN}(P)\right]\psi_{VCO}$$

From where it follows that the noise spectra out of the dashed block in the frequency synthesizer is given by

$$S_F(f) = N^2|H_{SYN}(f)|^2\,S_{VCXO}(f) + |1 - H_{SYN}(f)|^2\,S_{VCO}(f) \qquad (5\text{-}105)$$

From the above and the block diagram of the synthesizer it follows that

$$S_{FSYN} = (MN)^2|H_{SYN}(f)|^2\,S_{VCXO}(f) + M^2|1 - H_{SYN}(f)|^2\,S_{VCO}(f) \qquad (5\text{-}106)$$

Using now (5-106) in (5-90) and assuming the $F_{SYN}N(f) \simeq S_{\Delta\psi}(f)$ we get

$$\sigma^2_{\Delta\psi} = (MN)^2\int_{-\infty}^{\infty}|1 - H\phi(f)|^2|H_{SYN}(f)|^2\,S_{VCXO}(f)\,df + M^2\int_{-\infty}^{\infty}|1 - H\phi(f)|^2|1 - H_{SYN}(f)|^2\,S_{VCO}(f)\,df. \qquad (5\text{-}107)$$

5.3.2.3 Results and Computations

Once the carrier power to noise ratio is determined (ρ = S/No) and a noise bandwidth B_I for the data filters adopted, it is clear that $\sigma^2_{2\phi}$ in (5-97) is only a function of the loop bandwidth B_L, i.e.,

$$\sigma^2_{2\phi} = \frac{4B_L}{\alpha\rho}\left[1 + \frac{B_I}{2\alpha\rho}\right]$$

The nominal numbers adopted for the above parameters where B_I = 500 kHz, ρ = 64 dB-Hz, $\alpha_{72\ kbs}$ = .842 and $\alpha_{216\ kbs}$ = .68.

The VCO and VCXO models adopted have single sided phase spectra (rad^2/Hz) given by

(1) VCO

22 dB/decade to -140 dBc/Hz at 1 MHz

$$S_\theta(f) = \left(\frac{10^6}{f}\right)^{2.5} 10^{-14.5} \qquad 0 \leq f \leq 1 \text{ MHz}$$

$$S_\theta(f) = 10^{-14.5} \qquad f > 1 \text{ MHz}$$

(2) VCXO

-80 dBc at 10 Hz

-109 dBc at 100 Hz

-137 dBc at 1000 Hz

-147 dBc at 10 kHz

-152 dBc at $\geq$ 25 kHz

so that we model the VCXO spectra as

$$S_{\theta VCXO}(f) = \frac{10^9}{f^3}\ 10^{-13.8} \qquad 0 \leq f \leq 1 \text{ kHz}$$

$$S_{\theta VCXO}(f) = \left(\frac{10^4}{f}\right) 10^{-14.7} \qquad 1 \text{ kHz} \leq f \leq 10 \text{ kHz}$$

$$S_{\theta VCXO}(f) = \left(\frac{25{,}000}{f}\right) 1.25\ _{10}{}^{-15.2} \qquad 10 \text{ kHz} \leq f \leq 25 \text{ kHz}$$

$$S_{\theta VCXO}(f) = 10^{-15.2} \qquad f > 25 \text{ kHz}$$

When the damping factor in a second order PLL is $\zeta = .707$, it can be shown that

$$|H\phi(\omega)|^2 = \frac{1+2(\omega/\omega_n)^2}{1+(\omega/\omega_n)^4}$$

and

$$|1 - H\phi(\delta)|^2 = \frac{\omega^4/\omega_n^4}{1+(\omega/\omega_n)^4}$$

where $\omega_n = B_L/.53$. Then we have that the mean square phase error due to oscillator instabilities is (in degrees square)

$$\sigma^2_{\Delta\psi} = (57.3)^2(751.69)^2\, 2\int_0^\infty S_{VCXO} \frac{1+2(f/f_{syn})^2}{1+(f/f_{syn})^4} \cdot \frac{(f/f_{CL})^4}{1+(f/f_{CL})^4}\, df$$

$$+ (57.3)^3(50.11)^2\, 2\int_0^\infty S_{VCO}(P) \frac{(f/f_{syn})^4}{1+(f/f_{syn})^4} \cdot \frac{(f/f_{CL})^4}{1+(f/f_{CL})^4}\, df$$

where f_{syn} = 10 kHz and $f_{CL} = B_L/.53$. The above integration was performed numberically for 200 Hz $\leq B_L \leq$ 16000 Hz.

From the above it follows that the variance of the phase error due to the additive noise is proportional to B_L, while the component due to $\Delta\psi$ is inversely proportional to B_L. This means that the value of B_L can be chosen so as to minimize σ^2_T. This was done and B_L was chosen to be B_L = 5000 Hz. With this loop bandwidth $\sigma^2_T = 6.37°$.

Once B_L has been fixed, then using the criteria in reference [17] and [20] which follows Frazier and Page acquisition time and sweep rate can be determined. For $\zeta = .707$ and $B_L = \omega_n 0.53$ the sweep rate is for a squaring loop.

$$R_{90} = 0.5431\ (1 - \sqrt{\tfrac{2}{\rho_T}})\ B_L^2 \text{ Hz/sec.} \qquad (5\text{-}108)$$

This means that the sweep rate we have to adopt for Costas loop is $R_{90}/2$. According to Frazier and Page (reference [21]) by sweeping at this rate across the uncertainty band there is a 90% chance of acquiring the signal. This means with a .9 probability the loop can acquire in

$$T_{ACQ} = \frac{fd}{\frac{R_{90}}{2} - |\dot{fd}|}$$

$$= \frac{2fd}{R_{90}} \text{ , } R_{90} >> |\dot{fd}| \qquad (5\text{-}109)$$

where fd is the total (positive frequency) uncertainty band. In our system fd = 2.226 MHz and $|\dot{fd}|$ is the doppler rate. It is possible to assume that by sweeping at half the range given by (5-108) we can increase the probability of acquisition to .99, it is clear then that we pay a penalty of doubling the acquisition time as given by (5-109). It is preferable to decrease the sweep rate to half instead of assuming two consecutive sweeps in order to determine the time it takes to acquire with .99 probability due to hardware advantages and at the same time decrease the possibility of falling out of lock while trying to kill the sweep. It also follows from (5-109) that $T_{ACQ} = f(B_L)$, the larger B_L, the larger the sweep rate and the smaller the acq time. For the system design B_L was chosen to minimize phase jitter and the resulting B_L is such that the acq time is very much within acceptable values. The results of the above analysis is presented in Figures 5-22, 5-23, and 5-24.

Once B_L has been fixed (B_L = 5 kHz) we can compute the mean to first slip time according to [22].

$$\bar{T}slip = \frac{\pi}{4B_L} e^{1.5\rho'} \qquad (5\text{-}110)$$

for the above values of B_L and $4\sigma^2 T$ we have $\bar{T}slip = 2.3 \times 10^9 S$.

It is also important to observe that due to the fact the loop bandwidth B_L has been chosen to maximize the SNR in the loop (ρ') and not to satisfy acquisition time requirements there is no need to switch filters once in the tracking mode. In fact to do that would imply a higher BEP degradation.

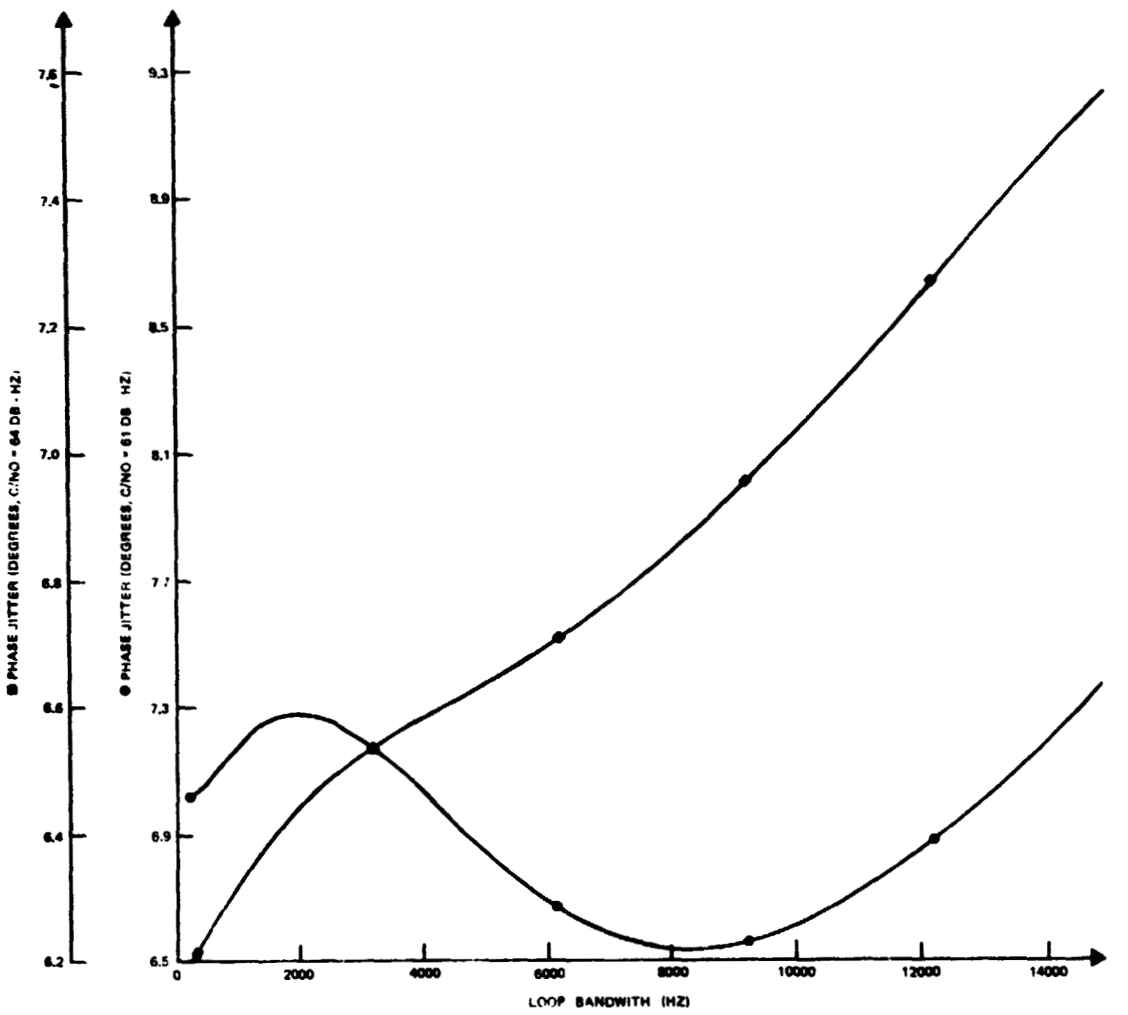

Figure 5-22. Phase Jitter Vs. Loop Bandwidth. The Data Rate is 216 Kbps.

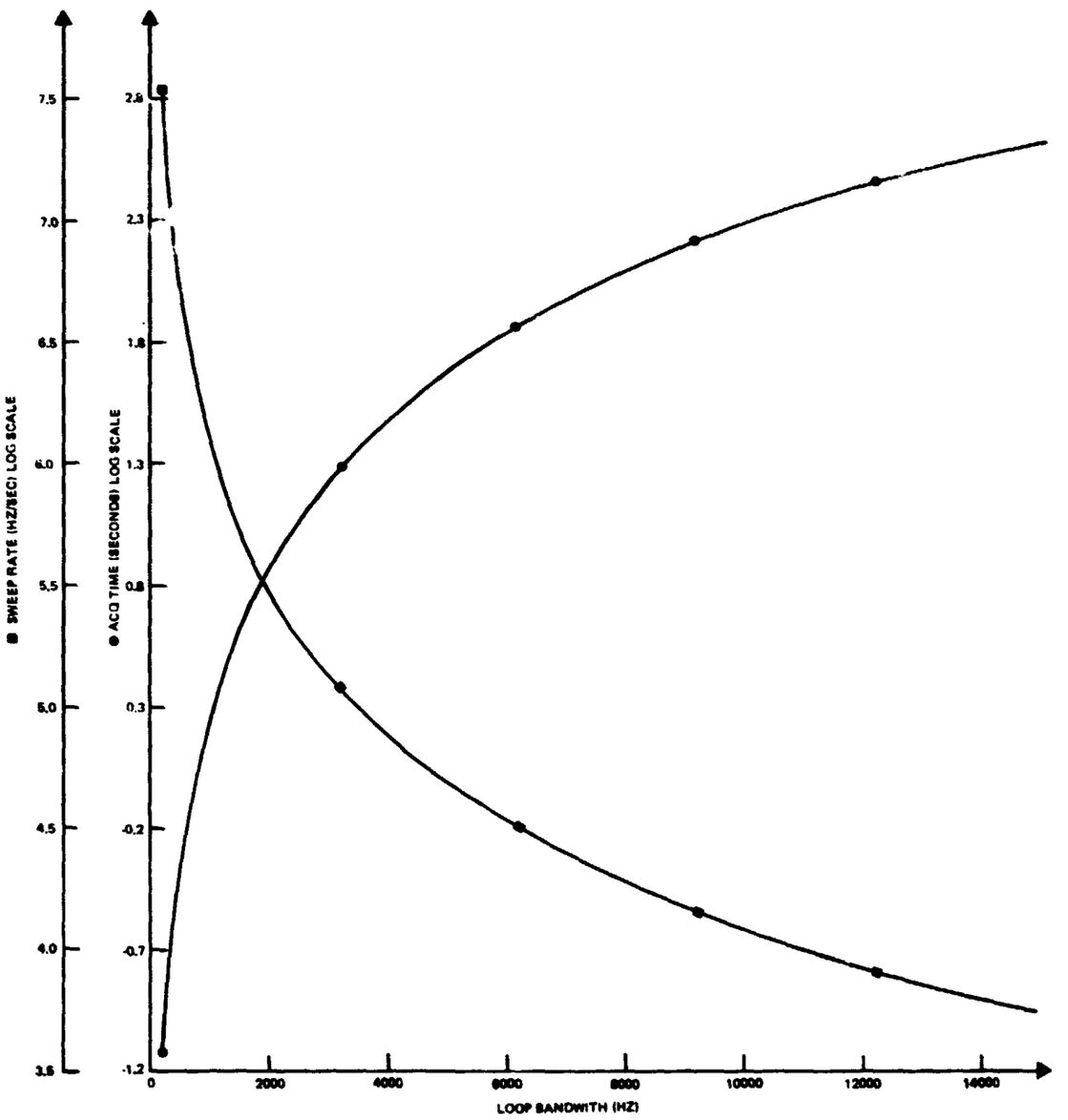

Figure 5-23. Acquisition Time and Sweep Rate Vs. Loop Bandwidth. R = 216 Kbps and C/N_0 = 64 dB-Hz.

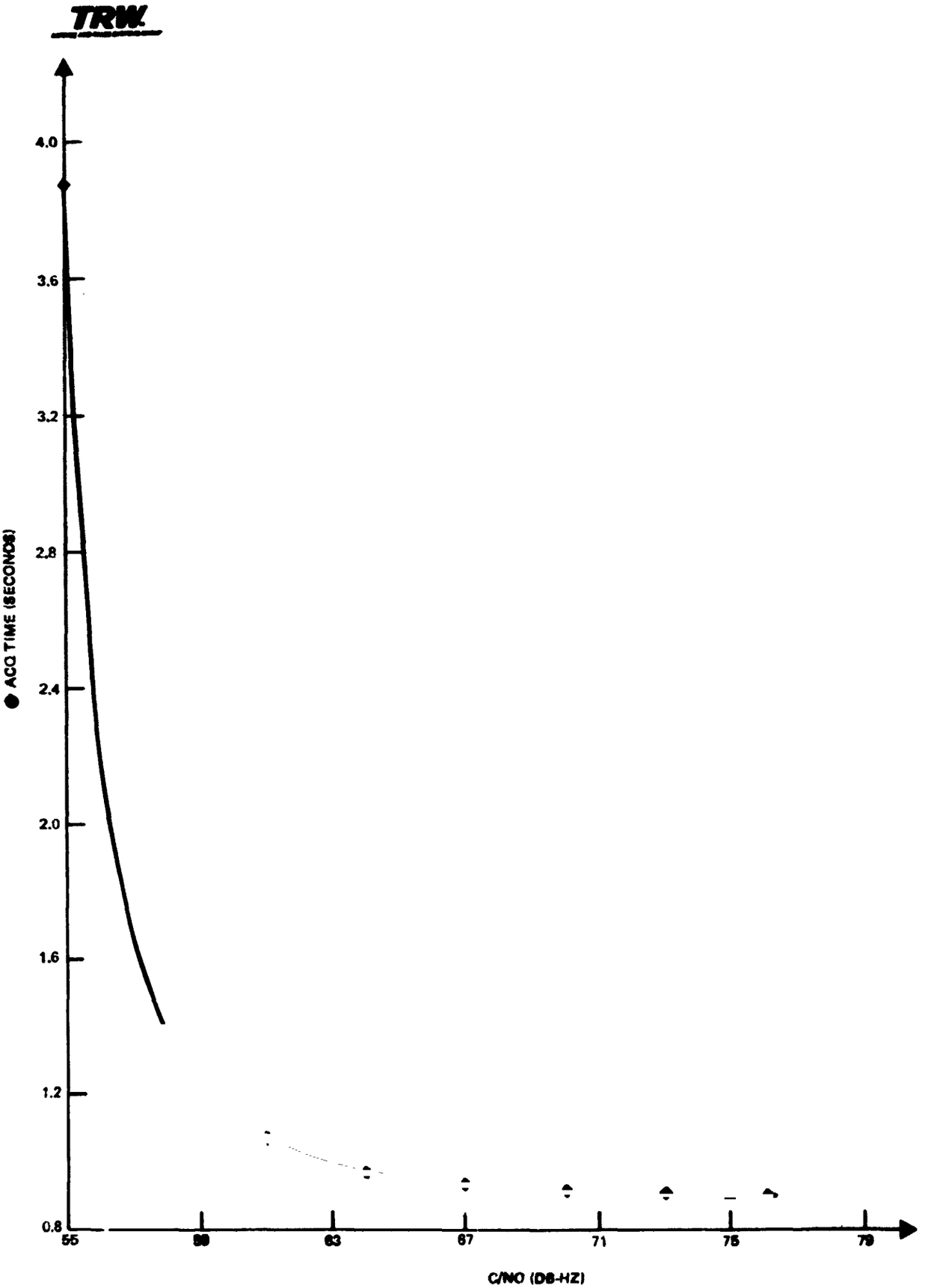

Figure 5-24. Acquisition Time Vs. C/N_0. R = 216 Kbps; P_r = 0.99.

5.3.3 Recommended Carrier Synchronization Design

The carrier recovery loop recommended for use in the K-band Orbiter receiver is the Costas detector implementation shown in Figure 5-25.

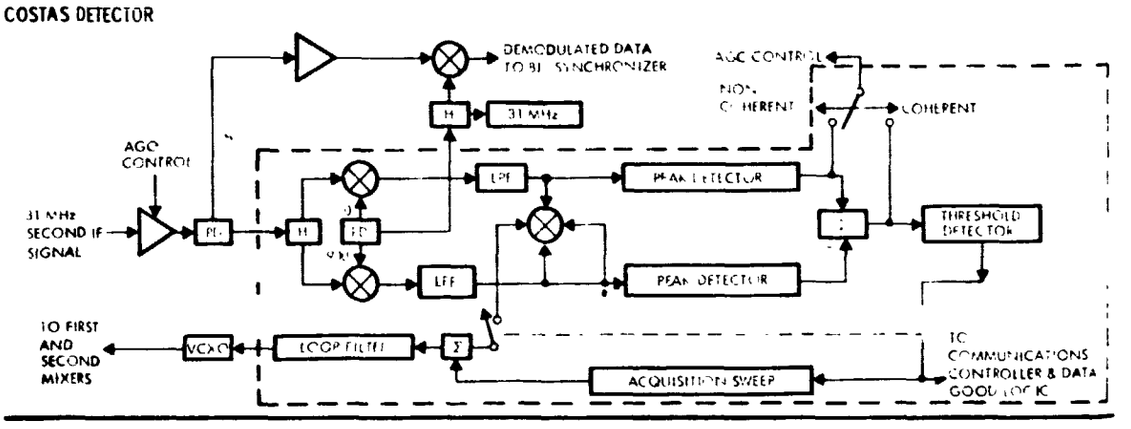

Figure 5-25. Costas Detector

Pertinent loop parameters are indicated in Table 5-4 and the tradeoff between loop bandwidth and acquisition time is shown in Figure 5-26. Note that for the chosen loop bandwidth of 5 kHz the loop will acquire with a 0.99 probability in 1.4 seconds. This acquisition time is consistent with a 3.4 dB margin for the 36.6 dBW minimum EIRP from TDRS.

Table 5-4. Performance and Design Parameters

PERFORMANCE AND DESIGN PARAMETERS	
LOOP BANDWIDTH	5 KHz
ACQUISITION TIME	1.4 SEC
ACQUISITION SWEEP RATE	2 MHz/SEC
SWEEP RANGE	±1.3 MHz
VCXO PHASE NOISE	5.39 DEG RMS
VCO PHASE NOISE	0.71 DEG RMS
BER DEGRADATION	0.7 dB
17 DEG STATIC PHASE ERROR	0.6 dB
7 DEG RMS PHASE ERROR	0.1 dB

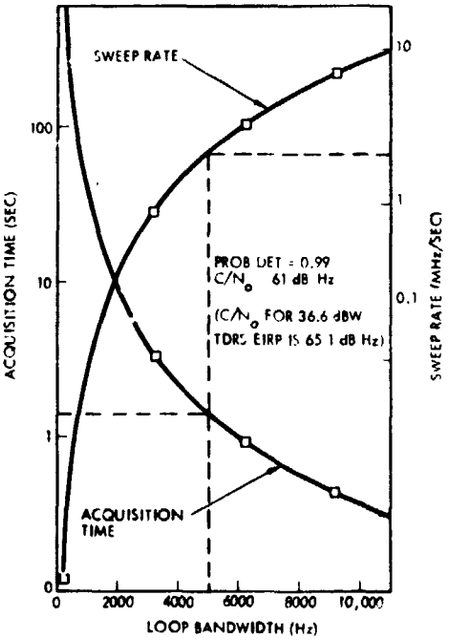

Figure 5-26. Loop Bandwidth Selection

The ±1.4 MHz sweep range was sized to accommodate the following factors: 500 kHz doppler, 500 kHz offset, 100 kHz receiver local oscillator offset, and 200 kHz allowance for variation in sweep circuitry.

The degradation due to phase noise for the 5 kHz loop bandwidth is shown in Figure 5-27. The phase jitter estimates reflect both the front

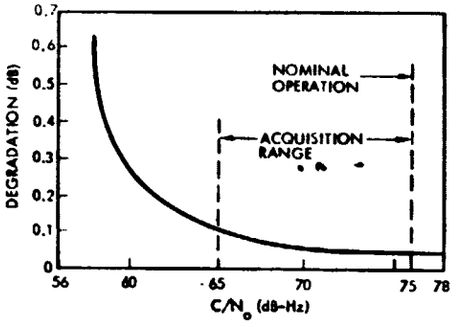

Figure 5-27. Phase Noise Degradation BEP for 5 kHz B_L

end thermal noise and the contribution of the VCO in the indirect X15 multiplier. In addition to the 0.1 dB degradation to bit error rate at nominal TDRS EIRP due to phase jitter, an additional 0.6 dB degradation is contributed by a static phase error of 17 degrees (current worst-case SCTE estimate). This is due to phase shift differences in the signal paths to the Costas loop and the wideband data demodulator.

5.4 BIT SYNCHRONIZER

The Orbiter receiver bit synchronizer receives as input the 216 kbps biphase data and derives a bit synchronous clock output plus the data (now NRZ) suitable for processing by the frame sync decoder. The data output of the frame sync decoder is in 16-bit bytes to the demultiplexer RAM which performs separation of the 144 kbps payload data and 72 kbps operational data. The 72 kbps data is the Ku-band input to the NSP synchronizer. This data flow is illustrated in Figure 5-28.

A complete redesign of the bit receiver was considered during the uplink study, however, the recommended unit is identical except for interface modifications, to the bit synchronizer previously developed by TRW for SC network signal processor (NSP).

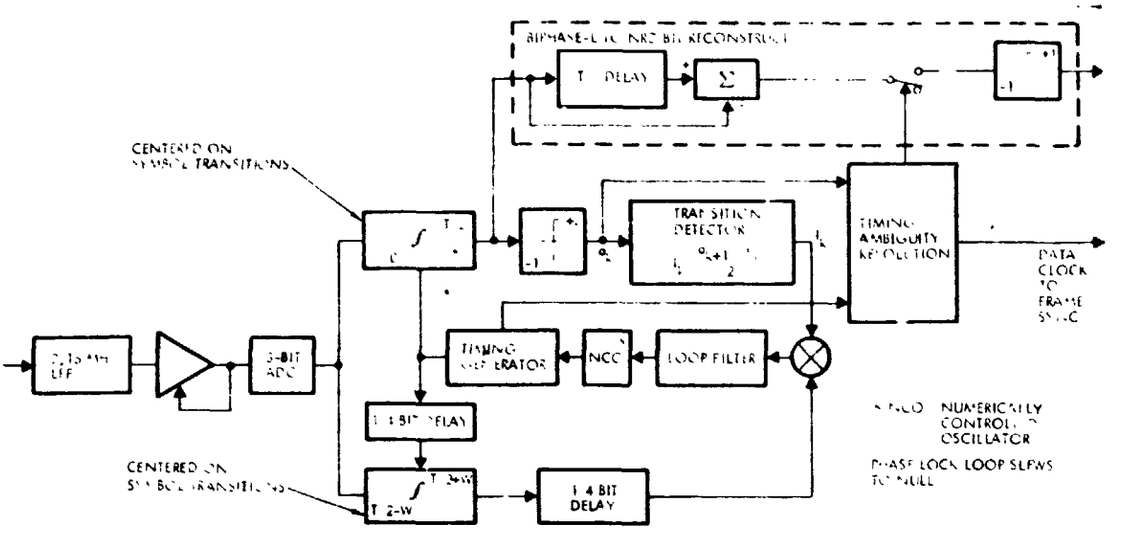

Figure 5-28. Bit Synchronizer and Data Detection Using Data Transition Tracking Loop

5.4.1 Functional Description

The bit synchronizer function is illustrated in the diagram of Figure 5-28. Signal conditioning in the analog front end consists of converting the differential signal to a single-ended signal then filtering through a 3-pole butterworth filter whose noise bandwidth is 10 times the incoming data rate or 2.16 MHz. The filter data signal is then applied to an absolute value detector AGC amplifier high pass cutoff < 1 kHz (ac coupled) which provides a constant output level. The data signal is next applied to a 3-bit A/D converter which converts the signal into digital words in two's complement format The A/D converter utilizes a 50 percent duty cycle clock at a rate 32 times the data rate of 6.912 MHz. Eight samples at a time are clocked into a quarter-symbol accumulator. The resulting 6-bit digital word which represents the final value for a quarter-symbol integration, is reclocked, delayed, and then added to the next quarter-symbol accumulation to obtain a 7 bit half-symbol integration. Once the half-symbol integration is performed, a full symbol adder completes the Manchester data detection by subtracting successive half-symbol integrals after a half-symbol period delay thus producing an NRZ data stream.

To generate the bit synchronous clock, the half-symbol integrations previously performed in the data detector are sent to the phase detector and CAD lock detector together with a sign bit of a half-symbol integration. The phase detector operates by integrating about an assumed transition and multiplying the result by +1, 0, -1 depending on the sense of the data transition about the integration. The sense of the transition and magnitude of the phase error is obtained by comparing successive half-symbol integrations in the phase detector. The phase error output of the phase detector consists of 7 bits plus 1 control bit depending on the sense of the data transition. This phase error is then smoothed by the digital loop filter before being applied to the numerically controlled oscillator (NCO). The NCO varies the derived bit synchronizer clock so that the phase error between the incoming data and locally-derived bit synchronizer clock tend to zero. Finally the half-symbol integrations from the analog board are used to perform a coherent amplitude detection which is used to indicate locked or unlocked status of the loop.

5.4.2 Performance Summary

The Ku-Band Orbiter bit synchronizer, identical to the SCTE unit, has demonstrated the capability of highly efficient operation at low signal-to-noise ratios, performing within 0.5 dB of theoretical at the forward link data rate of 216 kbps as shown in Figure 5-29. A summary of requirements and capabilities is shown in Table 5-5.

The key requirements for the bit synchronizer are a BER degradation of less than 1.0 dB and a capability of acquiring and tracking down to 0 dB signal-to-noise ratio. These requirements are met by an all-digital implementation to obtain accurate and stable matched filter detection and by employing a data transition tracking loop (DTTL) to allow the bit sync to operate at low values of signal-to-noise ratio.

A summary of the design values in given in Table 5-6 for both acquisition and tracking. Mean acquisition times are plotted in Figure 5-30 for various values of SNR parametrically with transition density.

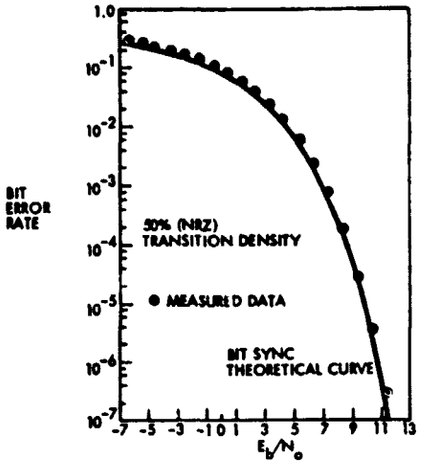

Figure 5-29. Bit Sync Bit Error Rate is Within 0.5 dB of Theoretical

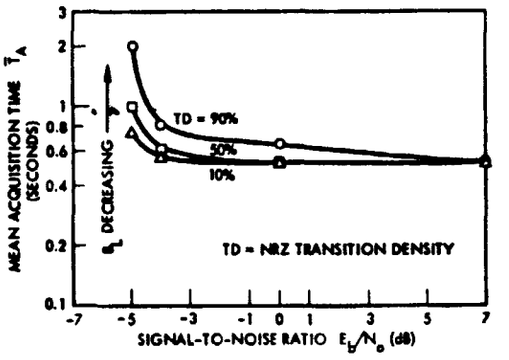

Figure 5-30. Mean Acquisition Time As a Function of E_b/N_o

Table 5-5. Shuttle Bit Synchronizer Requirements Versus Capabilities

INPUT CODE	MANCHESTER II, BIPHASE L
BIT RATE	216 KBPS
THRESHOLD SNR (E_b/N_o)	< -5 dB
BER DEGRADATION	0.5 dB
OUTPUT CODE	NRZ-L
AMBIGUITY RESOLUTION	PROVIDED
MEAN ACQUISITION TIME	< 0.7 SEC
LOCK INDICATION	PROVIDED

Table 5-6. Design and Performance Values

$\frac{E_b}{N_o}$ (dB)	TRANSITION DENSITY (%)	LOOP BAND WIDTH B_L (Hz)	LOOP SNR (dB)	SYNC JITTER (%)	ACQ TIME (SEC)
0	50	80	36	<1.0	0.5
7	50	122	43	0.2	0 5

At the specified minimum of 0 dB SNR, the bit sync mean acquisition time is less than 0.7 seconds. For SNR's 5 dB below specification, acquisition time is only a few seconds and is relatively insensitive to transition density variations over a large range.

The frame sync decoder acquires frame synchronization in an average of 9 milliseconds (four and one half frame periods). The total time for bit and frame sync acquisition is $\sim$ 0.5 seconds at a 0 dB SNR. The frame sync decoder senses data polarity and inverts the data if required.

6. DOWNLINK PERFORMANCE EVALUATION

An additional task undertaken during the Ku-Band Uplink Signal Study was the performance evaluation of the downlink signal by means of computer simulation to obtain realistic estimates of BER degradation. This section summarizes the results of that investigation. Both downlink modes are considered.

6.1 DOWNLINK SIGNAL DESCRIPTION

Computer link simulations were performed for the downlink signal which may perform in either of two modes as described below.

6.1.1 Mode 1

Mode 1 is an all digital data mode in a three-channel configuration The data in the three channels is asynchronous. The channel capacities are:

Channel 1 - 192 kbps (Biphase L)

Channel 2 - Variable from 16 kbps to 2 Mbps (Biphase L or NRZ-L)

Channel 3 - Variable from 3 Mbps to 50 Mbps (NRZ)

Channels 1 and 2 are uncoded. Channel 3 is convolutionally encoded at rate one-half.

The formation of the Mode 1 downlink signal is illustrated in the block diagram of Figure 6-1. Channels 1 and 2 are orthogonally mixed with an 8.5 MHz squarewave. The modulated squarewave outputs are mixed with the convolutionally encoded (R = 1/2; K = 7) digital data of Channel 3. The three resulting channels are summed after appropriate weighting and the resultant is phase modulated to form the Mode 1 downlink.

6.1.2 Mode 2

The Mode 2 downlink signal shall consist of one of the following.

1) Three Simultaneous Channels of Data:

Channel 1 - 192 kbps Biphase L format data

Channel 2 - 16 kbps to 2 Mbps (variable) NRZ-L or 1024 kbps Biphase L data

Channel 3 - 4.5 megahertz TV, or up to 4 Mbps digital NRZ format data, or 4.5 megahertz analog data or other data that are compatible with the response characteristics of this channel

Channels 1 and 2 are modulated onto an 8.5 megahertz plus or minus 0.1 megahertz subcarrier oscillator and then combined with the analog Channel 3 data in the spectral range of 3 hertz to 4.5 megahertz. The Channel 1 and 2 data are unbalanced QPSK modulated with a power split of 80 percent for the I-channel (Channel 2) and 20 percent for the Q-channel (Channel 1). The composite, summed signal must be established with adequate filtering to prevent the analog data from reducing the BEP of the digital data or the digital data on the nominal 8.5 megahertz subcarrier from the degrading TV performance. The composite signal maintains dc response into the FM modulator, where an appropriate bias shall be added to provide symmetrical frequency deviation about the nominal center frequency. The 8.5 megahertz subcarrier deviates the carrier plus or minus 11 megahertz, each about the nominal center frequency.

2) Two Channels of Simultaneous Data:

Channel 1 - A subcarrier oscillator of 8.5 MHz modulated by a data signal format described below

Channel 2 - An analog on digital channel identical to Channel 3 of (1) above

Data for the 8.5 MHz SCO Channel are TDB, but are typically up to 16 kbps PSK modulated on a 1.025 MHz sinusoidal signal. The input modulated signal is phase modulated onto the 8.5 MHz SCO of a modulation index of TBS. The following performance parameters shall be used:

		TBS
a)	Modulation Loss	
b)	FM Discriminator Degradation	-1 dB
c)	TV Interference	-2 dB
d)	PM Demodulation Degradation	-1 dB

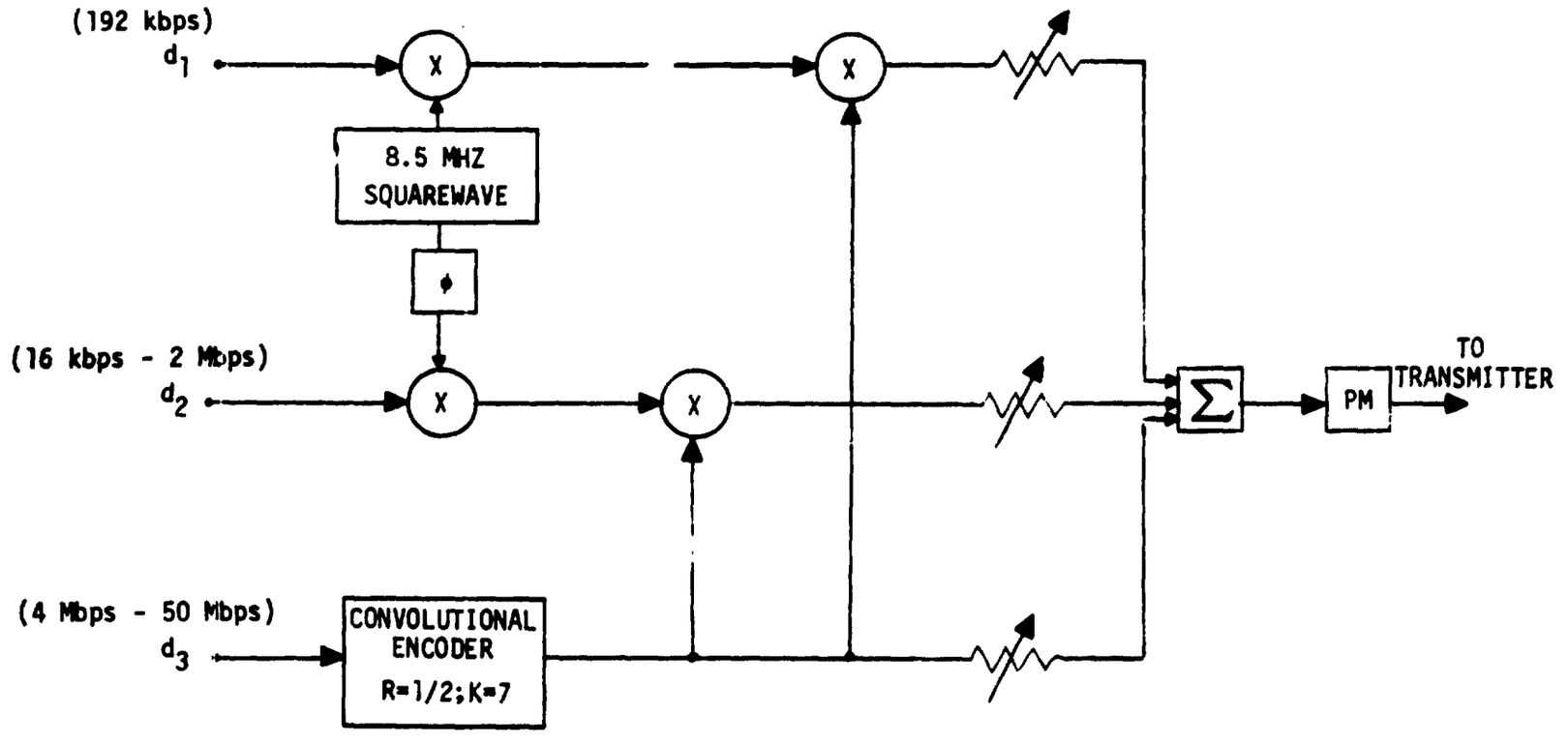

Figure 6-1. Formation of the 3-Channel PM (Interplex) Model 1 Return Link

6.2 COMPUTER LINK SIMULATION FOR DOWNLINK MODE 1

All significant sources of distortion were analyzed and performance simulations were made to obtain the resultant BER degradations.

The primary tool used in evaluating link BER degradation was the TRW link simulation program described in Section 3.4. The simulation was modified to accommodate the three-channel model configuration. This configuration consists of a 192 kbps signal and a 2 Mbps signal in quadrature on an 8.5 MHz squarewave subcarrier which itself is in quadrature with a 50 Mbps, rate 1/2 convolutionally encoded signal. The simulation was modified to generate this signal structure, with the appropriate power levels, which was used as the input signal for the simulation. The simulation model as well as typical waveforms at the output of the modulator, orbiter and the ground station demodulator are shown in Figure 6-2.

The simulation, which included all significant distortion sources (except data asymmetry discussed below), gave a BER degradation of 1.8 dB for Channel 3. The sensitivity of BER degradation to variation in each of the more critical link parameters was determined by varying each parameter in the simulation individually and observing the resulting change in degradation (Figure 6-3).

The BER degradation is fairly insensitive to variations in RF parameters over and beyond worst-case values. The sensitivity of BER degradation to TDRS AM-to-PM conversion was determined; the additional degradation caused by 5°/dB of TDRSS AM-to-PM was only 0.15 dB.

The sensitivity to variation in baseband parameters over the range specified in the [28] are shown in Figure 6-4. For power division (i.e., the division of power among the three channels) several parameters are varying simultaneously and, therefore, only the nominal and worst-case point have been shown. Power division causes the most variation over the allowable range of variation; however, the additional degradation for an extreme condition is only 0.4 dB.

It is worth noting that while the Orbiter passband phase and gain variation are larger than for TDRS, the degradation due to the Orbiter passband characteristics is only a few tenths of a dB. More important is the fact that the passband is specified in [3] have good passband

Figure 6-2. Simulation Model

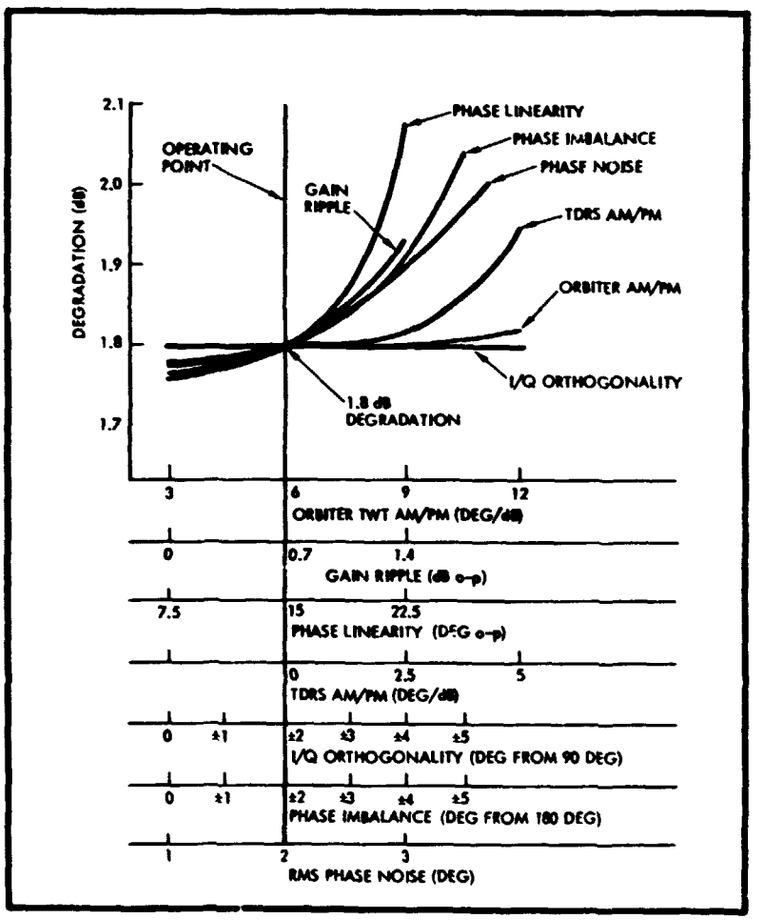

Figure 6-3. Parameter Sensitive Analysis - RF Parameters

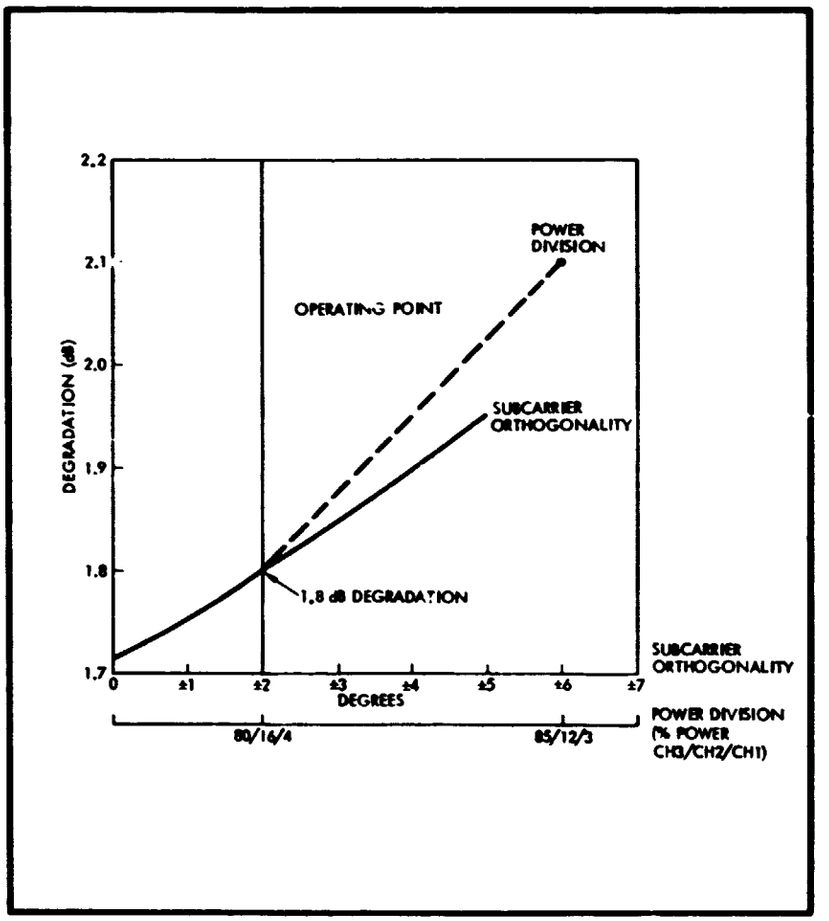

Figure 6-4. Parameter Sensitivity Analysis - Baseband Parameters

characteristics over 225 MHz while the TDRS has good passband characteristics over only 160 MHz. Thus if higher data rates than 50 Mbps (100M symbols/sec) are desired, the Orbiter passband will be nonconstraining and the maximum achievable data rate will be limited by the TDRS bandpass (approximately 75 to 80 Mbps or 150 to 160M symbols/sec per I or Q channel). For Channels 1 and 2, the data rates are lower, the distortion effects of the channel elements are less, and the resulting BER degradation will be < 1.8 dB. Since Channels 1 and 2 have large margins (19.2 and 15.0 dB, respectively), 1.8 dB was used as an upper bound.

Transmission of data from the signal processor to the transmitter assembly over approximately 60 feet of 75 ohm coaxial cable causes lenthening of rise and fall times. This, in combination with dc offsets due to differences in ground potential, results in data asymmetry (the percentage increase or decrease in a bit time) of up to ± 8 percent for the high rate (Channel 3) signals. Analysis shows a BER degradation of 0.75 dB at 50 Mbps. As the data rate decreases, the data asymmetry introduced decreases so that at 10 MHz, the degradation is only 0.1 dB. The asymmetry can be reduced by adding circuitry to reclock the data at the end of the cable. Given the ample margin provided (7.0 dB), the small improvement does not warrant the added complexity of reclocking circuitry.

For Channels 1 and 2, data rates are low enough (192 kbps and 2 Mbps, respectively) so that no significant data asymmetry is introduced by the cable.

6.3 COMPUTER ANALYSIS FOR DOWNLINK MODE 2

The Mode 2 return link is FM with two possible baseband configurations: a three-channel configuration consisting of wideband signal (analog or digital) and an unbalanced QPSK subcarrier at 8.5 MHz; or a two-channel configuration consisting of the same wideband signal and a PM subcarrier at 8.5 MHz.

Differential phase and gain are primarily determined by RF time delay distortion and by baseband (including modulator) intermodulation, respectively. The TWT is the primary contributor to time delay distortion. The primary contributor to differential gain is the FM modulator nonlinearity (manifested in intermodulation). Both the Ku-band and SCTE FM modulators

are specified to be linear to within ±2 percent over their respective deviation ranges.

In order to prevent the wideband Channel 3 signals from interfering with the subcarrier signals, and vice versa, filtering of these signals prior to summing is necessary. These filters and the subcarrier filter were chosen to cause minimal distortion in the passband, while rolling off fast enough to reduce interference in the stop band. Because of the impracticality of simultaneously achieving in one filter very low time delay distortion for the TV channel and high out-of-band rejection for the digital signal (the digital signal has much more power in the subcarrier band than do the other signals) a different filter is used for the digital signal. The filter degradation was typically 0.5 dB with a maximum of 1 dB.

A source of noise often significant in FM links is intermodulation noise due to modulator nonlinearities, transmission deviations (i.e., gain slope and phase nonlinearity), and AM/PM conversion. An analysis based on the work of Cross [24] and Garrison [25] has been done to determine the intermodulation distortion introduced by these factors. The details of this analysis are presented in Appendix B. The results are shown in Figure 6-5 for the digital Channel 3/QPSK subcarrier mode. The rms signal-to-intermodulation ratio has been determined for the operating point and then each distortion causing parameter has been varied individually to determine the sensitivity of the distortion level to variations in that parameter.

For the TV signal case, the intermodulation is much lower than for the digital signal case. The lower intermodulation which results when the digital signal is replaced by the TV signal is due to two effects. These are the higher power in the digital signal relative to analog signal (approximately 3 dB difference) and the fact that the TV signal spectrum is much more concentrated near dc.

Since the required link rms signal to rms noise is 26 dB for the analog channel (35 dB peak-to-peak signal to rms noise) and approximately 10.5 dB for the subcarrier and digital signal, it is clear that this intermodulation distortion causes negligible reduction in link performance margins.

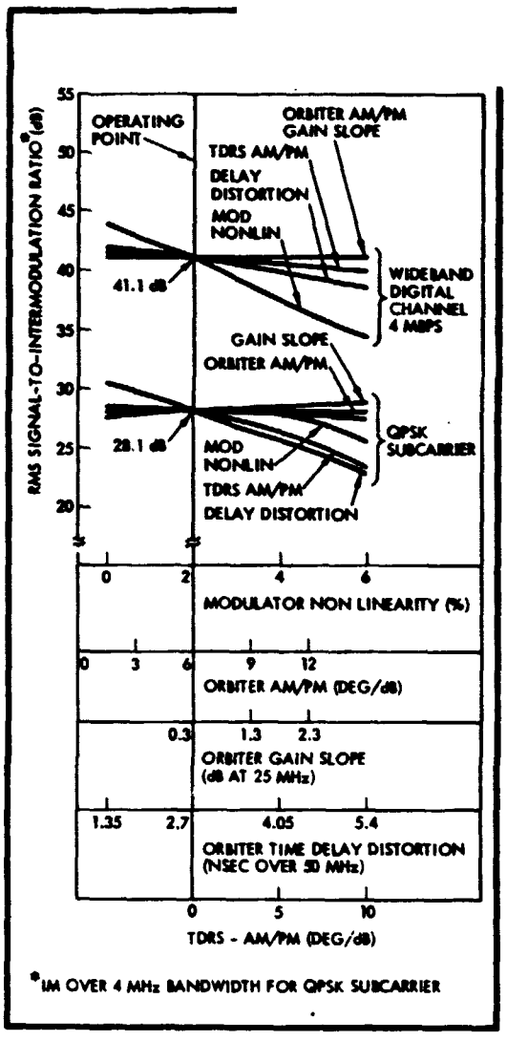

Figure 6-5. Signal-to-IM Ratio Parameter Sensitivity Analysis-Digital Channel 3 Data

6.4 DOWNLINK POWER BUDGETS

The downlink power budgets for Modes 1 and 2 are shown in Tables 6-1 and 6-2 , respectively. Reference sources for each item are taken from the Rockwell RFP [28], the TRW proposal [3], and this study.

The Mode 1 return link distributes the effective P_{REC}/N_0 among the three channels. Margins for Channels 1 and 2 including all degradations, are 19.2 and 15.0 dB, respectively. Margins for Channel 3 are computed for various data rates between 10 and 50 Mbps. These are shown to vary between 7.0 and 16.3 dB as the Channel 3 data rate varies in this range.

The Mode 2 return link budgets of Table 6-2 show both the two- and three-channel configurations. For the three-channel case, Channels 1 and 2 show margins of 13.6 and 10.3 dB, respectively. Channel 3 has a computed margin of 8.9 dB for analog data and 13.6 dB for digital. The two-channel configuration has a 13.6 dB margin for the 8.5 MHz SCO channel and margins of 8.9 and 13.6 dB for the analog wideband channel and the digital wideband channel, respectively.

Table 6-1. Return Link — Mode 1

ITEM	VALUE	SOURCE
ORBITER TRANSMIT POWER	19.5 dBw	[3]
TRANSMIT CIRCUIT LOSS	-1.6 dB	[3]
TRANSMIT ANTENNA GAIN	40.3 dBi	[3]
ORBITER EIRP	58.2 dBw	[3]
ANTENNA POINTING LOSS	-0.1 dB	[3]
ANTENNA POLARIZATION LOSS	-0.1 dB	[3]
SPACE LOSS	-208.5 dB	PS 70.2.3.2A [28]
TDRS RECEIVER G/T	24.1 dB/K	PS 70.2.3.1A [28]
BOLTZMANN'S CONSTANT	-228 6 dBw/Hz-K	-
P_{REC}/N_o	102.2 dB-Hz	CALCULATION
TDRS TRANSPONDER LOSS	-2.0 dB	PS 70.2.3.1B [28]
TDRS AUTOTRACK LOSS	-1.0 dB	PS 70.2.3.1C [28]
DEMODULATION LOSS	-1.0 dB	PS 70.2.3.1D [28]
EFFECTIVE P_{REC}/N_o	98.2 dB-Hz	CALCULATION

ITEM	CHANNEL					SOURCE
	1	2	3			
MODULATION LOSS	-14 dB	-8 dB	-1 dB	, dB	-1 dB	RFP AMENDMENT 1 [28]
DATA RATE (MBPS)	0.192	2.0	50.0	30.0	10.0	-
DATA RATE (dB-Hz)	52.8	63.0	77.0	74 8	70.0	-
E_b/N_o (dB)	31.4	27 2	20.2	22.4	27.2	CALCULATION
BAND LIMITING EFFECT (dB)	0.0	0.0	-0.7	-0.3	0.0	PS TABLE XXVIII [28]
BIT SYNC DEGRADATION (dB)	-2.0	-2.0	-3.5	-3.0	-2.5	PS TABLE XXVIII [28]
OTHER LOSSES (dB)	-1.8	-1.8	-2 5	-2.1	-1.9	STUDY
BEP	10^{-4}	10^{-4}	10^{-6}	10^{-6}	10^{-6}	-
CODING GAIN (dB)	N/A	N/A	4.0	4.0	4.0	PS TABLE XXVIII [28]
REQUIRED E_b/N_o (dB)	8.4	8.4	10.5	10.5	10.5	-
CIRCUIT MARGIN (dB)	19.2	15.0	7 0	10.5	16 3	CALCULATION

Table 6-2. Return Link — Mode 2

ITEM	VALUE	SOURCE
ORBITER TRANSMIT POWER	19.5 dBw	[3]
TRANSMIT CIRCUIT LOSS	-1.6 dB	[3]
TRANSMIT ANTENNA GAIN	40.3 dBi	[3]
ORBITER EIRP	58.2 dBw	[3]
ANTENNA POINTING LOSS	-0.1 dB	[3]
ANTENNA POLARIZATION LOSS	-0.1 dB	[3]
SPACE LOSS	-208.5 dB	PS 70.2.3.2A [28]
TDRS RECEIVE G/T	24.1 dB/K	PS 70.2.3.1A [28]
BOLTZMANN'S CONSTANT	-228.6 dBw Hz-K	-
TDRS P_{REC}/N_o	102.2 dB-Hz	CALCULATION
TDRS TRANSPONDER LOSS	-2.0 dB	PS 70.2.3.1B [28]
TDRS AUTOTRACK LOSS	-1.0 dB	PS 70.2.3.1C [28]
EFFECTIVE P_{REC}/N_o	99.2 dB-Hz	CALCULATION
PREDETECTION BW	75.6 dB-Hz	PS 70.2.3.3.3.3A[28]
SNR AT DISCRIMINATOR INPUT	23.6 dB	CALCULATION
FM THRESHOLD	10 dB	PS 70.2.3.3.3.3B [28]
FM THRESHOLD MARGIN	13.6 dB	CALCULATION

ITEM	CHANNEL 1 (192 KBPS)	CHANNEL 2 (≤ 2 MBPS)	CHANNEL 3 ANALOG OR DIGITAL		SOURCE
FM IMPROVEMENT (dB)	16.7	6.5	23.8	23.8	CALCULATION PS 70.2.3.3.3.1.2C [28]
FM DISCRIMINATOR DEGRADATION (dB)	-1.0	-1.0	-1.0	-1.0	PS 70.2.3.3.3.1.1C [28]
MODULATION LOSS (dB)	-7.0	-1.0	N/A	N/A	PS 70.2.3.3.3.1.1B [28]
QPSK DEMODULATION LOSS (dB)	-1.0	-1.0	N/A	N/A	PS 70.2.3.3.3.1.1A
POST DETECTION SNR (dB)	31.3	27.1	46.4 $(\frac{rms}{rms})$	46.4	CALCULATION [28]
SNR OF INPUT DATA (dB)	35.0	35.0	45.0 $(\frac{P-P}{rms})$	35.0	PS 3.2.1.2.3.3.1 [28]
SIGNAL TO IM RATIO (dB)	41.0	31.1	>60.0 $(\frac{P-P}{rms})$	41.1	STUDY
COMBINED SNR (dB)	29.4	25.2	44.5 $(\frac{P-P}{rms})$	33.8	CALCULATION
BANDPASS FILTERING LOSS (dB)	-0.4	-0.4	-0.1	-0.6	STUDY [28]
TV INTERFERENCE (dB)	-2.0	-2.0	N/A	N/A	PS 70.2.3.3.3.1.1D
SUBCARRIER INTERFERENCE	N/A	N/A	-0.5	-0.5	STUDY
BIT SYNC DEGRADATION (dB)	-1.5	-2.0	N/A	-2.0	[28] PS 70.2.3.3.3.1.1E
SNR (dB)	25.5	20.8	41.9	30.7	CALCULATION
BEP	10^{-6}	10^{-6}	N/A	10^{-6}	-
REQUIRED SNR (dB)	10.5	10.5	35.0 $(\frac{P-P}{rms})$	10.5	-
DATA MARGIN (dB)	15.0	18.3	8.9	20.2	CALCULATION
CIRCUIT MARGIN (dB)	13.6*	10.3	8.9	13.6*	CALCULATION

ITEM	8.5 MHz SCO CHANNEL	WIDEBAND CHANNEL ANALOG OR DIGITAL		SOURCE
POST DETECTION SUB-CARRIER/N_o (dB)	93.2	N/A	N/A	CALCULATION
FM IMPROVEMENT (dB)	N/A	23.8	23.8	CALCULATION
FM DISCRIMINATOR DEGRADATION (dB)	-1.0	- 0	-1.0	PS70.2.3.3.3.1.2C** PS 70.2.3.3.3.1.2C**
DATA RATE (dB)	42.0	N/A	N/A	PS 70.2.3.3.3.1.1C**
POST DETECTION SNR (dB)	30.2	46.4 $(\frac{rms}{rms})$	46.4	CALCULATION
SNR OF INPUT DATA (dB)	35.0	45.0 $(\frac{P-P}{rms})$	35.0	PS 3.2.1.2.3.3.1 [28]
SIGNAL TO IM RATIO (dB)	48.0	60.0 $(\frac{P-P}{rms})$	41.1	STUDY
COMBINED SNR (dB)	34.7	44.5 $(\frac{P-P}{rms})$	33.8	CALCULATION
MODULATION LOSS (dB)	3.3	N/A	N/A	CALCULATION
FM DEMODULATION DEGRADATION (dB)	-1.0	N/A	N/A	PS 70.2.3.3.3.2.1d[28]
BANDPASS FILTERING LOSS (dB)	-0.2	-0.1	-0.6	STUDY
TV INTERFERENCE (dB)	-2.0	N/A	N/A	PS 70.2.3.3.3.1.1d[28]
SUBCARRIER INTERFERENCE	N/A	-0.5	-0.5	STUDY
BIT SYNC DEGRADATION (dB)	-1.5	N/A	-2.0	PS 70.2.3.3.3.1.1e[28]
SNR (dB)	26.7	43.9	30.7	CALCULATION
BEP	10^{-6}	N/A	10^{-6}	-
REQUIRED SNR (dB)	10.5	35.0 $(\frac{P-P}{rms})$	10.5	-
DATA MARGIN (dB)	16.2	8.9	20.2	CALCULATION
CIRCUIT MARGIN (dB)	13.6*	8.9	13.6*	CALCULATION

*CIRCUIT MARGIN IS CONSTRAINED BY FM THRESHOLD MARGIN **[28]

(REVERSE OF THIS PAGE LEFT BLANK)

REFERENCES

[1] "Radio Frequency Allocations for Space and Satellite Requirements," Mission and Data Operation Directorate, Goddard Space Flight Center, Greenbelt, Maryland, 15 June 1973.

[2] "Space Shuttle RF Link Circuit Margins," NASA/JSC, January, 1976.

[3] "Proposal for Ku-Band Integrated Radar and Communications Equipment, Volume 2. Technical," TRW Defense and Space Systems Group, Redondo Beach, California, 17 May 1976.

[4] Poza, H., Sarkozy, Z., and Berger, H., "A Wideband Data Link Computer Simulation Mode," National Aerospace and Electronics Conference Proceedings, June, 1975.

[5] Poza, H. and Berger, H., "Performance Characterization of Advanced Wideband Data Links," International Communications Conference Proceedings, June, 1975.

[6] D. E. Cartier, "A Frequency Domain Approach to Shuttle PN Code Acquisition," NTC Record, San Diego, California, 1974, pp. 714-17.

[7] J. I. Marcum, "A Statistical Theory of Target Detection by Pulsed Radar," Transaction IRE, IT-6, 1960.

[8] W. B. Davenport, Jr., and W. L. Root, An Introduction to the Theory of Random Signals and Noise, McGraw-Hill, New York, 1958.

[9] H. P. Hartmann, "Analysis of a Dithering Loop for PN Code Tracking," IEEE Transaction on AES, AES-10, 1974.

[10] P. T. Nielsen, "On the Acquisition Behavior of Binary Delay-Lock Loops," IEEE Transaction on AES, AES-11, 1975.

[11] Lindsey, W. C. and Woo, K. T., "Costas Versus Squaring Loop Implementations," SCTE-50-76-172, 17 March 1976.

[12] Lindsey, W. C. and Simon, M. K., "The Performance of Suppressed Carrier Tracking Loops in the Presence of Frequency Detuning," Proceedings of the IEEE, Volume 58, No. 9, September, 1970.

[13] Lindsey, W. C. and Simon, M. K., Telecommunication Systems Engineering, Prentice-Hall, Inc., Inglewood Cliffs, New Jersey, 1973.

[14] Wolfgang Grobren and Nikoloau Hofreiter, "Integraltafel Zweiter Teil Teil Bestimmte Integrale," Springer-Verlag, 1961.

[15] Lindsey, W. C., Synchronization Systems in Communication and Control, Prentice-Hall, Inc., Inglewood Cliffs, New Jersey, 1972.

[16] Lindsey, W. C., "Carrier Tracking Phase Jitter Due to Oscillator Instabilities, Data Sidebands and Thermal Noise," IOC SCTE 50-76-176,WLL.

[17] Holmes, J. K., "Preliminary Carrier Acquisition Time Calculations for the Shuttle Orbiter," IOC SCTE-50-75-031/JKH, 2 July 1975.

[18] Holmes, J. K., "Performance and Stability Considerations of the DNSS Receiver I-Q Loop," IOC DNSDP-JKH-154, December, 1973.

[19] Holmes, J. K., "Recommendation to Use 200 Hz ±10% for TDRS Modes," IOC SCTE-50-76-190/JKH, April, 1976.

[20] Holmes, J. K., "Correction to the Acquisition Theory of a Costas and a Squaring Loop Applied to the Shuttle Orbiter," IOC 7130.60-007, June, 1974.

[21] Frazier, J. P., and Page, J., "Phase-Lock Loop Frequency Acquisition Study," IRE Transaction on Space Electronics and Telemetry, September, 1962.

[22] Lindsey, W. C., Private Communciation.

[23] "Telecommunication Services Via a Tracking and Data Relay Satellite System; Part II Technical Proposal," The Western Union Telegraph Company, Upper Saddle River, NJ, 15 January 1976.

[24] Cross, T. B., Intermodulation Noise in FM Systems Due to Transmission Deviations and AM/PM Conversion, Bell System Technical Journal, Volume 45, pp. 1749-1773, December, 1966.

[25] Garrison, G. J., "Intermodulation Distortion in Frequency-Division-Multiplex FM Systems — A Tutorial Summary," IEEE Transactions on Communication Technology, Volume COM-16, pp. 289-303, April, 1968.

[26] Franks, L. E., "A Model for the Random Video Process," BSTJ, April, 1966, pp. 600-630.

[27] "Performance Specification for Telecommunications Services Via the Tracking and Data Relay Satellite System," S-805-1, June, 1976.

[28] "Ku-Band Integrated Radar and Communications Equipment," Procurement Specification MC409-0025, Volume II, Space Division Rockwell International, 15 March 1976.

[29] Haney, E. M., "Diplexer/Filter Requirements," TRW IOC 7300.10-76.71, 26 February,1976.

APPENDIX A

NONCOHERENT AGC PERFORMANCE FOR KU-BAND UPLINK RECEIVER

1. INTRODUCTION

The TDRSS/Shuttle Orbiter Ku-Band Uplink spread-spectrum receiver shall be required to operate over a wide range (40-100 dB) of input power levels. The need for a constant input power level within ± 1 dB for proper despreader operation levies a requirement for some form of automatic level control. Two methods are generally available — coherent and noncoherent automatic gain control (AGC).

To implement a synchronous AGC loop one must have a coherent reference for the signal derived from a phase-locked loop. In this case, control voltages may be generated which are proportional to the instantaneous signal amplitude. During acquisition, however, such a reference is not available and therefore only noncoherent AGC techniques may be used.

The noncoherent AGC loop operates to maintain the total instantaneous power (signal + noise) input to the despreader constant. The baseline approach utilizes an envelope detector before the despreader to provide a measure of the IF power, which is compared to a fixed reference. The difference is filtered to drive the gain control elements which are both variable attenuators and variable bias amplifiers.

The following sections constitute the performance analysis of the noncoherent AGC loop. Section 2 is a self-contained summary of analysis results. Sections 3 through 5 may be considered appendices to Section 2. In Section 2, the linear AGC loop model is developed which allows the calculation of loop frequency and transient respons together with the steady state tracking error in Section 4. Section 5 includes some specific design applications.

2. SUMMARY

The principal difficulty which arises in the analysis of the noncoherent AGC is the development of a linear model for the transfer function between the AGC voltage and input signal plus noise envelope. As seen in Figure 3, which is a simplified block diagram of the noncoherent AGC loop, the AGC voltage is derived by a nonlinear squaring operation or half-wave rectification. Section 3 describes in detail the derivation of the AGC loop model. The control block diagram for the AGC control voltage may be realized by an integrator or low-pass filter with negative feedback as shown in Figures 8(a) and 8(b), respectively. The AGC voltage transfer function resulting from the low-pass filter implementation is

$$H_v(S) = \frac{k_L}{(\tau S + 1 + k_L)k_c}$$

where k_L = AGC loop gain, k_c = attenuation or gain coefficient, and τ is the time constant of the filter.

Using the above AGC voltage transfer function, it is a straightforward procedure to obtain the frequency response of the loop. The 3 dB cutoff frequency occurs at

$$\omega_c = \frac{1 + k_L}{\tau} \text{ rad/sec}$$

and falls off at the rate of 20 dB/decade as shown in Figure 9. The resulting loop two-sided noise bandwidth is

$$f_L = \frac{1 + k_L}{4\pi\tau} \text{ Hz.}$$

The AGC transient response is obtained for a step input, a ramp input, and for a typical antenna acquisition scan. Figure 10 shows the AGC response and steady-state tracking error for a step input. If the envelope follows a ramp input, the loop filter produces a steady-state transient error that grows linearly in time. However, short duration ramp inputs can be tolerated by making the AGC loop gain large.

It is of interest to compute the AGC response during the antenna acquisition scan approximated as a "half-sinusoid" as shown in Figure 11. This response is obtained as sketched in Figure 12.

In summary, the basic analytical tasks for the prediction of the noncoherent AGC loop performance are developed in Sections 3 and 4. The application of these design techniques follow in Section 5. Two specific devices are considered. These are: 1) the MC1590F AGC amplifier – presently under consideration for the S-Band Shuttle Communications 2nd IF noncoherent AGC amplifier, and 2) the 1H407 pin diode attenuator – presently under development by Aertech for the S-Band Shuttle Communications 1st IF AGC. Using assumed values for the desired output level, the AGC amplifier is treated in some detail, yielding values for loop gain, loop bandwidth, and response time.

Some further work is required in the analysis of the noncoherent AGC loop in noise. In particular, an expression for the stability of the AGC gain for low signal-to-noise ratios is desired. Some progress has been made in this area and results will be published at a later date.

3. AGC LOOP MODEL

The desired AGC function holds the output power at a constant level despite significant variations in the received power. This basic operation is shown conceptually in Figure 1. The input envelope-squared function $A^2(t)$ is composed not only of a (signal x signal) -term but (spread signal x noise) and (noise x noise) terms as well and the AGC loop must operate on observations of the total instantaneous power. The operational concept for AGC is one of normalizing the envelope-squared to a desired value using an estimate of $A^2(t)$ designated as $\hat{A}^2(t)$. This operational concept is illustrated in Figure 2. The noise-term instantaneous power fluctuations can be smoothed by implementing an estimator structure with delay taking care that the integration time constant is faster than the variations in received signal. The resulting AGC configuration is one based on energy detection. Related analysis work by Victor, Brockman, and Tausworthe ([1],[2]) on the behavior of synchronous AGC loops which require a coherent signal reference for operation, and Oliver [3] on automatic volume control does not apply directly to the above AGC configuration and a somewhat different approach is required.

One practical implementation of an AGC circuit is shown in the block diagram of Figure 3. The AGC action is accomplished by monitoring the output of a variable gain amplifier with an envelope detector, comparing the detector output to a fixed reference voltage V_R, and using the filtered incremental voltage bias to adjust the amplifier gain to produce the desired output envelope. The envelope detector is either a half-wave linear or square-law device. Additional loop sensitivity may be obtained by a gain element, usually a high gain operational amplifier, in the feedback path. The performance analysis for this technique, the baseline front-end AGC for the Ku-band uplink receiver, follows in the sequel.

First the linearized model of the AGC circuit is developed. The purpose here is the derivation of the transfer function relating the AGC control voltage $V_C(t)$ to the input (signal + noise) -envelope A(t).

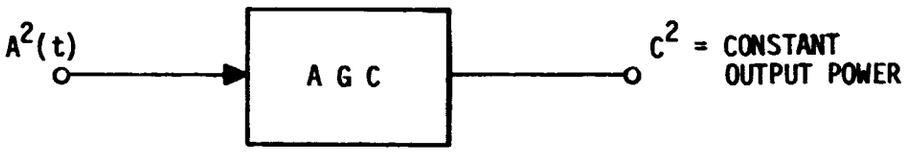

Figure 1. AGC Function

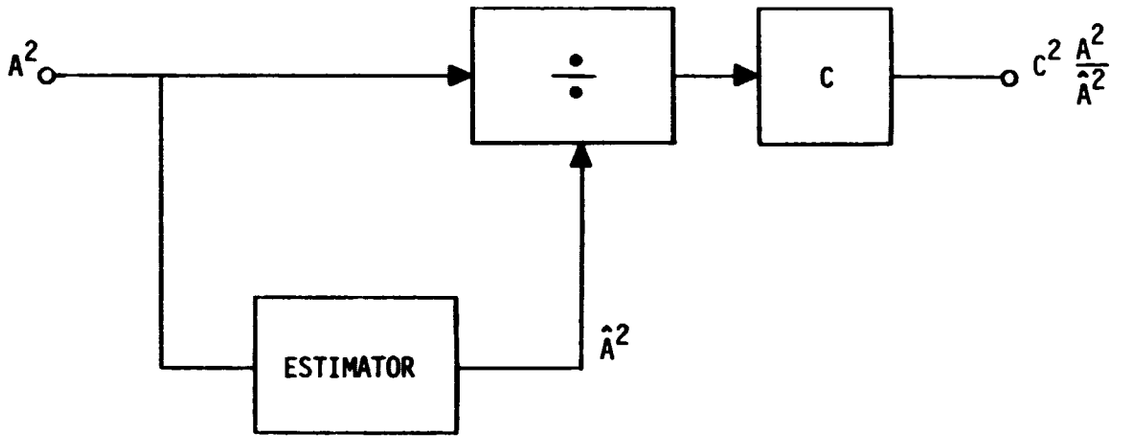

Figure 2. Operational Concept

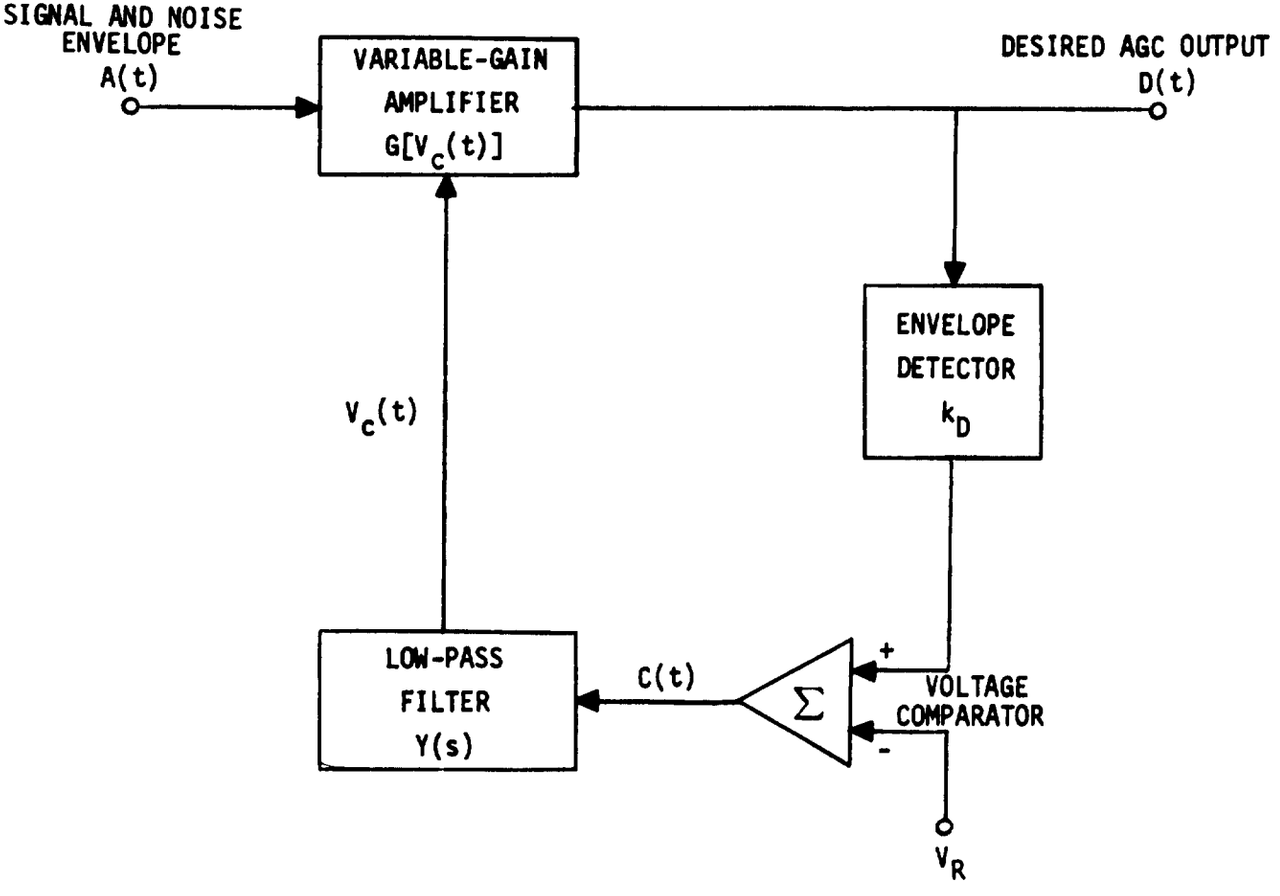

Figure 3. Noncoherent AGC Circuit

Variable-Gain Amplifier. The variable-gain amplifier is assumed to have a gain characterisic G(t) which is an exponential function of the AGC control voltage $V_C(t)$

$$G(t) = 10^{-\frac{1}{20}[k_C V_C(t) + k_R]} \tag{1}$$

or equivalently an attenuation characteristic

$$a(t) = 1/G(t) = 10^{\frac{1}{20}[k_C V_C(t) + k_R]} \tag{2}$$

The action of the variable-gain amplifier can be modeled as two operations ① a block operating on V_C according to (1) to produce G(t), and ② a multiplication of G(t) and A(t). This model is shown in Figure 4. Now if the input envelope and the attenuation function are both expressed in dB, the variable-gain amplifier model of Figure 4 can be transformed to the linear model of Figure 5, since

$$20 \log a(t) = k_C V_C(t) + k_R \tag{3}$$

and the AGC output may be expressed as

$$D(t) = 20 \log \frac{A(t)}{a(t)} = 20 \log A(t) - 20 \log a(t) \tag{4}$$

The constants k_C (in dB/volt) and k_R (in dB) depend on the construction of the variable-gain amplifier (or attenuator). More on this later in Section 5.

Envelope Detector and Comparator. The envelope detector and voltage comparator comprise the next portion of the AGC circuit and are isolated in Figure 6. The envelope detector output is $\sim A/a$. Let k_D be a proportionality constant associated with the detector (i.e., scaled envelope output) times the gain of any amplifier in the feedback loop. The envelope detector output is then summed with the reference voltage - V_R in the voltage comparator to obtain

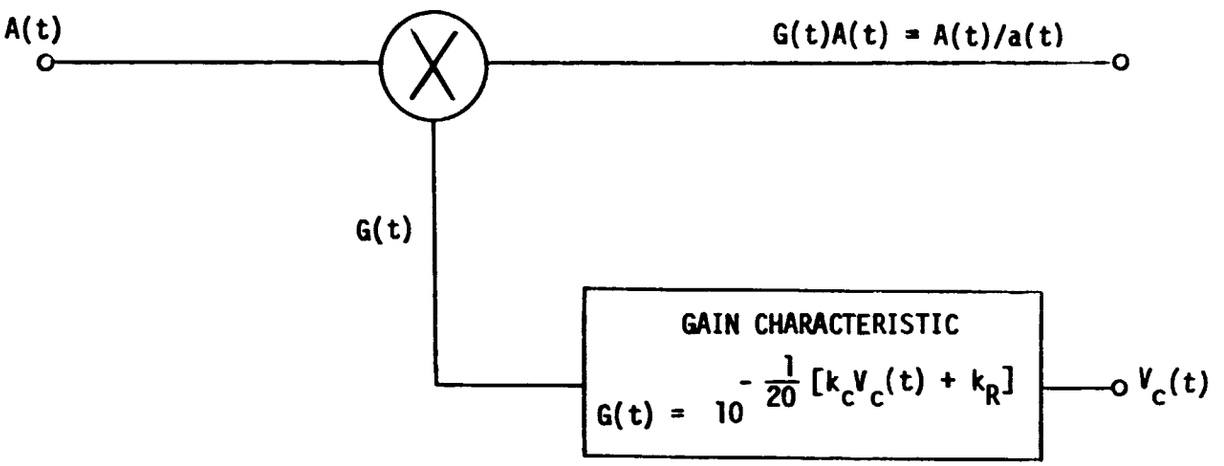

Figure 4. Voltage-Controlled Variable-Gain Amp

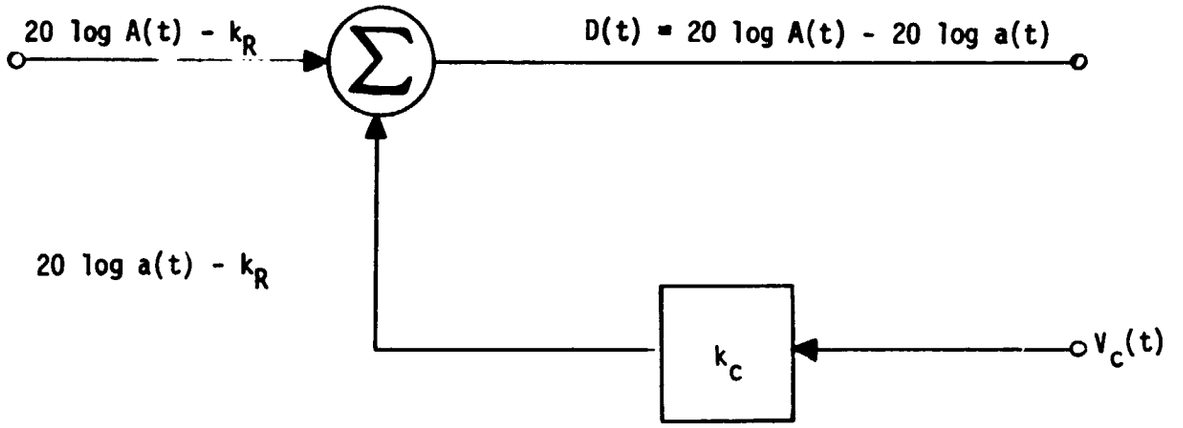

Figure 5. Linearized Model of Variable-Gain Amp

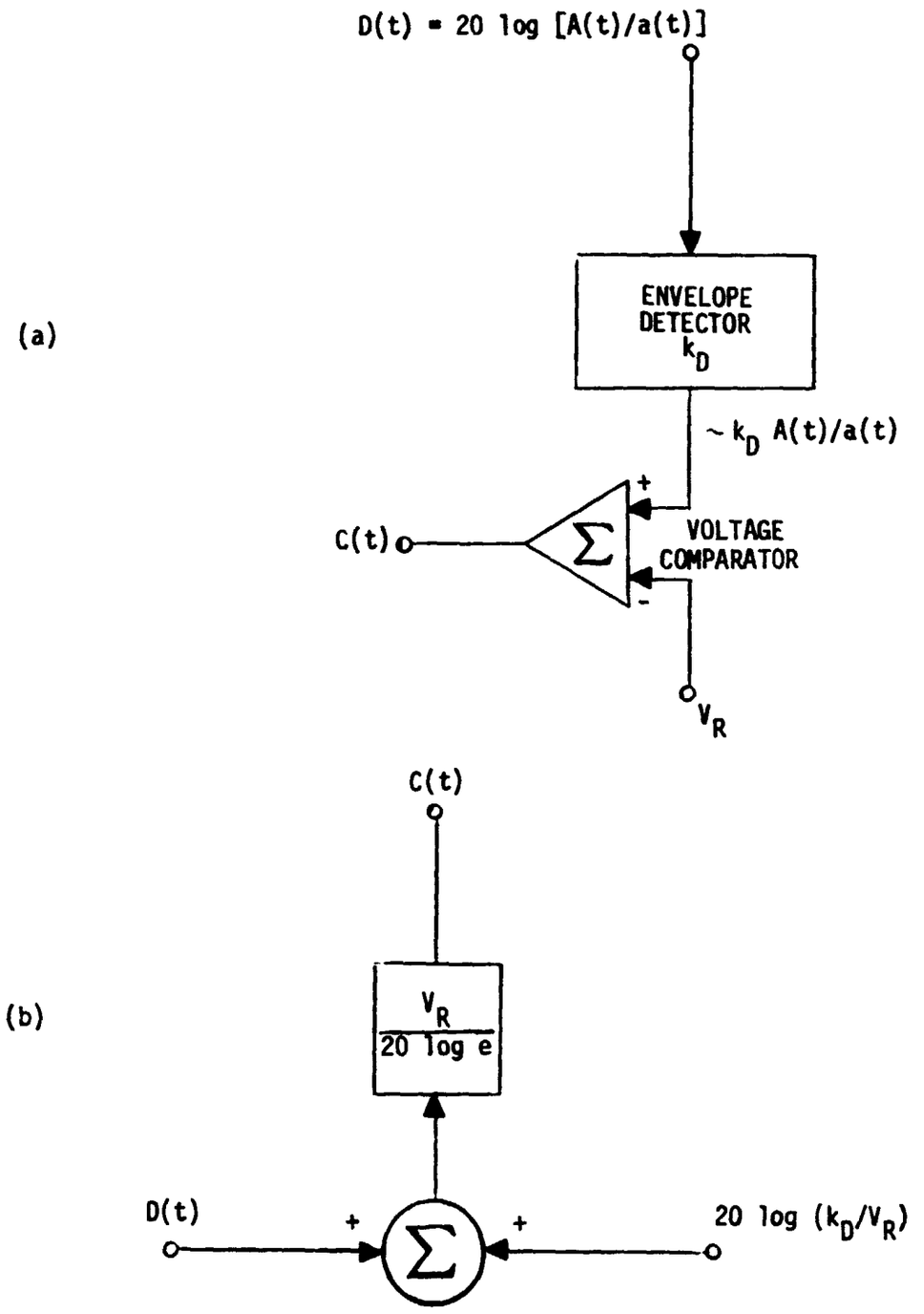

Figure 6. (a) Envelope Detector and Comparator
(b) Linearized Model

$$C(t) = k_D(A/a) - V_R$$

$$= V_R\,[k_D\,A/aV_R - 1]$$

The reference voltage V_R is chosen so that nominally $k_DA/aV_R \approx 1$. Recalling the series representation for the natural logarithm of X

$$\ln x = (x-1) - \frac{1}{2}(x-1)^2 + \frac{1}{3}(x-1)^3 + \ldots \qquad (0<x\leq 2)$$

Neglecting the higher-order terms for $x \approx 1$ the comparator output may be approximated as

$$C(t) \approx V_R \ln (k_DA/aV_R) \qquad (5)$$

which allows the linearization of this portion of the AGC circuit as follows

$$C(t) = V_R \ln A - V_R \ln (aV_R/k_D)$$

$$= \frac{V_R}{20 \log e}(20 \log A) - \frac{V_R}{20 \log e}(20 \log aV_R/k_D)$$

=>

$$C(t) = \frac{V_R}{20 \log e}[D(t) + 20 \log (k_D/V_R)]$$

The above developments allow a total linearization of the AGC circuit as shown in Figure 7.

AGC Voltage Transfer Function. The output of the filter Y(s) is the AGC control voltage $V_C(t)$. Let the symbol * denote convolution and $L^{-1}\{Y(s)\} = y(t)$, the filter impulse response. The AGC voltage may then be written

$$V_C(t) = y(t) * C(t)$$

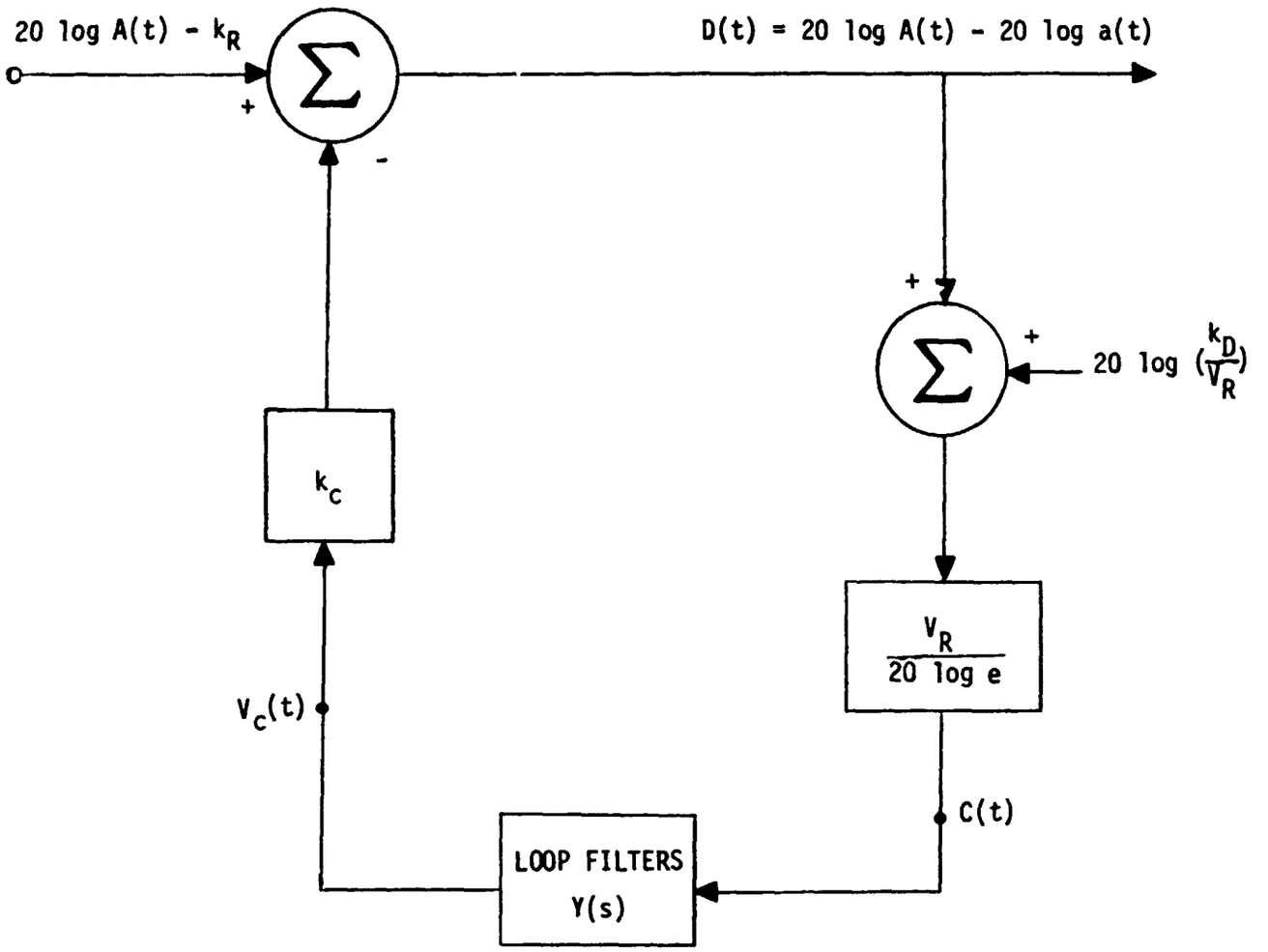

Figure 7. Linear AGC Loop Model

or

$$V_C(t) = \frac{V_R}{20 \log e} \left\{ y(t) * [D(t) + 20 \log (k_D/V_R)] \right\} \qquad (6)$$

but from (4), then (3)

$$D(t) = 20 \log A(t) - 20 \log a(t)$$

$$= 20 \log A(t) - [k_C V_C(t) + k_R]$$

Substituting in (6)

$$V_C(t) = \frac{V_R}{20 \log e} \left\{ y(t) * [20 \log A(t) - k_C V_C(t) - k_R + 20 \log (k_D/V_R)] \right\}$$

$$= \frac{V_R}{20 \log e} \left\{ y(t) * [20 \log (k_D A/V_R) - k_R] - k_C y(t) * V_C(t) \right\}$$

Taking Laplace transforms of both sides yields

$$\frac{V_C(s)}{L\{20 \log (k_D A/V_R) - k_R\}} = \frac{\frac{V_R}{20 \log e} Y(s)}{1 + \frac{V_R k_C}{20 \log e} Y(s)}$$

Now, let

$$A'(t) = 20 \log A(t) + C$$

where

$$C = 20 \log k_D - 20 \log V_R - k_R$$

and the AGC voltage transfer function is conveniently expressed in terms of the rescaled input envelope as

$$H_V(s) \triangleq \frac{V_C(s)}{A'(s)} = \frac{k_L Y(s)}{[1 + k_L Y(s)]k_C} \tag{7}$$

where k_L is AGC loop gain

$$k_L = \frac{V_R k_C}{20 \log e} \tag{8}$$

Note that the AGC voltage may also be written as

$$V_C(s) = H_V(s) \left[A(s) + \frac{C}{S}\right] \tag{9}$$

where $A(s) = L\{20 \log A(t)\}$.

4. AGC LOOP FREQUENCY AND TRANSIENT RESPONSE

The synthesis of Y(s) by an ideal integrator and a low-pass filter is discussed. These ultimately determine the final form of the AGC voltage transfer function, derived in Section 3, and allow the derivation for the frequency and transient response of the AGC loop.

Ideal Integrator. If the AGC loop filter can be realized by an ideal integrator with a time constant τ-sec, then $Y(s) = 1/\tau s$ and the AGC voltage transfer function becomes

$$H_V(s) = \frac{k_L/k_C}{\tau s + k_L}$$

The feedback control block diagram for $V_C(s)$ is shown in Figure 8(a) for the ideal integrator implementation.

Low-Pass Filter. In practice the loop filter is usually realized by a low-pass filter instead of an ideal integrator. The low-pass filter implementation is therefore chosen for further analysis. For this case $Y(s) = (1+\tau s)^{-1}$ and the AGC voltage transfer function is

$$H_V(s) = \frac{k_V}{\tau s + 1 + k_L} \qquad (10)$$

where for convenience $k_V \triangleq k_L/k_C$. The control block diagram for $V_C(s)$ using the LPF implementation is shown in Figure 8(b).

Frequency Response. The frequency response of the noncoherent AGC loop may be obtained from (10). The 3 dB cutoff frequency occurs at

$$\omega_C = \frac{1 + k_L}{\tau} \approx \frac{k_L}{\tau} \quad \text{for } k_L >> 1$$

and falls off at a rate 20 dB/decade as sketched in Fig. 9. Note that the AGC loop noise bandwidth is

$$\omega_L = \frac{2k_L}{\tau}$$

for a double-sided noise power density $\frac{N_0}{2}$.

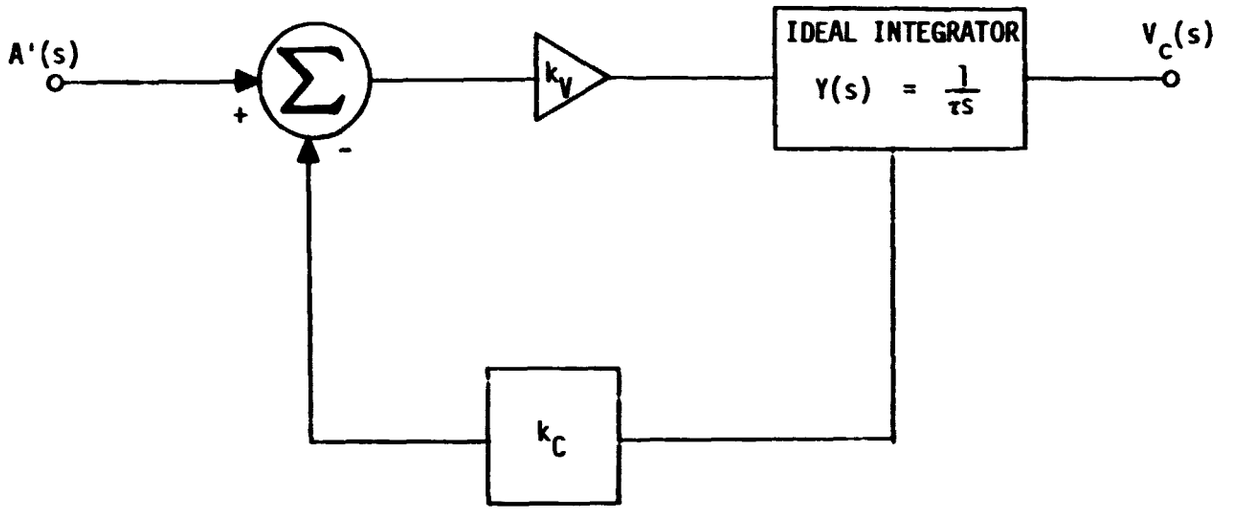

Figure 8(a). AGC Loop Model: Integrator with Feedback

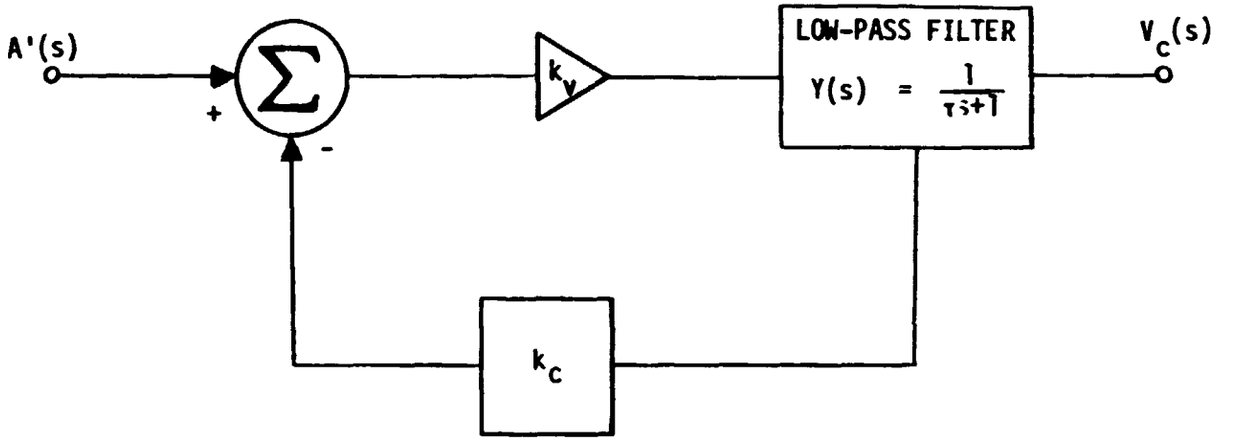

Figure 8(b). AGC Loop Model for the Usual LPF Implementation

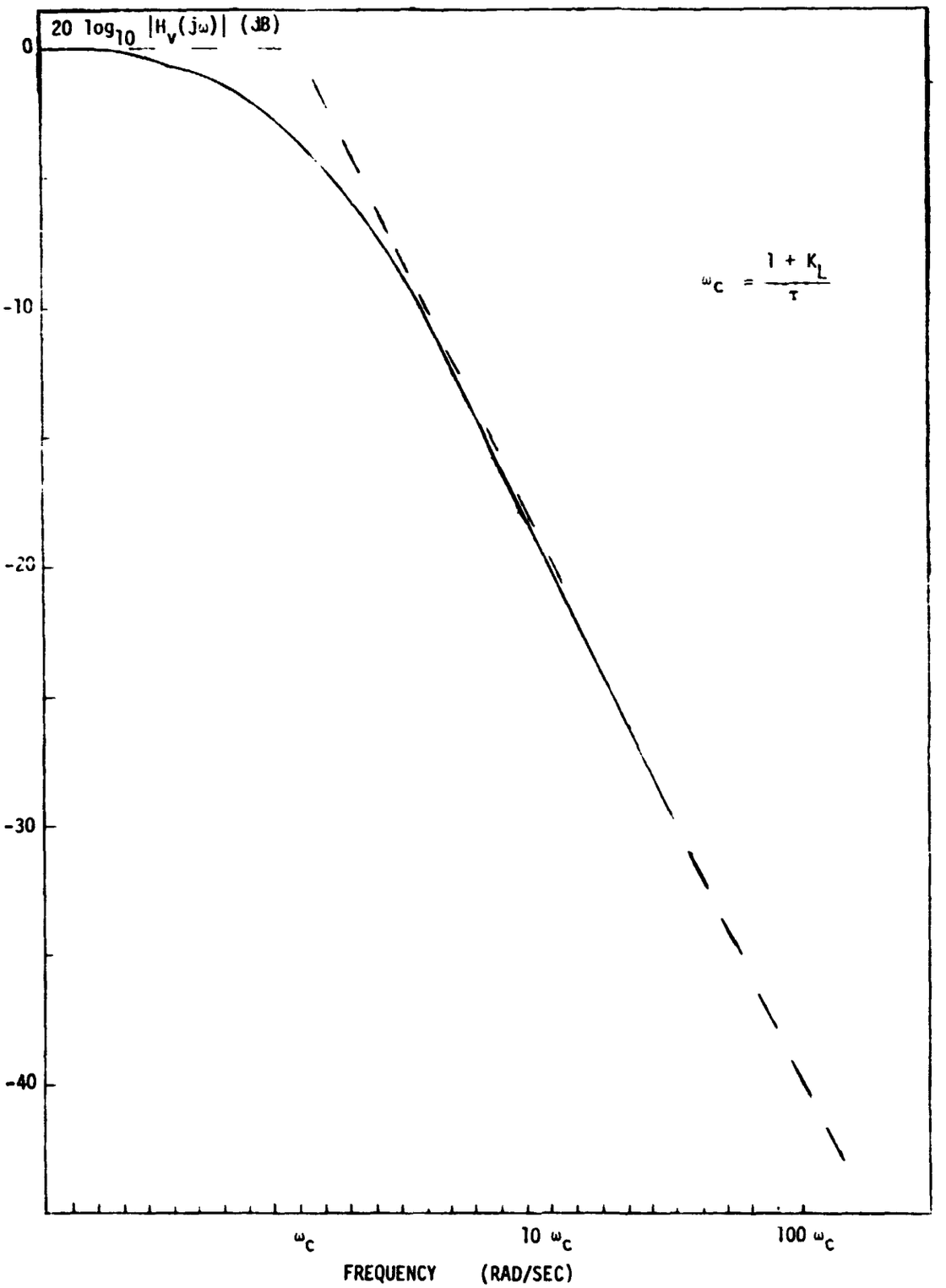

Figure 9. AGC Loop Frequency Response

Transient Analysis. Assume that the input amplitude A(t) undergoes a step fractional increase $a_o u(t)$. The corresponding change in a'(t) is

$$\Delta a'(t) = 20 \log(Aa_o) + C - (20 \log A + C)$$

$$= 20 \log a_o = (a_o)dB$$

The AGC voltage step response is

$$V_C(s) = H_V(s)A'(s) = \frac{k_V}{\tau s+1+k_L} \cdot \frac{a_o}{s}$$

$$= \frac{k_V/\tau}{s + (\frac{1+k_L}{\tau})} \cdot \frac{a_o}{s} = \frac{-\frac{k_V a}{1+k_L}}{\tau(\frac{1+k_L}{\tau})} + \frac{\frac{k_V a_o}{1+k_L}}{\tau(\frac{1+k_L}{\tau})}$$

$$= \frac{k_V a_o}{1+k_L}\left[\frac{1}{s} - \frac{1}{s+(\frac{1+k_L}{\tau})}\right]$$

=>

$$V_C(t) \text{ [step response]} = \frac{k_V a_o}{1+k_L}\left[1 - e^{-(\frac{1+k_L}{\tau})t}\right] u(t)$$

For a large loop gain ($k_L >> 1$), the step response may be written

$$V_C(t) \approx \frac{a_o}{k_C}\left[1 - e^{-\frac{k_L}{\tau}t}\right] u(t) \qquad (11)$$

as shown in Figure 10. The steady-state tracking error is obtained below for both a step and ramp input.

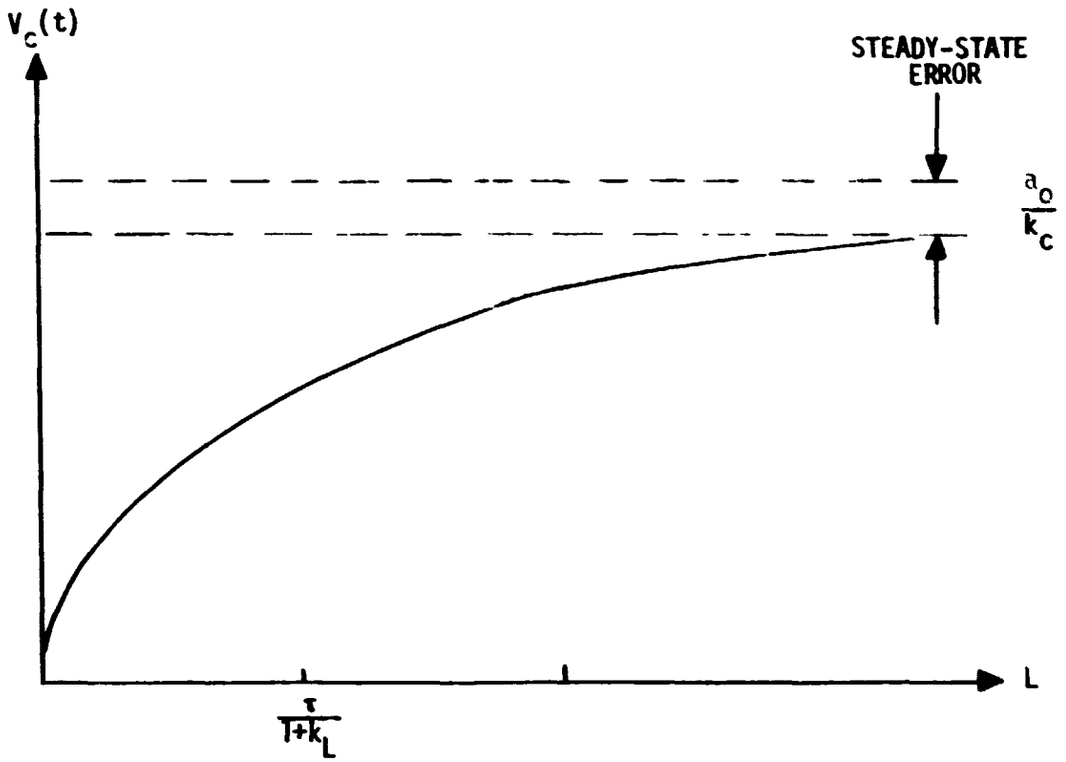

Figure 10. AGC Response to Step Input

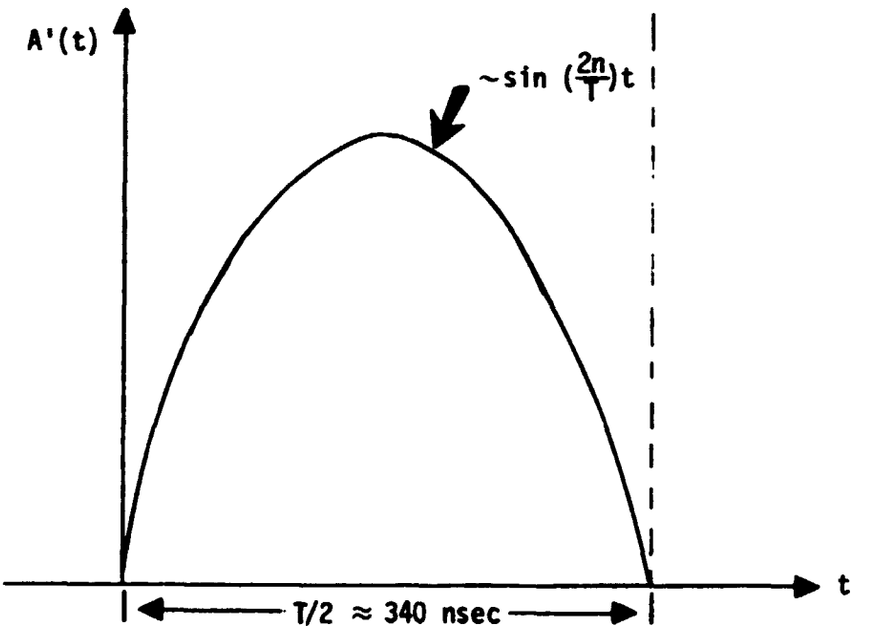

Figure 11. Antenna Receiver Pattern During Antenna Acquisition Scan

Steady-State Tracking Error

$$e_{ss} = \lim_{t\to\infty} V_C(t) = \lim_{s\to 0} \; s\, A'(s)\,[1 - H_V(s)]$$

(for a step input) $a'(t) = (a_o)_{dB}u(t)$

$$e_{ss} = \lim_{s\to 0}\left\{ S\,\frac{a_o}{s}\;\left[1 - \frac{k_V}{\tau s+1+k_L}\right]\right\} = a_o\left[1 - \frac{k_V}{1+k_L}\right]$$

$$\simeq a_o\left[1 - \frac{1}{k_C}\right] \quad \text{for } k_L >> 1$$

(for a ramp input) $a'(t) = \frac{1}{2}\, a_1 t\, u(t)$ (in dB)

$$e_{ss} = \lim_{s\to 0}\left\{ S\,\frac{a_1}{s^2}\;\left[1 - \frac{k_V}{\tau s+1+k_L}\right]\right\} \to \infty$$

Hence, the AGC loop will not track a ramp input. However if the loop gain is large, small duration ramp inputs may be briefly tolerated by the loop.

AGC Response During Antenna Scan. If the antenna receive pattern during the acquisition scan is modeled as the "half-sinusoid" depicted in Figure 11, the envelope input to the AGC may be written as

$$A'(t) = \sin\omega[u(t) - u(t-T/2)]$$

where $T/2 \simeq 170$ msec $= \pi/\omega$, one obtains for the Laplace Transform of $A'(t)$

$$A'(s) = \int_0^{\infty} A'(t)e^{-st}dt = \int_0^{T/2} \sin(\tfrac{2\pi}{T})t\ e^{-st}dt$$

$$= \left\{ \frac{e^{-st}(-s \sin \frac{2\pi}{T}t - \frac{2\pi}{T} \cos \frac{2\pi}{T} t)}{s^2 + (2\pi/T)^2} \right\} \Bigg|_0^{T/2}$$

=>

$$A'(s) = \frac{(\frac{2\pi}{T})}{s^2+(\frac{2\pi}{T})^2} \left[1 + e^{-\frac{1}{2}sT} \right]$$

The AGC voltage response, therefore, is

$$\frac{V_c(s)}{} = \frac{\frac{2\pi k_v}{\tau T}(1 - e^{-\frac{1}{2}sT})}{[s+(\frac{1+k_L}{\tau})][s^2+(\frac{2\pi}{T})^2]}$$

Let $k_1 = \frac{2\pi k_v}{\tau T}$ and $k_2 = (\frac{1+k_L}{\tau})$, the partial fraction expansion of V(s) is

$$V(s) = [1 - e^{-sT}] \left\{ \frac{k_1}{\frac{k_2^2+(\frac{2\pi}{T})^2}{s + k_2}} + \frac{\frac{k_1(k_2-s)}{k_2^2+(\frac{2\pi}{T})^2}}{s^2 + (\frac{2\pi}{T})^2} \right\}$$

Hence, the AGC voltage response during the antenna acquisition scan is (for $k_L >> 1$)

$$V_c(t) = \frac{\frac{2\pi k_v}{\tau T}}{\left(\frac{k_L}{\tau}\right)^2+\left(\frac{2\pi}{T}\right)^2} \left\{ \left[e^{-\left(\frac{k_L}{\tau}\right)t} + \frac{k_L}{\tau} \sin\left(\frac{2\pi}{T}\right)t - \cos\left(\frac{2\pi}{T}\right)t \right] u(t) \right.$$

$$\left. - \left[e^{-\left(\frac{k_L}{\tau}\right)(t-T/2)} + \frac{k_L}{\tau} \sin\left(\frac{2\pi}{T}\right)(t-T/2) - \cos\left(\frac{2\pi}{T}\right)(t-T/2) \right] u(t-T/2) \right\}$$

shown in Figure 12.

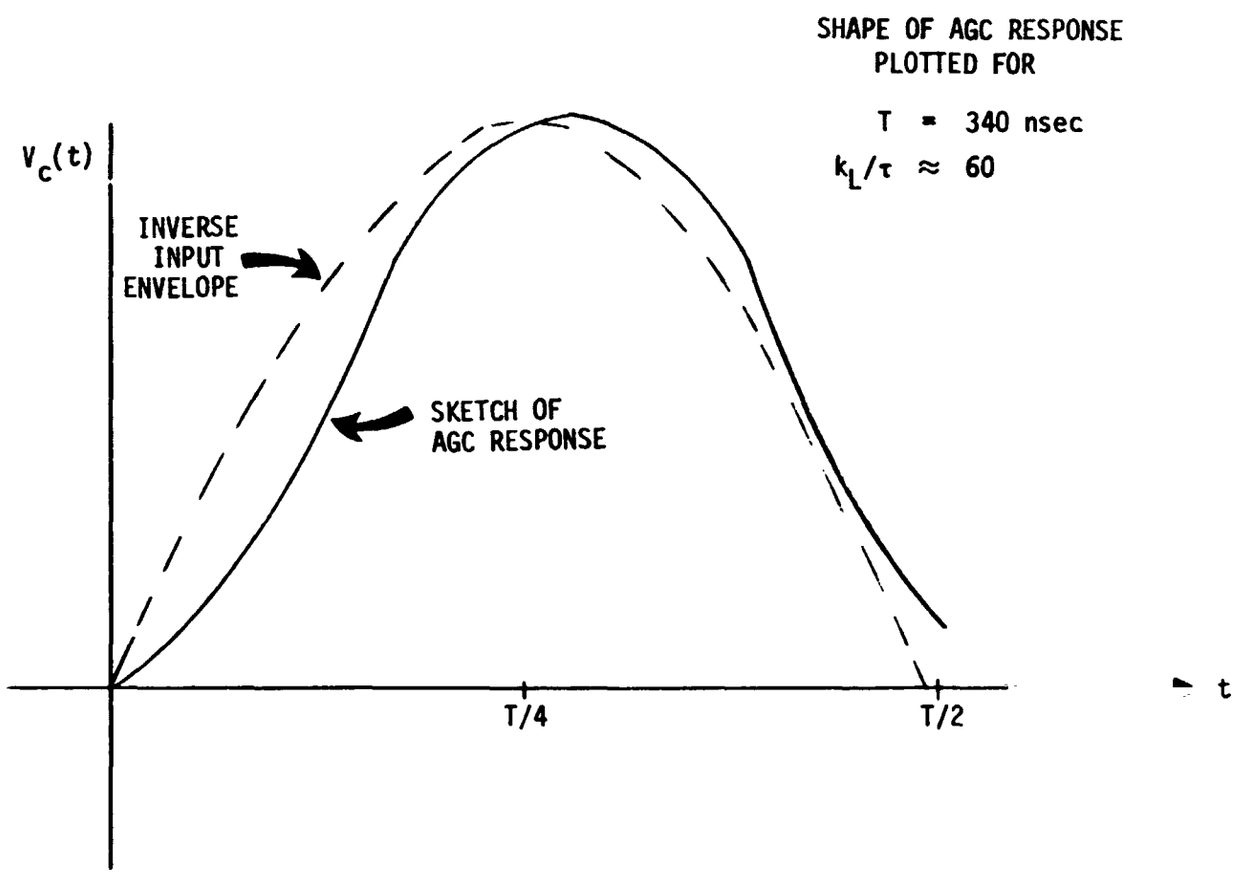

The dashed curve represents the reciprocal of the input envelope. The above is an illustrative sketch only.

Figure 12. AGC Voltage Response for Antenna Scan Input of Figure 11

5.0 DESIGN APPLICATIONS

Now consider the application of the above analysis techniques to obtain the performance characteristics of a specific AGC amplifier. The device chosen for analysis is the MC 1590F AGC amplifier - presently under consideration for the S-band Shuttle communications 2nd IF noncoherent AGC amplifier. The gain characteristic of this device (single-stage) is shown in Figure 13. Note the characteristic is very linear in the range of gains -10 dB to +20 dB (at room ambient temperature ~ 70°F). Over this range of gain the control voltage changes only 0.4 volt (from -5.5 volts to -5.9 volts). The gain vs V_c slope is

$$\Delta = \frac{30\text{dB}}{-0.4\text{v}} = -75 \text{ dB/V.}$$

In the linear range of operation the MC1590F fits well with the previously assumed gain characteristic

$$G = 10^{-\frac{1}{20}[k_c V_c(t)+k_R]}$$

or

$$20 \log G = - k_c V_c(t) - k_R \qquad \text{(Gain in dB)}$$

by letting $k_C = 75$ and $k_R = 422.5$, for which

$$G_{dB} = -75\ V_c(t) - 422.5$$

The gain characteristic is now matched to the MC1590F single-stage AGC amplifier, and the previous results apply.

The AGC loop gain (8) is

$$k_L = \frac{V_R(\text{volts}) x k_c(\text{dB/volt})}{20 \log e}$$

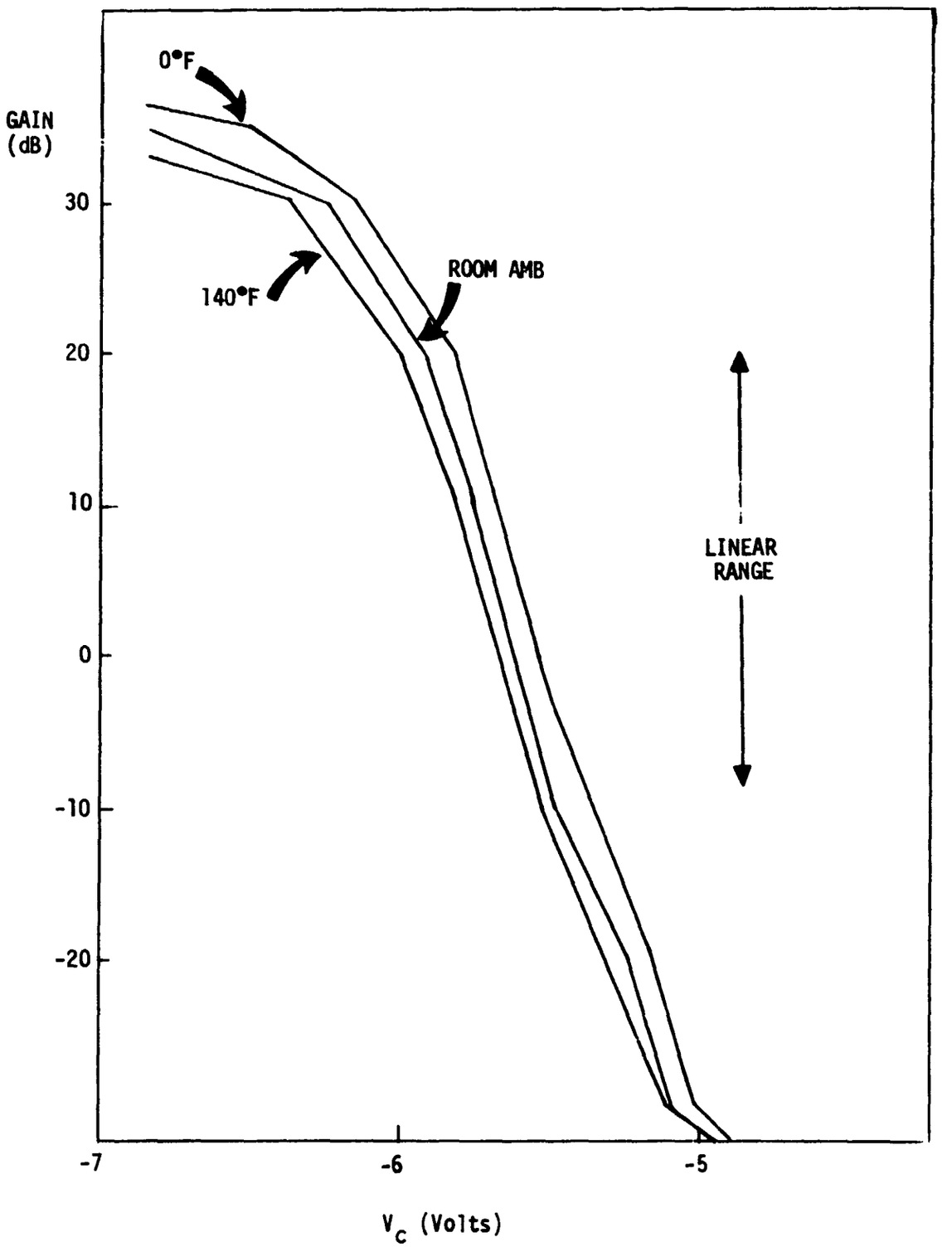

Figure 13. MC1590F Gain Characteristic
Reference [4]

and, therefore, dependent on the reference voltage V_R which as shown previously is related to the desired AGC output D by $V_R = k_D D(t)$. The desired input to the despreader is taken as -15 dBm. Hence, the input to the four-way power divider between the AGC and despreader should be $\sim$ -9 dBm. Assuming a nominal 50 ohm impedance into the power divider the desired AGC output voltage should be approximately 0.08 volts. The AGC loop gain follows, for the above point design as

$$k_L = 0.46\, k_D \qquad \text{(in dB)}$$

For a large value of loop gain the AGC loop bandwidth for this AGC amplifier becomes

$$\omega_c = \frac{0.46\, k_D}{\tau}$$

To complete the design example, assume k_D = 90 dB and τ = 1 sec, for which f_c = 6.6 Hz. The AGC response time (defined as the time required for the AGC loop to change its gain to within 90% of its final value for a step input) is

$$e^{-\frac{k_L}{\tau} t} = e^{-2\pi(6.6)t_r} = 0.1$$

$$\Rightarrow t_r = 0.06 \text{ sec}$$

Pin Diode Attenuator. The control voltage $V_c(t)$ may also be used to control the inverse gain or attenuation of a pin diode and thereby augment the AGC dynamic range. Consider the use of a voltage source to drive a pin diode variable attenuator as shown in Figure 14. The RF resistance R of the pin diode varies over a wide range with bias current as shown in Figure 15. In general the RF resistance is

$$R = KI^{-X}$$

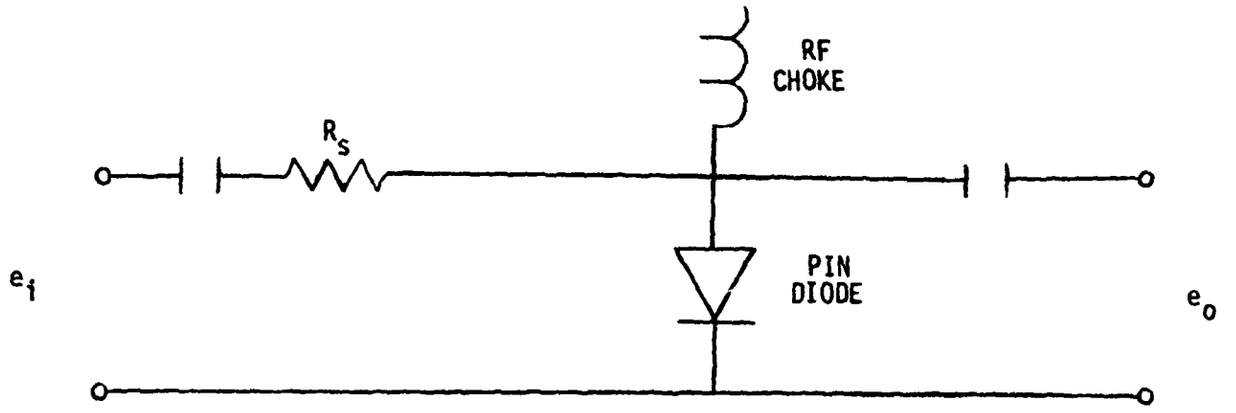

Figure 14. Pin Diode Attenuator

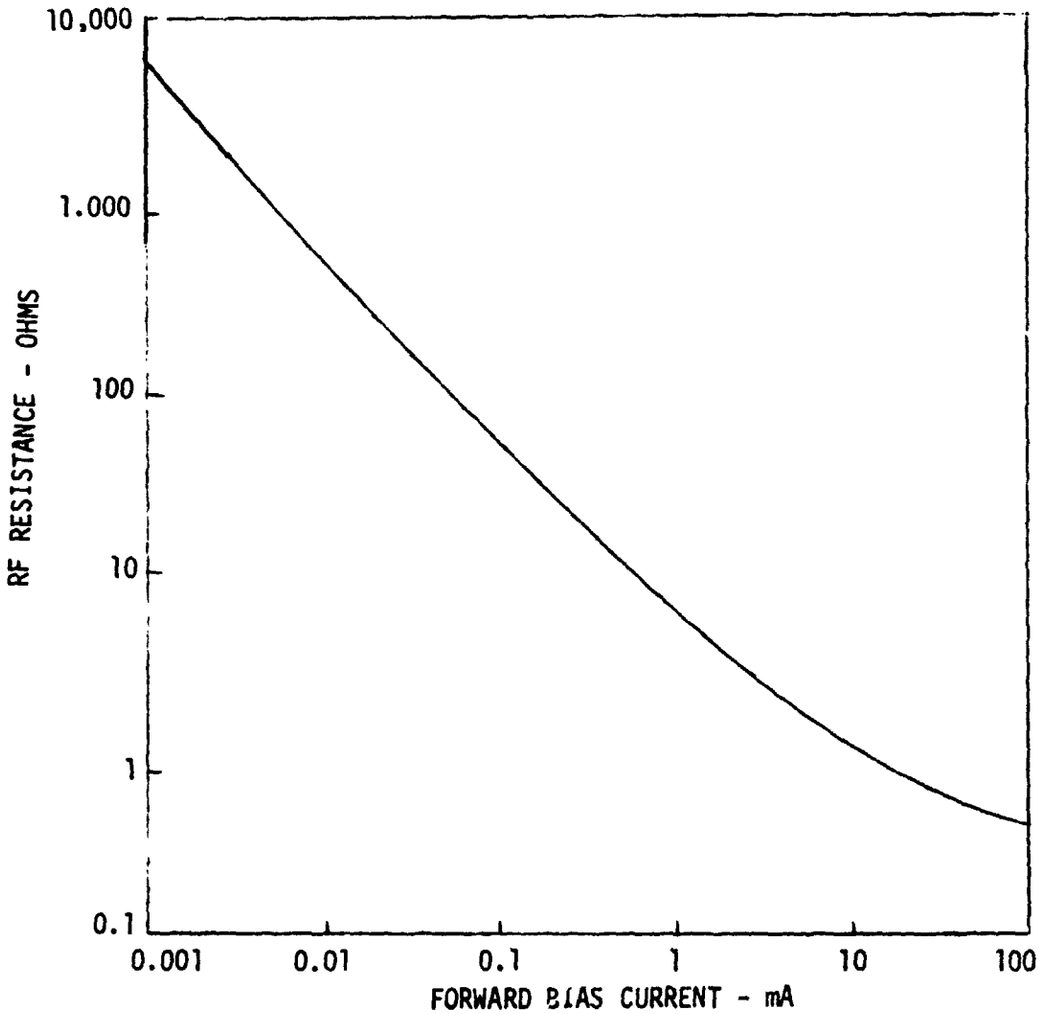

Figure 15. RF Resistance of Typical Microwave Pin Diode Under Forward Bias

where K is a constant depending on the construction of the diode.

I = the bias current

x = a constant.

A very good approximation to the current emitted across the forward-biased diode junction

$$I \approx I_o \exp(q V_c/kT)$$

where I_o is the leakage current

q is the electron charge

k is Boltzman's constant

T is the diode junction temperature in degrees Kelvin

kT/q is approximately 26 mV for T = 300°K. Hence one can write

$$R \approx K [I_o e^{38.46V_c}]^{-x} = K \frac{e^{-38.46V_c}}{I_o}^{x}$$

From Figure 14, note that the ratio of the output to the input voltage for the attenuator is

$$G = \frac{e_o}{e_i} = \frac{R}{R + R_s}$$

So the attenuation is

$$a = \frac{1}{G} = \frac{R + R_s}{R} \approx \frac{R_s}{R} \qquad (\text{for } R_s >> R)$$

In terms of our previous relations the attenuation may be written

$$a = \frac{R_s}{K} [I_o e^{38.46V_c}]^{x}$$

and

$$20\log a = [(20\log e)38.46x]V_c + 20\log[\frac{RI_o x}{K}]$$

Hence, if

$$k_c = (20\log e)38.46x$$

and

$$k_R = 20\log\left[\frac{RI_o x}{K}\right]$$

the resulting attenuation characteristic

$$20\log a = k_c V_c + k_R$$

is the form previously assumed and the previous analysis techniques apply for the pin diode attenuator.

One specific device presently under development by Aertech for the S-band comm is the 1H407 whose attenuation characteristic is specified as shown in Figure 16. The gain-voltage slope is

$$k_c = \frac{-80 - (-15)}{0 - 8} = -8.125$$

and the ordinate intercept is $k_R = 80$, hence the nominal attenuation characteristic for the 1H407 pin diode attenuation is

$$20 \log a = -8.125 V_c + 80$$

The design procedure may be continued by the previously described methods.

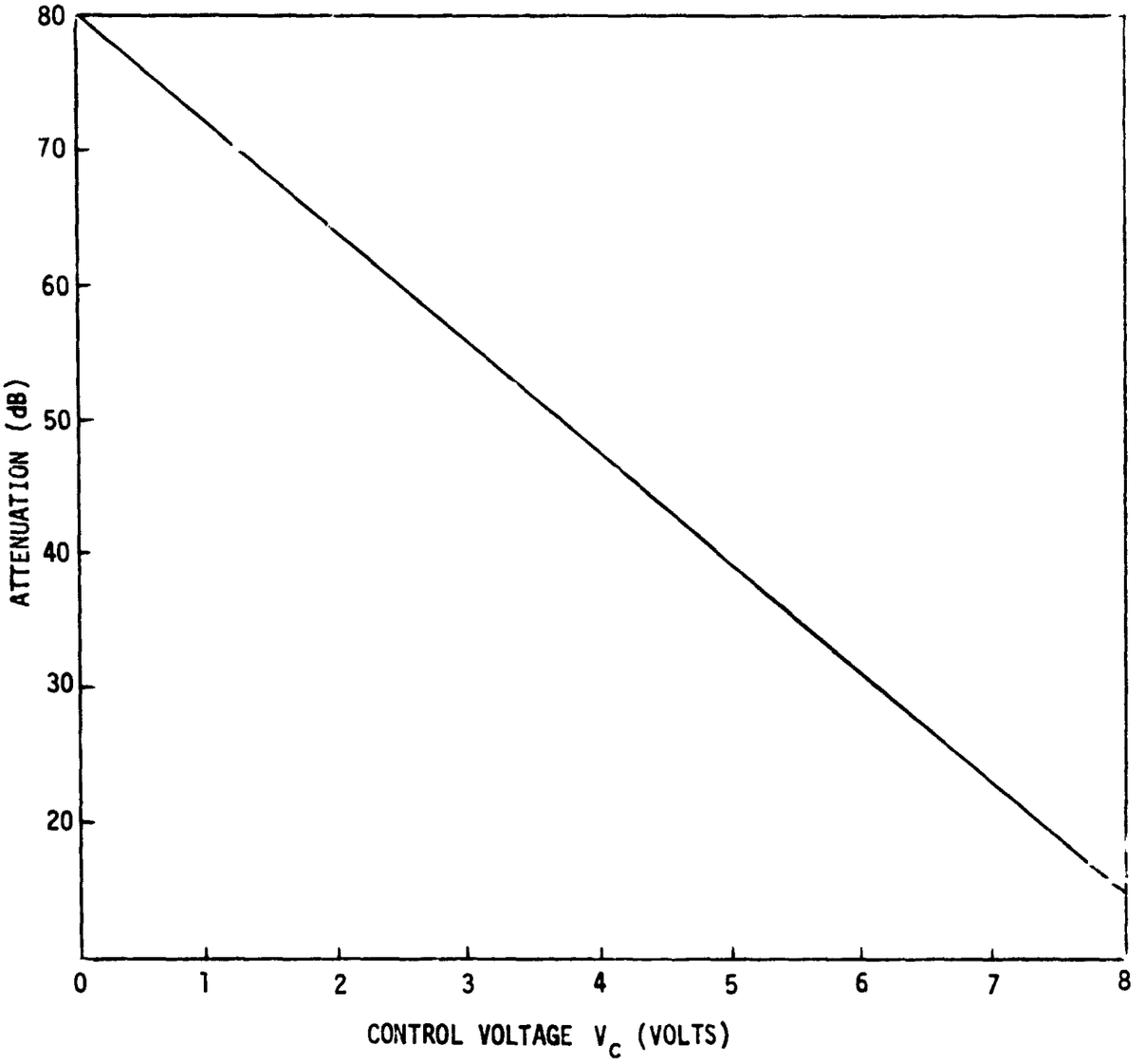

Figure 16. Pin Diode Attenuation Spec Being Developed By Aertech for S-Band (Ref. B. Craig - TRW)

References

[1] Victor, W. K. and Brockman, M. H., "The Application of Linear Servo Theory to the Design of AGC Loops," IRE Proceedings, Vol. 48, pp. 234-238, February 1960.

[2] Tausworthe, R. C., "Theory and Practical Design of Phase-Locked Receivers," Technical Report 32-819, Jet Propulsion Laboratory, February 1966.

[3] Oliver, B. M., "Automatic Volume Control as a Feedback Problem," IRE Proceedings, Vol. 46, pp. 466-473, April 1948.

[4] "Second IF and Detectors Conceptual Design Review," (for SCTE) TRW Systems, 19 November 1975, page 70.

APPENDIX B

INTERMODULATION DISTORTION IN THE KU-BAND SHUTTLE MODE 2 RETURN LINK

The mode 2, three-channel configuration, for the Ku-band Orbiter return lirk consists of unbalanced QPSK modulated on to an 8.5 MHz subcarrier which is combined with a 4.5 MHz analog signal and then FM modulated. A sketch of the spectral occupancy for this link is shown in Figure 1.

Previous analysis (ref 1) has shown that for FDM-FM links intermodulation distortion produced bv the FM modulator, RF transmission equipment and FM demodulator is significant. This memo extends the analysis of reference 1 to the signal structure of the mode 2 return link and presents a computer program to calculate the IM distortion for this link.

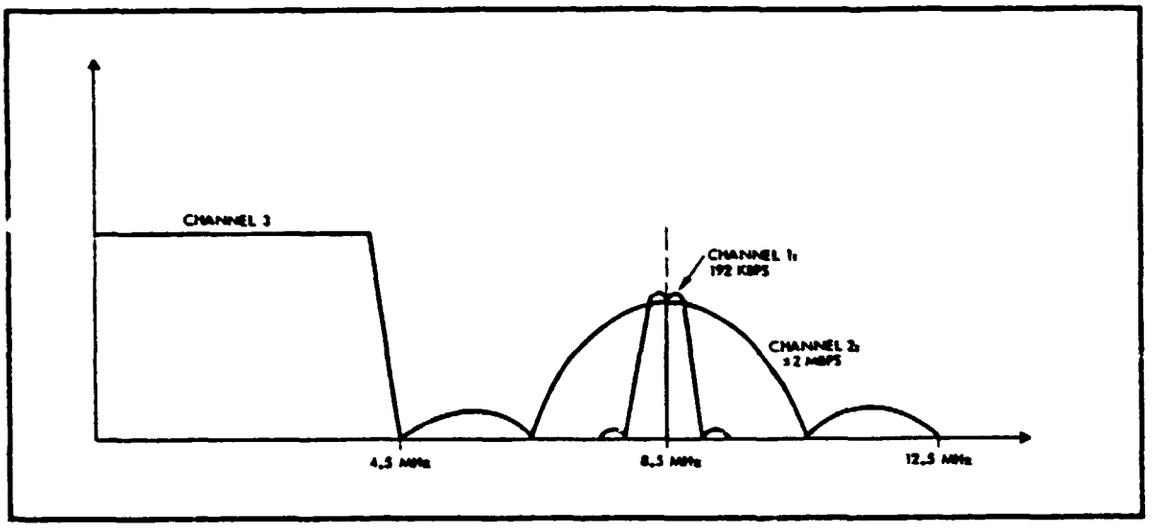

Figure 1. Spectral Occupancy

Summary of Previous Analysis

The analysis of reference 1 considers the effects of the FM deviator, RF transmission path and the FM discriminator. Figure 2 shows the system that has been analyzed.

FM Deviator. It was assumed that the output of the deviator can be represented as a power series

$$\frac{d}{dt}\phi(t) = \dot{\phi}(t) = V(t) + a_2V^2(t)+a_3V^3(t) \qquad (1)$$

where $\dot{\phi}(t)$ = Instantaneous angular-frequency variation from carrier at modulator output

$V(t)$ = Input baseband signal

a_2, a_3 = Nonlinear amplitude characteristics

RF Transmission Path. The RF transmission path includes those components that make up the transmitter, the channel and the receiver. These devices can generate intermodulation noise in two ways: phase distortion and AM-to-PM conversion. Distortion arises from devices in the transmission path having amplitude and phase characteristics that are nonlinear functions of frequency. These devices introduce amplitude modulation and phase modulation to the RF signal. The amplitude modulation by itself will not effect the FM signal, however if a device that generates AM is followed by a device (such as a TWTA) that converts amplitude variation in the phase variations the intermodulation noise will be increased. This second source of distortion is referred to as AM-to-PM conversion.

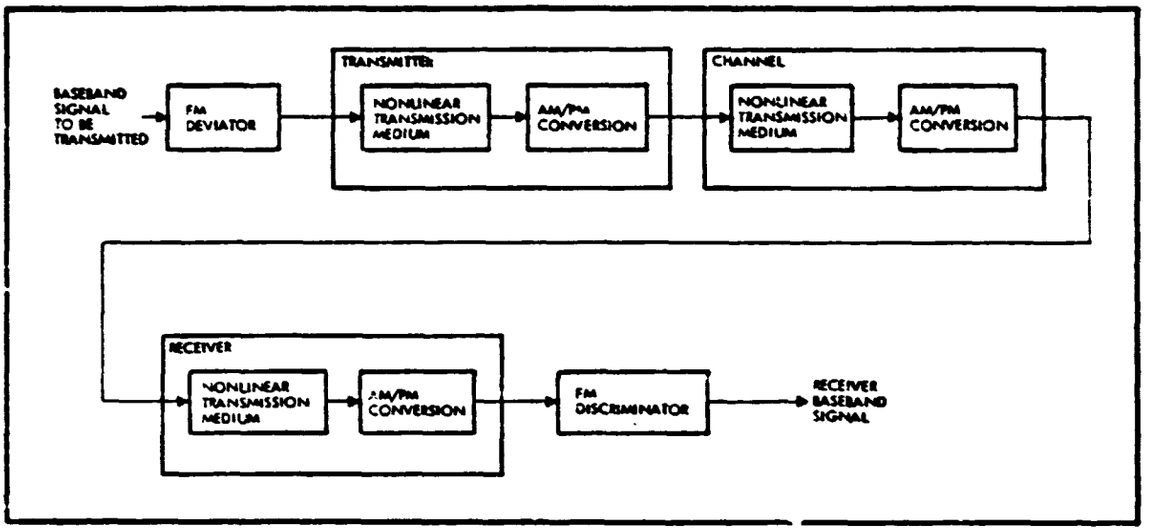

Figure 2. FM Link

The nonlinear transmission media are described by transfer functions of the form

$$H(\omega) = A(\omega)\, e^{-jB(\omega)} \tag{2}$$

$$A(\omega) = 1 + g(\omega-\omega_c)$$

$$-B(\omega) = b_2(\omega-\omega_c)^2 + b_3(\omega-\omega_c)^3$$

where $\frac{\omega_c}{2\pi}$ = carrier frequency

g = amplitude coefficient representing gain slope

b_2 = phase coefficient representing parabolic phase distortion

b_3 = phase coefficient representing cubic phase distortion

If the amplitude modulation introduced by a nonlinear transmission medium is p(t) then the phase modulation at the output of the conversion device will include a term $\theta_0 p(t)$, where θ_0 is the AM-to-PM conversion coefficient. It is also assumed that the AM/PM converter does not distort the input AM, but only scales it by a constant K. (Note: K=0 for a saturating device.)

Following the analysis of reference 1 when distortion to distortion terms have been neglected the effect of the total RF transmission path upon the phase of the input signal is

$$\psi_T(t) = \phi(t) + [\phi'(t)]^2\{b_2^t + b_2^c + b_2^r - 2(g_1^t\, b_3^t + g_1^c\, b_3^c + g_1^r\, b_3^r)\frac{d^2}{dt^2}$$

$$+ \{(\tfrac{3}{2}\, b_3^t + g_1^t\, b_2^t)\theta_o^t + [[\tfrac{3}{2}\, b_3^t + g_1^t\, b_2^t]k^t + [\tfrac{3}{2}\, b_3^c + g_1^c\, b_2^c]]\theta_o^c \qquad (3)$$

$$+ [(\tfrac{3}{2}\, b_3^t + g_1^t\, b_2^t)k^c k^t + (\tfrac{3}{2}\, b_3^c + g_1^c\, b_2^c)k^c + (\tfrac{3}{2}\, b_3^r + g_1^r\, b_2^r)]\theta_o^r]\}[\tfrac{d}{dt}]\}$$

$$+ [\phi'(t)]^3\{b_3^t + b_3^c + b_3^r + [\theta_o^t\, g_1^t\, b_3^t + \theta_o^c[g_1^t\, b_3^t\, k^t + g_1^c\, b_3^c]$$

$$+ \theta_o^r\,[g_1^t\, b_3^t\, k^t k^c + g_1^c\, b_3^c\, k^c + g_1^r\, b_3^r]](\tfrac{d}{dt})\}$$

where the superscripts t,c and r indicate transmitter, channel and receiver, respectively.

Discriminator. Discriminators show curvature resulting from the nonlinear relationship between the incoming frequency modulation and the resulting amplitude modulation. This has been modeled by a power series.

$$O(t) = c_1\, \dot{\psi}_T(t) + c_2\, [\dot{\psi}_T(t)]^2 + c_3\, [\dot{\psi}_T(t)]^3 \qquad (4)$$

where $O(t)$ is the output voltage

c_i are constants

Substitution of equation 1 into equation 3 and then into equation 4 results in an output signal

$$O(t) = V(t) + m_2V^2(t) + m_3V^3(t)$$

$$+ \{h_1 - 2h_2 \frac{d^2}{dt^2} + h_3 \frac{d}{dt}\}[\frac{d}{dt} V^2(t)] \qquad (5)$$

$$+\{h_4 + h_5 \frac{d}{dt}\}[\frac{d}{dt}V^3(t)] + \text{higher order terms}$$

where

$$m_2 = a_2 + c_2$$

$$m_3 = a_3 + c_3$$

$$h_1 = b_2^t + b_2^c + b_2^r$$

$$h_2 = (g_1^t b_3^t + g_1^c b_3^c + g_1^r b_3^r)$$

$$h_3 = (\tfrac{3}{2} b_3^t + g_1^t b_2^t)\theta_o^t + [(\tfrac{3}{2} b_3^t + g_1^t b_2^t)k^t + \tfrac{3}{2} b_3^c + g_1^c b_2^c]\theta_o^c$$

$$+ [(\tfrac{3}{2} b_3^t + g_1^t b_2^t)k^c k^t + (\tfrac{3}{2} b_3^c + g_1^c b_2^c)k^c + \tfrac{3}{2} b_3^r + g_1^r b_2^r]\theta_o^r$$

$$h_4 = b_3^t + b_3^c + b_3^r$$

$$h_5 = \theta_o^t g_1^t b_3^t + \theta_o^c [g_1^t b_3^t k^t + g_1^c b_3^c] + \theta_o^r [g_1^t b_3^t k^t k^c + g_1^c b_3^c k^c + g_1^r b_3^r]$$

Baseband Signal Model

Since the mode 2 return link baseband signal structure differs from the frequency division multiplex signal of reference 1, we can no longer follow the analysis of reference 1. Instead the baseband signal will be mo[illegible] NRZ signal in quadrature with a Bi-ϕ-L signal on an 8.5 MHz s[illegible] a[illegible] V signal below 4.2 MHz (see Fig. 1). A model of a TV [illegible] ranks (ref 2) will be used.

Thus the baseband signal is

$$V(t) = x_1(t) + x_2(t) + x_3(t) \qquad (6)$$

where $x_1(t)$ is the TV signal

$x_2(t)$ is the NRZ signal

$x_3(t)$ is the Bi-ϕ-L signal.

Calculation of Signal Distortion

The signal distortion is that part of the autocorrelation of O(t) that is not signal that is (as derived in Attachment A):

$$\begin{aligned}
\text{Distortion}(\tau) = {} & \left[m_2^2 + (2m_3h_3 - h_1^2)\frac{d^2}{dt^2} + (h_3^2 - 2h_1h_2)\frac{d^4}{dt^4}\right. \\
& \left. - h_2^2\,\frac{d^6}{dt^6}\right] R_{22}(\tau) \\
& + \left[m_2 - h_1\,\frac{d}{dt} - h_2\,\frac{d^3}{dt^3} + h_3\,\frac{d^2}{dt^2}\right] R_{12}(\tau) \\
& + \left[m_2 + h_1\,\frac{d}{dt} + h_2\,\frac{d^3}{dt^3} + h_3\,\frac{d^2}{dt^2}\right] R_{21}(\tau) \\
& + \left[m_3^3 + 2(m_3h_5 - m_4^2)\,\frac{d^2}{dt^2} + h_5^2\,\frac{d^4}{dt^4}\right] R_{33}(\tau) \\
& + \left[m_3 - h_4\,\frac{d}{dt} + h_5\,\frac{d^2}{dt^2}\right] R_{13}(\tau)
\end{aligned}$$

$$+ \left[m_3 + h_4 \frac{d}{dt} + h_5 \frac{d^2}{dt^2}\right] R_{31}(\tau)$$

$$+ \left[m_2 m_3 + (m_3 h_1 - h_2 h_4) \frac{d}{dt} + (m_5 - h_1 h_4) \frac{d^2}{dt^2}\right.$$

$$\left. + (m_2 h_2 + h_1 h_5 - h_3 h_4) \frac{d^3}{dt^3} + (h_3 h_5 - h_2 h_4) \frac{d^4}{dt^4}\right. \qquad (7)$$

$$\left. + h_1 h_5 \frac{d^5}{dt^5}\right] R_{23}(\tau)$$

$$+ \left[m_2 m_3 + (m_2 h_4 - m_3 h_1) \frac{d}{dt} + (m_2 h_5 + h_3 h_4 - h_1 h_4) \frac{d^2}{dt^2}\right.$$

$$\left. - (m_3 h_1 + h_1 h_4 + h_1 h_5) \frac{d^3}{dt^3} + h_3 h_5 \frac{d^4}{dt^4} - h_2 h_5 \frac{d^5}{dt^5}\right] R_{32}(\tau)$$

where $R_{ij}(\tau) = E[V^i(t+\tau)V^j(t)]$. The $R_{ij}(\tau)$'s are evaluated in Attachment B.

The power spectral dersity of the distortion is found by taking the Fourier Transform of the distortion, i.e.,

$$S_{DIST}(f) = \int_{-\infty}^{\infty} \text{Distortion } (\tau)\, e^{-2\pi j f \tau}\, d\tau \qquad (8)$$

Since a computer will be used to evaluate the intermodulation distortion, its power spectral density will not be evaluated explicitly, but rather the transform will be performed on the computer.

Computer Program to Evaluate Equation 8

Due to the complex signal structure of the mode 2 return link signal and the large number of terms required to evaluate equation 8, a computer program was written.

The program requires the following inputs: RF bandwidth, modulator/demodulator nonlinearities (m_2 and m_3 of equation 5) and RF transmission path characteristics (g_1,b_2,b_3,θ_0 and k of equation 5). The program accepts these in terms of degrees and dB and normalizes them as required. The frequency deviation, 11 MHz for TV and 6 MHz for the subcarrier has been preprogrammed.

After accepting and normalizing inputs the various signals are generated and the autocorrelations of Attachment C are calculated. These are combined to produce the $R_{ij}(\tau)$'s of Attachment B. Finally, equation 7 is evaluated and a fast Fourier transform is done to obtain the spectrum of the intermodulation distortion. Throughout the calculations any correlation whose result is identical to the signal is ignored, resulting in a worst case situation.

The program calculates integrated signal-tp-intermodulation ratios for both the TV and digital signals and outputs these. The program also generates plots of the signal spectrum and the spectrum of the intermodulation. A typical input sequence and the outputs it generates are shown in Figures 3 and 4.

```
 ENTER: RF BANDWIDTH
? 50E6
 ENTER: MOD/DEMOD NONLINEARITIES - M1,M2
? .02,.02
 ENTER: NONLINEARITIES - GAIN SLOPE,QUAD PHASE,CUBE PHASE
 FOR TRANSMITTER
? 0.,0.,0.
 FOR CHANNEL
? .5,3.5,7.8
 FOR RECEIVER
? 0.,3.,3.
 ENTER: AM/PM,AM/AM
 FOR TRANSMITTER
? 6.,0.
 FOR CHANNEL
? 4.7,.7
 FOR RECEIVER
? 0.,1.
```

(a) Typical Input

```
FOR TELEVISION SIGNAL, 0-4.5 MHZ
  INTEGRATED SIGNAL POWER  223.95 DB
  INTEGRATED NOISE POWER  164.79 DB
  CNR   59.16 DB


FOR DATA SIGNAL, 6.5-10.5MHZ
  INTEGRATED SIGNAL POWER  215.59 DB
  INTEGRATED NOISE POWER  187.68 DB
  CNR   27.91 DB
```

(b) Typical Output

Figure 3

Figure A. Typical Output Plot

Attachment A - Derivation of Equation 7

From equation 4 the autocorrelation of the output signal is calculated by

$$
\begin{aligned}
E[O(t+\tau)O(t)] &= E[V(t+\tau)V(t)] \\
&+E[(m_2V^2(t+\tau) + m_3V^3(t+\tau))(m_2V^2(t) + m_3V^3(t))] \\
&+ E[(\{h_1-2h_2\frac{d^2}{dt^2} + h_3\frac{d}{dt}\}[\frac{d}{dt}V^2(t+\tau)] + \{h_4+h_5\frac{d}{dt}\}[\frac{d}{dt}V^3(t+\tau)]) \\
&\quad (\{h_1-2h_2\frac{d^2}{dt^2} + h_3\frac{d}{dt}\}[\frac{d}{dt}V^2(t)] + \{h_4+h_5\frac{d}{dt}\}[\frac{d}{dt}V^3(t)])] \\
&+ E[(m_2V^2(t+\tau) + m_3V^3(t+\tau)(\{h_1-2h_1\frac{d^2}{dt^2} + h_3\frac{d}{dt}\}[\frac{d}{dt}V^2(t)] \\
&\quad + \{h_4+h_5\frac{d}{dt}\}[\frac{d}{dt}V^3(t)]) + (\{h_1-2h_2\frac{d^2}{dt^2} + h_3\frac{d}{dt}\}[\frac{d}{dt}V^2(t+\tau)] \\
&\quad + \{h_4+h_5\frac{d}{dt}\}[\frac{d}{dt}V^3(t+\tau)])(m_2V^2(t)+m_3V^3(t))] \\
&+ E[V(t+\tau)(m_2V^2(t) + m_3V^3(t) + \{h_1-2h_2\frac{d^2}{dt^2} + h_3\frac{d}{dt}\}[\frac{d}{dt}V^2(t)] + \\
&\quad \{h_4+h_5\frac{d}{dt}\}[\frac{d}{dt}V^3(t)]) + (m_2V^2(t+\tau) + m_3V^3(t+\tau) + \\
&\quad \{h_1-2h_2\frac{d^2}{dt^2} + h_3\frac{d}{dt}\}[\frac{d}{dt}V^2(t)] + \{h_4+h_5\frac{d}{dt}\}[\frac{d}{dt}V^3(t)])V(t)]
\end{aligned}
\tag{A.1}
$$

Note that the terms in equation A.1 have been collected so that they represent signal-signal, modulator-modulator, nonlinearity-nonlinearity, modulator-nonlinearity and signal-(modulator + nonlinearity) correlations respectively.

We will proceed by calculating the power spectral density for each term of equation A.1 individually, substituting for V(t) from equation 6 as appropriate. Finally, these terms will be combined to obtain the total power spectral density of the distortion. The evaluation of the various correlation terms of the form $R_{ij}(\tau) = E[V^i(t+\tau)V^j(t)]$ are presented in Attachment B. Attachment C presents the evaluation of the correlation of each of the three signals with itself.

Modulator-Modulator Terms:

The distortion term that results from modulator-modulator correlations in equation A.1 is

$$MM(\tau) = E[(m_2V^2(t)+\tau) + m_3V^3(t+\tau))(m_2V^2(t)+m_3V^3(t))] \quad (A.2)$$

$$= m_2^2 R_{22}(\tau) + m_2m_3R_{23}(\tau)+m_2m_3R_{32}(\tau) + m_3^2 R_{33}(\tau)$$

Nonlinearity-Nonlinearity Terms:

The nonlinearity-nonlinearity distortions are represented by the third term of equation A.1. That is

$$NN(\tau) = E[((h_1-2h_2 \frac{d^2}{dt^2} + h_3 \frac{d}{dt})[\frac{d}{dt} V^2(t+\tau)+(h_4+h_5 \frac{d}{dt})[\frac{d}{dt} V^3(t+\tau)]) \quad (A.3)$$

$$((h_1-2h_2 \frac{d^2}{dt^2} + h_3 \frac{d}{dt})[\frac{d}{dt} V^2(t)] + (h_4+h_5 \frac{d}{dt})[\frac{d}{dt} V^3(t)])]$$

Using the fact that

$$E\left[\frac{d^i V^\ell(t+\tau)}{dt^i}\ \frac{d^j V^m(t)}{dt^j}\right] = (-1)^j \frac{d^{i+j}}{dt^{i+j}} E[V^\ell(t+\tau)V^m(t)] \qquad (A.4)$$

equation A.3 becomes

$$\begin{aligned} NN(\tau) = &\left[-h_1^2 \frac{d^2}{dt^2} + (h_3^2 - 2h_1h_2) \frac{d^4}{dt^4} - h_2^2 \frac{d^6}{dt^6}\right] R_{22}(\tau) \\ &+ \left[-h_1h_4 \frac{d^2}{dt^2} + (h_1h_5 - h_3h_4) \frac{d^3}{dt^3} + (h_3h_5 - h_2h_4) \frac{d^4}{dt^4}\right. \\ &\left. + h_2h_5 \frac{d^5}{dt^5}\right] R_{23}(\tau) \qquad (A.5) \\ &+ \left[(h_3h_4 - h_1h_4) \frac{d^2}{dt^2} + (-h_1h_4 - h_1h_5) \frac{d^3}{dt^3}\right. \\ &\left. + h_3h_5 \frac{d^4}{dt^4} - h_2h_5 \frac{d^5}{dt^5}\right] R_{32}(\tau) \\ &+ \left[-h_4^2 \frac{d^2}{dt^2} + h_5^2 \frac{d^4}{dt^4}\right] R_{33}(\tau) \end{aligned}$$

Modulator-Nonlinearity Term:

The fourth term of equation A.1 represents the modulator-nonlinearity distortion term. Again using equation A.4 this term becomes

$$MN(\tau) = \left[(m_3h_1 - m_2h_4)\frac{d}{dt} + m_2h_5\frac{d^2}{dt^2} + m_3h_2\frac{d^3}{dt^3}\right] R_{23}(\tau)$$

$$+ \left[(m_2h_4 - m_3h_1)\frac{d}{dt} + m_2h_5\frac{d^2}{dt^2} - m_3h_2\frac{d^3}{dt^3}\right] R_{32}(\tau)$$

$$+ 2m_2h_3\frac{d^2}{dt^2} R_{22}(\tau) + 2m_3h_5\frac{d^2}{dt^2} R_{33}(\tau) \qquad (A.6)$$

Signal-(Modulator+Nonlinearity) Term:

The last term of equation A.1 is the signal-(modulator + nonlinearity) term. Carrying out the indicated multiplication and using equation A.4 yields

$$SM(\tau) = \left[m_2 - h_1\frac{d}{dt} - h_2\frac{d^3}{dt^3} + h_3\frac{d^2}{dt^2}\right] R_{12}(\tau)$$

$$+ \left[m_2 + h_1\frac{d}{dt} + h_2\frac{d^3}{dt^3} - h_3\frac{d^2}{dt^2}\right] R_{21}(\tau)$$

$$+ \left[m_3 - h_4\frac{d}{dt} + h_5\frac{d^2}{dt^2}\right] R_{13}(\tau) \qquad (A.7)$$

$$+ \left[m_3 + h_4\frac{d}{dt} + h_5\frac{d^2}{dt^2}\right] R_{31}(\tau)$$

Combining the various terms evaluated above equation A.1 becomes

$$E[O(t+\tau)\, O(t)] = R_{11}(\tau) + SS(\tau) + MM(\tau) + NN(\tau) + MN(\tau) + SN(\tau)$$

$$= R_{11}(\tau)$$

$$+ \left[m_2^2 + (2m_2h_3 - h_1^2)\frac{d^2}{dt^2} + (h_3^2 - 2h_1h_2)\frac{d^4}{dt^4}\right.$$

$$
\begin{aligned}
&- h_2^2 \frac{d^6}{dt^6}] R_{22}(\tau) \\
&+ [m_2 - h_1 \frac{d}{dt} - h_2 \frac{d^3}{dt^3} + h_3 \frac{d^2}{dt^2}] R_{12}(\tau) \\
&+ [m_2 + h_1 \frac{d}{dt} + h_2 \frac{d^3}{dt^3} + h_3 \frac{d^2}{dt^2}] R_{21}(\tau) \\
&+ [m_3^3 + (2m_3 h_5 - h_4^2) \frac{d^2}{dt^2} + h_5^2 \frac{d^4}{dt^4}] R_{33}(\tau) \\
&+ [m_3 - h_4 \frac{d}{dt} + h_5 \frac{d^2}{dt^2}] R_{13}(\tau) \\
&+ [m_3 + h_4 \frac{d}{dt} + h_5 \frac{d^2}{dt^2}] R_{31}(\tau) \\
&+ [m_2 m_3 + (m_3 h_1 - m_2 h_4) \frac{d}{dt} + (m_5 h_2 - h_1 h_4) \frac{d^2}{dt^2} \\
&\quad + (m_3 h_2 + h_1 h_5 - h_3 h_4) \frac{d^3}{dt^3} + (h_3 h_5 - h_2 h_4) \frac{d^4}{dt^4} \\
&\quad + h_2 h_5 \frac{d^5}{dt^5}] R_{23}(\tau) \\
&+ [m_2 m_3 + (m_2 h_4 - m_3 h_1) \frac{d}{dt} + (m_2 h_5 + h_3 h_4 - h_1 h_4) \frac{d^2}{dt^2} \\
&- (m_3 h_2 + h_1 h_4 + h_1 h_5) \frac{d^3}{dt^3} + h_3 h_5 \frac{d^4}{dt^4} \\
&\quad - h_2 h_5 \frac{d^5}{dt^5}] R_{32}(\tau) \qquad \text{(A.8)}
\end{aligned}
$$

Attachment B - Calculation of Autocorrelation - $R_{ij}(\tau)$

This attachment calculates the autocorrelation terms

$R_{ij}(\tau) = E[V^i(t+\tau)V^j(t)]$ used in Attachment A.

B-1: $R_{11}(\tau)$

$$R_{11}(\tau) = E[V(t+\tau)V(t)].$$

$$= E[\sum_{i=1}^{3} x_i(t+\tau)\, x_i(t) + \sum_{i=1}^{3} \sum_{j\neq 1} x_i(t+\tau)\, x_j(t)]$$

$$= \sum_{i=1}^{3} R_i(\tau)$$

B-2: $R_{22}(\tau)$

$$R_{22}(\tau) = E[V^2(t+\tau)V^2(t)]$$

$$= E[\sum_{i=1}^{3} x_i^2(t+\tau)\, x_i^2(t) + \sum_{i=1}^{3} x_i^2(t+\tau) \sum_{j\neq 1} x_j^2(t)$$

$$+ \sum_{K=1}^{3} x_K^2(t+\tau)\,[\sum_{i=1}^{3} \sum_{j\neq K} x_i(t)\, x_j(t)] + \sum_{K=1}^{3} x_K^2(t)[\sum_{i=1}^{3} \sum_{j\neq i} x_i(t+\tau)x_j(t)]$$

$$+ 2 \sum_{i=1}^{3} \sum_{j\neq i} x_i(t+\tau)\, x_i(t)\, x_j(t+\tau)\, x_j(t)$$

$$+ 4 \sum_{i=1}^{3} \sum_{j\neq i} \sum_{K\neq j} x_j(t+\tau)\, x_i(t+\tau)\, x_i(t)\, x_K(t)]$$

$$= E[\sum_{i=1}^{3} x_i^2(t+\tau)\, x_i^2(t)] + \sum_{i=1}^{3} R_i(0) \sum_{j\neq i} R_j(0)$$

$$+ 2 \sum_{i=1}^{3} \sum_{j\neq i} R_i(\tau)\, R_j(\tau)$$

$$= 2 R_1^2(\tau) + R_1^2(0) + R_2^{22}(\tau) + R_3^{33}(\tau) + \sum_{i=1}^{3} R_i(0) \sum_{j\neq i} R_j(0)$$

$$+ 2 \sum_{i=1}^{3} \sum_{j\neq i} R_i(\tau)\, R_j(\tau)$$

B-3: $R_{21}(\tau)$

$$R_{21}(\tau) = E[V^2(t+\tau)V(t)]$$

$$= E[\sum_{i=1}^{3} x_i^2(t+\tau)\, x_i(t) + \sum_{i=1}^{3} \sum_{j\neq i} x_i^2(t+\tau)\, x_j(t)$$

$$+ \sum_{i=1}^{3} x_i^2(t+\tau) \sum_{j=1}^{3} \sum_{K\neq j} x_i(t)\, x_K(t)]$$

$$= R_2(\tau) + R_3^{21}(\tau)$$

B-4: $R_{12}(\tau)$

Similarly

$$R_{12}(\tau) = R_2(\tau) + R_3^{12}(\tau) = R_2(\tau) - R_3^{21}(\tau)$$

B-5: $R_{33}(\tau)$

$$R_{33}(\tau) = E[V^3(t+\tau)V^3(t)]$$

$$= E\Big[\sum_{i=1}^{3} x_i^3(t+\tau)\, x_i^3(t) + \sum_{i=1}^{3} x_i^3(t+\tau) \sum_{j\neq i} x_j{}^3(t)$$

$$+ 3\sum_{i=1}^{3} x_i^3(t+\tau)\, x_i(t) \sum_{j\neq i} x_j^2(t)$$

$$+ 3\sum_{j=1}^{3} x_i^3(t+\tau) \sum_{j\neq i} x_j(t) \sum_{\substack{K=j \\ K\neq i}} x_K^2(t)$$

$$+ 6\sum_{i=1}^{3} x_i^3(t+\tau)\, x_1(t)\, x_2(t)\, x_3(t)$$

$$+ 3\sum_{i=1}^{3} x_i^3(t)\, x_i(t-\tau) \sum_{j\neq i} x_j^2(t+\tau)$$

$$+ 3\sum_{i=1}^{3} x_i(t+\tau) \sum_{j\neq i} x_i^3(t) \sum_{K\neq i} x_K(t+\tau)$$

$$+ 9\sum_{i=1}^{3} x_i(t+\tau)\, x_i(t) \sum_{j\neq i} x_j^2(t) \sum_{K\neq j} x_K^2(t)$$

$$+ 9\sum_{i=1}^{3} x_i(t+\tau) \sum_{j\neq i} x_j^2(t+\tau) \sum_{K\neq i} x_K(t) \sum_{\substack{\ell\neq k \\ \ell\neq j}} x_\ell^2(t)$$

$$+ 18\sum_{i=1}^{3} x_i(t+\tau) \sum_{j\neq i} x_j(t-\tau)\, x_1(t)\, x_2(t)\, x_3(t)$$

$$+ 6\, x_1(t+\tau)\, x_2(t+\tau)\, x_3(t+\tau) \sum_{i=1}^{3} x_i^3(t)$$

$$+ 18\, x_1(t+\tau)\, x_2(t+\tau)\, x_3(t+\tau) \sum_{i=1}^{3} x_i(t) \sum_{j\neq i} x_j^2(t)$$

$$= 6\,R_1^3(\tau) + 9\,R_1(\tau)\,R_1^2(0) + 18\,R_1(\tau)\,R_1(0)\,[R_2(0) + R_3(0)]$$

$$+ R_2(\tau) + R_3(\tau) + 6\,R_1(0)\,[R_2(\tau)\,R_3(0) + R_3(\tau)\,R_2(\tau)]$$

$$+ 9\,R_1(\tau)\,[2R_2(0)\,R_3(0) + R_2^{22}(\tau) + R_3^{22}(\tau)2$$

$$+ 9\,R_2(\tau)\,[2R_1^2(\tau) + R_1^2(0) + R_3^{22}(\tau) + 2R_3(0)\,R_1'0)]$$

$$+ 9\,R_3(\tau)\,[2R_1^2(\tau) + R_1^2(0) + R_2^{22}(\tau) + 2R_2(0)\,R_1(0)]$$

B-6: $R_{31}(\tau)$

$$R_{31}(\tau) = E[V^3(t+\tau)\,V(t)]$$

$$= E\Big[\sum_{i=1}^{3} x_i^3(t+\tau)\,x_i(t) + \sum_{i=1}^{3} x_i^3(t+\tau) \sum_{j\neq i} x_j(t)$$

$$+ 3\sum_{i=1}^{3} x_i(t+\tau)\,x_i(t) \sum_{j\neq i} x_j^2(t)$$

$$+ 3\sum_{i=1}^{3} x_i(t+\tau) \sum_{j\neq i} x_j(t) \sum_{\substack{K\neq j \\ K\neq i}} x_K^2(t)$$

$$+ 6\sum_{i=1}^{3} x_i(t+\tau)\,x_1(t)\,x_2(t)\,x_3(t)$$

$$= 3R_1(\tau)\,R_1(0) + 3R_1(\tau)\,[R_2(0) + R_3(0)] + R_2(\tau) + R_3(\tau)$$

$$+ 3R_1(0)\,[R_2(\tau)\,R_3(0) + R_3(\tau)\,R_2(0)]$$

B-7: $R_{13}(\tau)$

Similarly

$$R_{13}(\tau) = 3R_1(\tau)\, R_1(0) + 3R_1(\tau)\, [R_2(0) + R_3(0)] + R_2(\tau) + R_3(\tau)$$

$$+ 3R_1(0)\, [R_2(\tau)\, R_3(0) + R_3(\tau)\, R_2(0)]$$

B-8: $R_{32}(\tau)$

$$R_{32}(\tau) = E[V^3(t+\tau)\, V^2(t)]$$

$$= E[\sum_{i=1}^{3} x_i^3(t+\tau)\, x_i^2(t) + \sum_{i=1}^{3} x_i^2(t+\tau) \sum_{j\neq i} x_i^3(t)$$

$$+ 3\sum_{i=1}^{3} x_i^2(t+\tau)\, x_i(t) \sum_{j\neq i} x_j(t)$$

$$+ 3\sum_{i=1}^{3} x_i^2(t+\tau) \sum_{j\neq i} x_i(t+\tau) \sum_{\substack{K\neq j \\ K\neq i}} x_K^2(t)$$

$$+ 6\sum_{i=1}^{3} x_i^2(t+\tau)\, x_1(t)\, x_2(t)\, x_3(t)$$

$$+ \sum_{i=1}^{3} x_i^3(t) [\sum_{j=1}^{3} x_j(t+\tau) \sum_{k\neq j} x_K(t+\tau)]$$

$$+ 3\sum_{i=1}^{3} x_i(t+\tau) \sum_{j\neq i} x_j(t+\tau) \sum_{K=1}^{3} x_K(t) \sum_{\ell\neq K} x_\ell(t)$$

$$= 3\sum_{i=1}^{3} R_i(\tau) \sum_{j\neq 1} R_j(\tau) + R_2(\tau) - R_3^{21}(\tau)$$

B-9: $R_{23}(\tau)$

Similarly,

$$R_{23}(\tau) = E[V^2(t+\tau)\ V^3(t)]$$

$$= 3 \sum_{i=1}^{3} R_i(\tau) \sum_{j \neq 1} R_j(\tau) + R_2(\tau) - R_3^{12}(\tau)$$

$$= 3 \sum_{i=1}^{3} R_i(\tau) \sum_{j \neq 1} R_j(\tau) + R_2(\tau) + R_3^{21}(\tau)$$

Attachment C - Calculation of Correlation Functions for Each Signal - $R_i(\tau)$

This appendix calculates the correlation functions for each of the three signals. The terms evaluated were used in the calculations of Attachment B.

TV Signal - Channel 3

The television signal, $x_1(t)$ has been modeled by a zero mean gaussian random process as described in reference 2. We define

$$R_1(\tau) = E[x_1(t+\tau)\, x_1(t)]$$

and calculated higher order correlation functions using the moment factoring property of gaussian random processes (reference 3).

$$\text{(i)}\quad E[x_1^2(t+\tau)x_1^2(t)] = E[x_1^2(t+\tau)]E[x_1^2(t)] + 2\{E[x_1(t+\tau)x_1(t)]\}^2$$

$$= 2R_1^2(\tau) + R_1(\tau)\, R_1(0)$$

$$\text{(ii)}\quad E[x_1^2(t+\tau)x_1(t)] = E[x_1(t+\tau)x_1^2(t)] = 0$$

$$\text{(iii)}\quad E[x_1^3(t+\tau)x_1^3(t)] = 6\{E[x_1(t+\tau)x_1(t)]\}^3$$

$$+ 9\, E[x_1(t+\tau)x_1(t)]E[x_1(t+\tau)x_1(t+\tau)]E[x_1(\tau)x_1(t)]$$

$$= 6\, R_1(\tau)^2 + 9\, R_1(\tau)\, R_1(0)$$

$$\text{(iv)}\quad E[x_1^3(t+\tau)x_1(t)] = E[x_1(t+\tau)x_1^3(t)]$$

$$= 3\,E[x_1(t+\tau)x_1(t)]E[x_1(t+\tau)x_1(t+\tau)]$$

$$= 3\,R_1(\tau)\,R_1(0)$$

$$\text{(v)}\quad E[x_1^3(t+\tau)x_1^2(t)] = E[x_1^2(t+\tau)x_1^3(t)] = 0$$

Digital Signal - NRZ - Channel 2

The NRZ signal consists of a series of pulses of duration T of level +1 or -1. (A single time pulse is shown in C-1a.) Since a long sequence of these pulses will have equal numbers of plus and minus ones this signal has zero mean. The autocorrelation function of the NRZ signal is shown pictorially in Figure C-1b. In addition, the other correlation functions used in Attachment B are

$$E[x_2^i(t+\tau)x_2^j(t)] = \begin{cases} R_2(\tau) & i \text{ even, } j \text{ even} \\ 0 & \text{otherwise} \end{cases}$$

Digital Signal - Bi-ø-L - Channel 3

As with the NRZ signal the Bi-ø-L signal and its correlation functions are best described pictorially. Those correlation functions used in Attachment B are shown in Figure C-2.

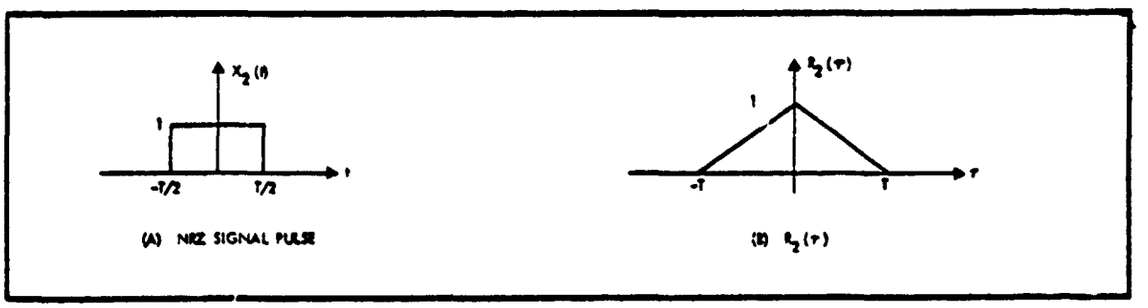

Figure C-1. NRZ Signal

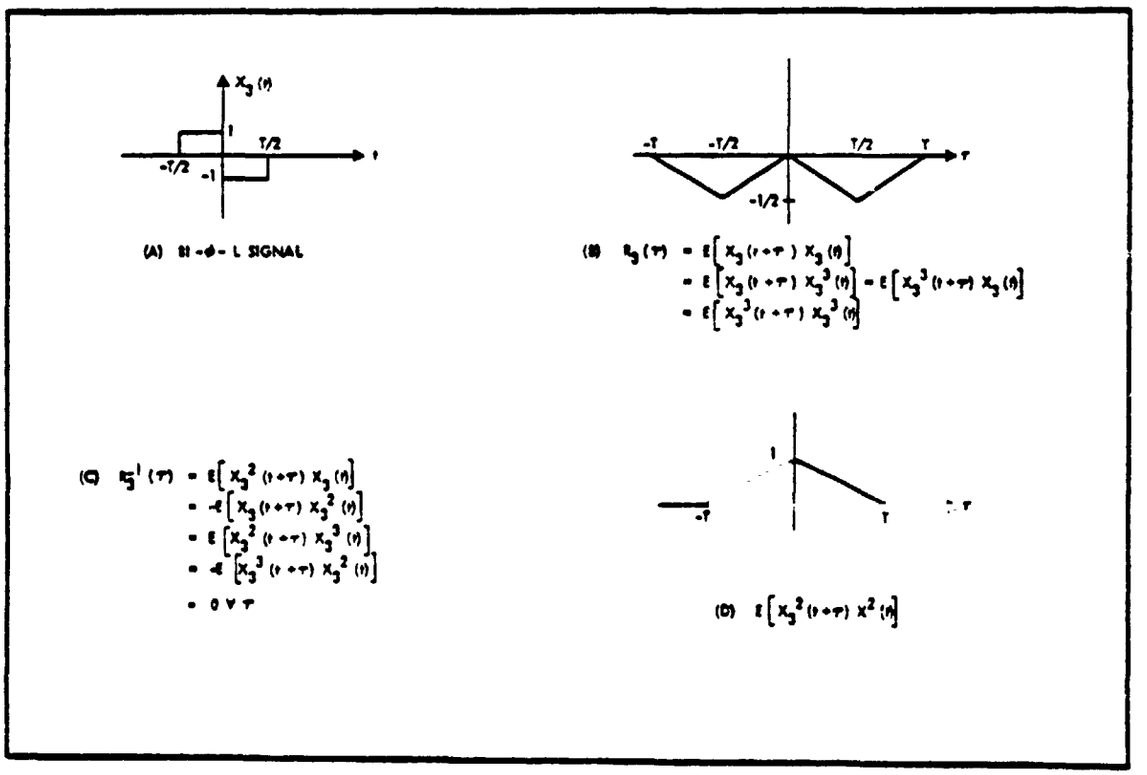

Figure C-2. BI-Φ-L Signal

References:

1. Stone, M.S., "Intermodulation in FDM-FM Systems", TRW IOC 7352.4-108, August 20, 1970.

2. Franks, L.E., "A Model for the Random Video Process", BSTJ, April 1966.

3. Papoulis, A., Probability, Random Variables, and Stochastic Processes, McGraw-Hill, 1965.